Characterization of Metamorphic Assemblages and Assessment of Cu-Pb-Ag-Au-Zn Mobility at the Lalor deposit, Snow Lake, Manitoba

by

Judy Lam

A thesis submitted in partial fulfillment
of the requirements for the degree of
Master of Science (MSc) in Geology

The Faculty of Graduate Studies
Laurentian University
Sudbury, Ontario, Canada

Abstract

The Lalor VMS deposit is located within the Snow Lake arc assemblage at the easternmost end of the Paleoproterozoic Flin Flon belt. A regional metamorphic event at 1.81 Ga, up to middle amphibolite facies (550˚C, 5kbar), recrystallized the mineral assemblages in the massive sulfide and hydrothermally altered rocks that are associated with the formation of VMS deposits in the area. The Lalor deposit differs from most VMS deposits in the area in that it contains low-sulfide Au rich zones that are proximal to but separate from the massive sulfide lenses.

Gold mineralization primarily occurs in three rock types at the Lalor deposit: massive sulfides, and calc-silicates to carbonate silicates, and Fe-Mg altered rocks. Electrum is the dominant form of gold, but gold also occurs in sulfosalt phases such as aurostibite ($AuSb_2$) and in tellurides such as petzite (Ag_3AuTe_2). It is often associated with hessite (Ag_2Te), altaite (PbTe), chalcopyrite ($CuFeS_2$), and galena (PbS). Gold mineralization occurs along fractures, grain boundaries, cleavage planes, and as discrete inclusions in metamorphic minerals.

There are two dominant metal associations with gold: Cu-Au and Pb-Au. The Cu-Au association is more common and occurs in a variety of rock types (including massive sulfides and Fe-Mg altered rocks), whereas the Pb-Au association is restricted to calc-silicate to carbonate silicate altered rocks.

In the massive sulfides, gold content and distribution are a function of primary VMS zone refining processes; however, Au has been locally remobilized during metamorphism and deformation. In the Fe-Mg altered rocks proximal to massive sulfide, the distribution and tenor of Au reflects primary zone refining and local remobilization due to metamorphism and deformation, whereas in Fe-Mg altered rocks distal to massive sulfide, gold distribution is

largely a product of pre-peak to peak metamorphic remobilization of primary VMS gold via fluid-dominated transportation.

In the calc-silicate to carbonate silicate rocks, which contained or contain carbonate, Au distribution reflects metamorphic remobilization. Metamorphic devolatilization of primary carbonate bearing rocks is responsible for adding components such as H_2O, CO_2 and S_2 into a fluid phase that remobilized Au and some metals (e.g. Cu, Pb) in the deposit, and in altered rocks located proximal and distal to the massive sulfide lenses. Gold was mobilized and transported as a sulfur complex, with CO_2 acting as a buffer for a low salinity fluid phase such that it could maintain an elevated gold content for transport and deposition. The result of this mobilization is responsible for the Pb-Au in calc-silicate to carbonate silicate altered rocks.

Acknowledgements

First and foremost, I would like to thank my supervisors Drs. Doug Tinkham and Harold Gibson for taking me on as a graduate student and seeing me through to the end of the project. I also extend my gratitude to the faculty and staff in the Department of Earth Sciences at Laurentian University who have helped me out during the completion of my Master's thesis, especially William Zhe for his assistance and flexibility while working on the SEM. I also want to thank the students in the department who motivated me and provided much needed breaks, especially in the late evening/early morning hours (Kate, Sarah, and Tif). I also want to thank Hudbay for their support on the project, as well as the other graduate students working in the Snow Lake area for good times and collaborating, especially during the field seasons.

I am very grateful to have found employment whilst editing my Master's dissertation, even though it was challenging to work all day and then come home to work some more on my thesis. I am thankful to the company (LSG/Tahoe) for their support and to Karin for helping me find a job and get settled in Timmins. Last but not least, I also want to thank my family and friends for their encouragement and distractions (especially Morgan and Greg). The last few years have been a good experience and I am looking forward to moving ahead with my career.

Table of Contents

List of Tables

List of Figures

List of Appendices

Chapter 1

1.0 Introduction

The Lalor volcanogenic massive sulfide (VMS) deposit is located on the eastern flank of the prolific Paleoproterozoic Flin Flon belt (Figure 1). It is part of the 1.89 Ga Snow Lake assemblage (David et al., 1996; Bailes and Galley, 1999), which has undergone metamorphism circa 1.81 Ga up to middle amphibolite facies (Machado and David, 1992). The Snow Lake assemblage comprises the Anderson sequence, Chisel sequence, and Snow Creek sequence (Figure 2a). The Lalor deposit occurs within the Chisel sequence along with 8 known VMS deposits (Figure 2b; Bailes, 2016).

The objective of this thesis is to determine if gold and associated metals were mobilized during metamorphism of the Lalor deposit, with a focus on the low-sulfide gold zones. Investigating metal mobility requires two steps. The first is to characterize the Au-Ag-Cu-Pb-Zn mineralization (visual and petrographic descriptions, and geochemical data) and its spatial association with hydrothermal alteration facies, location within the massive sulfide lenses (metal zoning), and metamorphic reaction history (mineral assemblages, textures and structures). The metamorphic reaction history is important as metamorphism could result in metal mobilization during production of fluids or melt phases. The second step is to use mineralization style and setting, in relation to the metamorphic reaction history, to infer mechanisms by which metals could be mobilized, such as by fluids or low temperature sulfarsenide/bismuthotelluride melts. This required detailed observations of drill core, followed by petrographic and geochemical studies.

1.1 Background

Volcanogenic massive sulfide deposits comprise one or more massive sulfide lenses and a stockwork mineralization system (Lydon, 1984). They form at or near the seafloor during a hiatus in volcanism from the precipitation of metals in hot hydrothermal fluids (Galley et al., 2007). As a result, these deposits can be hosted in either volcanic or sedimentary rocks (Gibson et al., 2007). A model of the typical metal zoning within VMS deposit and its hydrothermal alteration system is shown in Figure 3. The original massive sulfide lens configuration typically has a sphalerite-rich (Zn-rich) top, a pyrite-rich middle layer, and a chalcopyrite-rich (Cu-rich) bottom that transitions into a chalcopyrite stringer zone. The alteration zones are typically sericite, Mg-chlorite, and Fe-chlorite (Figure 3) towards the center of the deposit. As alteration intensity increases, there is alteration zoning due to the progressive decrease in certain elements and increase in others (i.e. decrease in Na and Fe while Mg and K increases as seen in the recharge zone in Figure 3; Galley et al., 2007).

Gold-rich VMS deposits are classified as those with Au grades greater than 3.46 g/t and at least 31 t of gold (Mercier-Langevin et al., 2011). Typical characteristics of some Au-rich VMS deposits include metamorphosed argillic alteration and silicification, which are common in high sulfidation gold deposits (Dube et al., 2007). By these definitions, the Lalor deposit, with an average grade of 2.78 g/t Au is not a gold-rich deposit (Mercier-Langevin et al., 2011), but it does contain low sulfide gold-rich zones (the 21, 24, 25, 26, 27, and 28 lenses) that are separate from the base metal zones. The gold associated with the massive sulfide zones at the Lalor deposit is typical of VMS deposits, but gold associated with low sulfide zones at the Lalor deposit is atypical of a VMS deposit.

Metamorphism of ore deposits above greenschist facies can result in significant textural, mineralogical and compositional changes, especially if the host rocks are hydrothermally altered

as at the Lalor deposit. An additional consequence is that primary textures are typically not well preserved in rocks hosting the Lalor deposit. During metamorphism, three mechanisms (or processes) can mobilize metals: mechanical remobilization, mobilization in a melt phase, and mobilization in a fluid phase.

Mechanical remobilization of metals can occur by deformation and emplacement of igneous intrusions. Deformation during metamorphism may result in differential mobility of sulfide minerals and the location of more mobile or ductile sulfides along planes of weakness. Igneous intrusions can locally aid in the mobilization of pre-existing metals as well as introducing more metals into a system. Mechanical remobilization alone is unlikely to be a dominant method for upgrading deposits since it only redistributes existing metals (Marshall et al., 2000).

Mobilization of metals in a melt phase can occur during partial melting of sulfides at medium- to high-grade metamorphism according to studies by Frost et al., (2002), Tomkins and Mavrogenes (2002) and Tomkins et al. (2004). VMS deposits typically have a pre-metamorphic assemblage of pyrite-pyrrhotite-sphalerite-galena-chalcopyrite with minor arsenopyrite. Initial partial melting of sulfides can begin with pyrite and arsenopyrite at 560°C and 5 kbar (Tomkins et al., 2007). Individual sulfides have relatively high melting temperatures, but in assemblages with other sulfides (such as galena), they typically melt at lower temperatures (Tomkins et al., 2007). Gold mineralization is often associated with low melting point chalcophile elements (Ag, As, Bi, Hg, Sb, Se, Te, Tl; Tomkins and Mavrogenes, 2002). These low melting point chalcophile elements typically occur together with remobilized sulfide minerals as they all exhibit similar behaviour (Basu et al., 1981, 1983; Hofmann 1994; Cook, 1996). During prograde metamorphism of massive sulfide deposits, the breakdown of pyrite to form pyrrhotite

can result in a high sulfur fugacity environment in which arsenopyrite can melt. An As-S melt can easily incorporate and mobilize gold, and it can also lower the melting temperature for other sulfide and sulfosalt phases (such as galena and stibnite; Tomkins et al., 2006). Regardless of what metals are in an auriferous melt phase, the role of deformation is important in mobilizing the melt so it can come in to contact with other ore minerals and incorporate them into the melt and thus, concentrate the metals. Tomkins et al. (2007) refer to this process as mobilization-assisted melting.

Mobilization of metals in a fluid phase results from metamorphic devolatilization reactions that release fluid phase capable of transporting metals such as gold (Phillips and Powell, 1993). Studies on the devolatilization model have primarily focused on the formation of "gold-only" deposits (Phillips and Powell, 2010). This model can also be applied to the Lalor VMS deposit since it has experienced amphibolite facies metamorphism that meets the temperature requirement for this model. Calc-silicate to carbonate silicate rocks occur in the Lalor deposit and may have contributed to a fluid phase during metamorphism that could have mobilized metals (Tinkham, 2013). Gold is a soft cation with a high (>2.00) electronegativity (Phillips and Powell, 2010). Other elements with high electronegativity, such as As, B, Bi, Hg, Mo, Sb, Se, Te, and W, exhibit a similar behavior as gold and are commonly found to variable degrees in association with Au (Phillips and Powell, 2010). Gold occurs in three oxidation states: Au^{+}, Au°, and Au^{3+} (Puddephatt, 1978). Au^{+} forms covalent bonds with soft bases such as S^{2-}, HS^{-}, and H_2S. Au° is the form of native gold. Au^{3+} occurs in saline fluids where it complexes with Cl^{-} in oxidizing conditions. Cl^{-} is a hard anion, so it preferably bonds with hard cations like Cu, Pb, Zn, and Ag (Phillips and Powell, 2010).

The metamorphic devolatilization model for the formation of gold deposits of Phillips and Powell (1993, 2010) and Phillips and Evans (2004) focuses on devolatilization that occurs at the greenschist to amphibolite facies transition in hydrated and mildly to moderately carbonated, metabasic rocks within an orogenic setting. During metamorphism (480 ± 20°C, 3-5 kbar), a significant amount of fluid can be released during dehydration reactions: 1 km^3 = 10 x 10^6 tonnes of fluid (1% of the original rock, which is a low estimate) (Phillips and Powell, 1993). The main mineralogical changes are illustrated by the reaction:

Chl + Ep + Ank – Dol + Ab + Qz (+ Py) = Ca-Amph + Pl + fluid (+ Po)

In this reaction, chlorite and carbonate break down at the greenschist to amphibolite facies transition. This devolatilization occurs at the mineral scale and can extract H_2O, CO_2, S, and Au from the rocks and incorporate them into a fluid phase (Phillips and Powell, 2010). The H_2O-CO_2 fluid generated is low salinity, with lower salinity than seawater (Phillips and Powell, 1993). The auriferous, low salinity fluid also has a low base metal content (Phillips and Powell, 2010). Sulfur in the fluid is sourced from the breakdown of abundant pyrite (Phillips and Powell, 1993). An advantage of this model is that gold can be dissolved into a fluid phase as the fluid is forming (Phillips and Powell, 2010). In a rock-dominated system, gold forms a complex with sulfur as a bisulfide complex, with H_2CO_3 buffering pH levels in the fluid for optimal gold solubility (Phillips and Powell, 1993). In a fluid-dominated system, the fluid phase preferentially travels along zones of low stress, allowing for focusing of mineralization unrelated to wall rock composition. The latter results in gold deposits, which occur in groups that are typically structurally controlled (Phillips and Powell, 2010).

Phillips and Evans (2004) suggested that CO_2 buffers the fluid pH to a range that maximizes gold solubility, allowing for transport of Au in the presence of a reduced sulfur complex (Eqn. 1).

(Eqn. 1) $Au + H_2S + HS = Au(HS)_2^- + ½ H_2$

Low salinity and the lack of base metals in the gold-only deposits indicate that the HS^- complex is the most significant ligand for transport of gold. At P-T conditions of 200-400°C and 200 MPa, and neutral pH, $Au(HS)_2^-$ is the dominant gold complex. These low salinity auriferous aqueous phases contain up to 20-30 mol% CO_2 and reduced S_2 (Phillips and Powell, 1993).

Phillips and Evans (2004) examined the solubility of gold as $Au(HS)_2^-$ in an auriferous CO_2-bearing fluid phase and an auriferous non-CO_2 bearing phase in the presence of a basalt. The interaction of the fluid with the ferrous wall rock resulted in a pH increase in the CO_2-free fluid, which increases the solubility of gold in the fluid and reduces the likelihood of deposition by sulfidation. In contrast, the CO_2-bearing fluid phase maintains its pH level, allowing for stable transport and deposition of gold in greater abundances through interaction with a favorable host rock such as Fe-rich basalt (sulfidation). CO_2-bearing fluids are more likely to form economic gold deposits since there is a narrow distance and temperature range in which Au is deposited. In contrast, non-CO_2 bearing fluids tend to deposit Au at a low concentrations and carry it greater distances from source. (Phillips and Evans, 2004).

Precipitation of gold from a fluid phase occurs between 250-400°C due to lower temperatures, sulfur activity (interaction with Fe-rich wall rocks to form Fe-sulfides), and changes in oxygen activity (lowering from interaction with carbonaceous sediments). Changes in P-T conditions (typically lowering) will result in fluid immiscibility and separation of the CO_2 and H_2O phases, the partitioning of which can release Au and H_2S from the fluid phase (Phillips

and Powell, 1993). Breakdown of the gold-thiosulfate complex due to reducing conditions, in the presence of carbon-bearing rocks or the sulfidation of wall rocks to form iron sulfides, will result in the deposition of gold (Phillips and Powell, 2010). Fluid:wall-rock interaction is not necessary for gold deposition but can localize it. Prominent gold deposits often have a strong structural control, such as localization of deposits at the brittle-ductile transition zone where the inelastic brittle zone is conducive to focusing fluid:wall rock interaction (Phillips and Powell, 1993).

Recent work on trisulfur (S_3^-) species in hydrothermal fluids indicates that it may play a role in the formation of gold deposits (Pokrovski et al., 2015). Raman spectroscopy has established that S_3^- is the dominant species of sulfur in aqueous solutions at 250-700°C and 5-50 kbar (Pokrovski and Dubrovinsky, 2011; Pokrovski and Dubessy, 2015). These conditions are met during magmatic fluid evolution in porphyry systems (>250°C) and during prograde metamorphism (>500°C) of orogenic gold deposits where desulfidation of pyrite to form pyrrhotite generates sulfur-rich fluids (Pokrovski and Dubessy, 2015). These settings contain 10-10 000 times more S_3^- than HS^- in the fluid phase (Pokrovski et al., 2015). However, due to fluid immiscibility at lower temperatures, common to many gold deposit-forming settings, the presence of a low-density vapour phase will cause the breakdown of $Au(HS)S_3^-$ to precipitate some gold, and then $Au(HS)_2^-$ becomes the main gold carrier (Pokrovski et al., 2015).

1.2 Methods

Fourteen diamond drill holes were logged across three sections of the Lalor deposit (Figures 4-7). Existing Hudbay data, including cross sections, assays, and lithogeochemical data guided core logging. Drill holes were selected based on the local occurrence of gold at greater than 5 g/t and on their spatial distribution across the deposit to accurately represent the ore environment (in

terms of the base metal versus gold zones and their host rocks). Graphic logs and log forms were used to collect drill core data. A specific graphic logging technique based on mineral associations was developed and used to record observations at the Lalor deposit because hydrothermal alteration and subsequent metamorphism and deformation often made identification of the protolith and primary textures impossible over large intervals of drill core. Representative drill holes were graphically logged to detail assemblage associations, the sum of minerals that are the product of metamorphosed hydrothermally alteration, and the distribution of these metamorphic minerals. This detailed logging constrained the environments in which metals occur in terms of qualitative alteration intensity and style, metamorphic mineral assemblages, reaction history, and textures. In conjunction with logging, representative drill core samples were collected for petrographic, lithogeochemical and metal chemistry studies.

Graphic logs provided a visual representation of data while log sheets record detailed descriptions of the rocks. Logging consisted of noting rock types, alteration style and zoning, contact relationships, mineralization style, as well as the distribution and variability of these components. Log sheets were used for detailed rock descriptions for each interval. Logging of drill core typically started in the less altered rocks above the first ore lens intercepted by the drill hole and then continued past the last ore zone into strong alteration zones. The abbreviations used for minerals in logging and in this thesis are listed in Table 1 and for the most part follow the abbreviations of Kretz (1983).

The graphic log style and technique illustrated in Figure 9 was specifically developed to represent the rock types encountered at the Lalor deposit. The rocks are logged as primary volcanic rocks (felsic, intermediate, or mafic in composition) when alteration is weak and was not texturally destructive, and by assemblage association where alteration intensity was strong

and characteristic alteration mineral assemblage associations were present (Figure 9). Sulfide-rich (including massive sulfide) intervals are indicated when sulfide content is greater than 30%. Examples of these rocks are shown in Figure 8 and the main alteration mineral assemblage associations are listed in Table 2. An assemblage association division reflects the differences in rock chemistry (primary and alteration) in terms of mineralogy, and in turn, VMS alteration types. Rather than attempting to list several assemblages on the log itself, which is not possible due to the large number of assemblages associated with one another within each chemical-mineralogical association (as seen in Table 2), only the characteristic minerals that occur in several associated assemblages within each chemical-mineralogical group are used to designate the assemblage association. The assemblage associations defined in this manner include: 1) chlorite-carbonate-talc-tremolite (Chl-Crb-Tlc-Tr), defined by mineral assemblages containing various combinations of the characteristic minerals chlorite, carbonate, talc and tremolite, representing a Ca-Fe-Mg chemical association; 2) Fe-Mg silicate (Fe-Mg) dominant assemblages with generally low to absent biotite and muscovite, reflecting Fe-Mg alteration and rocks low in K, Na, and Ca; 3) biotite-muscovite-quartz (Bt-Ms-Qz) dominant assemblages reflecting rocks with variable Fe-Mg content and relatively high K content compared to the Fe-Mg association; 4) a biotite-kyanite/sillimanite (Bt-Al_2SiO_5) association, and 5) a muscovite-kyanite/sillimanite (Ms-Al_2SiO_5) association. This scheme was developed because it is first and foremost defined by characteristic mineralogy easily identifiable at the hand sample scale, and yet reflects the compositional variability of the host rock in elements constrained by well-defined compositional changes associated with alteration in the generalized VMS alteration model. The sum of alteration minerals on the graphic log serves as an approximate proxy for alteration intensity and highlights the nature of alteration zoning. However, there are two exceptions: one, Fe-Mg-rich

garnets in less altered rocks (Hb- or Pl- rich) are not included and two, the occurrence of biotite was excluded, unless the other minerals present with biotite indicate the rock had undergone totally destructive alteration, and then half of the biotite mode was used. Modal mineralogy provided a mechanism to visualize minerals that persist across intervals. Intervals are used to indicate the observed changes in assemblage associations.

Detailed petrography was used to characterize the mineralization at the microscale by confirming mineralogy and resolving mineral textures to unravel the metamorphic reaction history. The peak metamorphic mineral assemblages are a good proxy in which timing relationships can be determined in relation to a prograde or retrograde phase. Reflected light microscopy was utilized to evaluate the nature of the ore minerals and their relationship to one another. Scanning electron microscopy (SEM) was used to characterize the gold mineralization in terms of its exact mineralogy, relationship to other ore minerals, and the mineral chemistry of host rocks.

Whole rock geochemistry was used to evaluate rock protoliths and alteration types, and establish stratigraphy and metal associations. Binary plots of various elements (i.e. Cu vs. Au, Pb vs. Cu, etc.) were plotted (using Igpet and Microsoft Excel) to test for associations between Au and base metals, Au and rock type, and Au and alteration type. Lithogeochemistry was used to help classify and correlate primary rock types of strongly altered lithologies and to elucidate the underlying deposit-scale stratigraphy. Traditional least mobile element geochemistry was used to define geochemical units by Winchester & Floyd (1977) Zr/TiO_2 vs. Nb/Y diagrams where samples plot in different protolith fields. The groupings were confirmed by observing the differences or similarities within and between them in a spider diagram (primitive mantle normalized trace element diagrams). Chemical indices were calculated using traditionally mobile

elements (major element geochemistry) to understand the nature of alteration-related compositional zoning. Calculated chemical indices used include the advanced argillic alteration index (AAAI), Ishikawa alteration index (AI), aluminum saturation index (ASI, also known as ACNK), and the chlorite-carbonate-pyrite index (CCPI; Tables 3-4). Alteration box plots in Figure 19, which use CCPI vs. AI as per Large et al. (2001), were used to define the dominant pre-metamorphism alteration trends.

Chapter 2

2.0 Geological Setting

2.1 Regional geology

The Lalor deposit, located on the eastern end of the Paleoproterozoic Flin Flon belt, was deformed during the Trans-Hudson Orogen (Figure 1). The Trans-Hudson orogeny, located between the Superior and Hearne cratons, represents a complete Wilson cycle with the opening and closing of the Manikewan Ocean over 150 Ma (2.07-1.80 Ga; Galley et al., 2007). It consists of the Hearne margin, Reindeer Zone, and Superior margin (Corrigan et al., 2009). The Reindeer Zone contains the Flin Flon-Glennie Complex, which was accreted circa 1.87 Ga (Lewry & Collerson, 1990; Lucas et al., 1996). It comprises the Glennie Domain, the Hanson Lake block, the Amisk collage, and the Snow Lake arc assemblage, all of which are fold-repeated and thrust stacked (Lewry & Collerson, 1990; Lucas et al., 1996; Ashton et al., 2005).

The Flin Flon belt contains the Amisk collage to the west and the Snow Lake arc assemblage to the east (Figure 1). It is exposed 200 km along strike over a 70 km exposed width (Galley et al., 2007). Regional metamorphism occurred at 1.81 Ga (Machado and David, 1992); the Amisk collage was metamorphosed to greenschist facies and the Snow Lake arc assemblage at greenschist facies to the south increasing to middle amphibolite facies adjacent to the Kisseynew domain. VMS mineralization formed in submarine oceanic volcanic arc and extensional volcanic arc settings at 1.91-1.88 Ga prior to the tectonic accretion and assembly of the Flin Flon belt (Galley et al., 2007). The Amisk collage comprises volcanic terranes intruded by plutons and overlain by sediments of the Missi Group (Syme, 1995; Lucas et al., 1996; Galley et al., 2007). It includes the West Amisk, Birch Lake, Flin Flon, and Fourmile Island arc assemblages, as well as the Sandy Bay and Elbow-Athapappuskow back-arc assemblages (Stern

et al., 1999; Syme et al., 1999). The Snow Lake arc assemblage consists of 1.89 Ga volcanic rocks (David et al., 1996; Bailes and Galley, 1999) exposed in a southwest verging 1.84-1.81 Ga fold-thrust belt (Kraus and Williams, 1999). It is divided into the Anderson, Chisel, and Snow Creek sequences (Figure 2).

2.2 Local geology

The location of the Anderson, Chisel, and Snow Creek sequences in the Snow Lake arc assemblage are shown in Figure 2a, with cross sections of the successions and their respective rock types and VMS deposits in Figure 2b. The Anderson sequence is a bimodal-mafic succession of primitive arc volcanic rocks dominated by the Welch basalt-basaltic andesite and three rhyolite complexes (Anderson, Sneath, Daly). The synvolcanic Sneath Lake tonalite-trondhjemite complex (1.886 Ga; Bailes et al., 1988, 1991) is part of the Anderson sequence. The Chisel sequence is the product of mature arc volcanism, dominated by subaqueous mafic flows and varied heterolithic volcaniclastic rocks, the latter of which comprises up to 50% of the succession. The synvolcanic Richard intrusive complex (1.889 Ga; Bailes et al., 1988, 1991) and associated dikes intrude the Chisel sequence. The Chisel sequence is divided into the Lower and Upper sequences, of which the synvolcanic dikes are the feeders. The nature of the contact between the Lower and Upper Chisel succession is interpreted to be conformable (Stewart et al., 2018). The Snow Creek sequence comprises massive-pillowed basalt flows and related basalt sills (Bailes and Galley, 1999) that are truncated by the Snow Lake thrust fault. However, the basalt is not hydrothermally altered and has an unfaulted lower stratigraphic contact, both of which indicate an arc-rifting environment.

Hydrothermal alteration and subsequent 1.81 Ga amphibolite facies metamorphism has resulted in the various metamorphic mineral assemblages in the Snow Lake arc assemblage. Three periods of alteration are observed (Bailes and Galley, 1996). The first is represented by stacked, semi-conformable zones in the Anderson-Stall and Daly rhyolites overlying discordant alteration pipes that truncate at the contact with the VMS deposits (Bailes and Galley, 2007). The second period of alteration manifests itself as a silicate and epidote alteration in the Welch basalts (Figure 2b), a 300-500 m thick zone underlying the Foot-Mud horizon at the top of the Anderson sequence (Bailes and Galley, 2007). The third period of alteration only affected the Lower Chisel sequence, where it is spatially associated with an early phase of the Richard intrusive complex and feeder dikes of the Powderhouse dacite (Bailes and Galley, 2007). At surface the resulting alteration is primarily observed in the Edwards mafic volcaniclastic rocks and Powderhouse dacite. The synvolcanic alteration zones (first and third period) are interpreted to be genetically associated with the formation of the VMS deposits, whereas the second period of alteration occurs during a hiatus in Anderson sequence volcanism (Bailes and Galley, 1996).

Four deformational events are observed in the Chisel-Anderson Lakes area of the Snow Lake arc assemblage (Kraus and Williams, 1999). D_1 and D_2 events are observed as tight isoclinal folds and low angle thrust faults that formed during SW-directed transport of Burntwood Group turbidite from the Kisseynew basin over the Flin Flon Domain. D_3 is interpreted to represent northwest-southeast transpressional shortening associated with syn- to post-peak regional metamorphism (Connors et al., 1999), resulting in open upright folds widely observed in units such as the Threehouse mafic volcaniclastic (Bailes, 2012). Overprinting D_4 structures are rarely seen, but occur south of Snow Lake as east-trending open upright folds (Kraus and Williams, 1999; Connors et al., 1999).

Recent work by Stewart et al. (2018) indicates that an earlier deformation event, which is expressed by the formation of isoclinal folds, preceded the deposition of the Burntwood turbidites. The updated stratigraphy of Upper Chisel sequence shows that folding and faulting repeats the Chisel sequence ore interval (most deposits have corroborating F_1 features). The early Lalor-Chisel thrust fault resulted in displacement of the hanging wall rocks of the Lalor deposit and crosscutting units in the VMS ore interval, which has the implication that this major D_1 structure may have shifted mineralization in the Snow Lake assemblage (Stewart et al., 2018).

Regional metamorphism up to middle amphibolite facies in the Snow Lake area has been documented in the diverse mineral assemblages that define the 1.81 Ga metamorphic event. Menard and Gordon (1997) concluded peak metamorphism occurred during the F_2 event, with conditions reaching up to 5 kbar and 550°C (middle amphibolite facies). Peak metamorphism resulted in assemblages including staurolite + garnet + biotite and kyanite + chlorite in altered volcanic rocks (Menard and Gordon, 1997).

2.2.1 VMS deposits in the Snow Lake arc assemblage

Volcanogenic massive sulfide (VMS) deposits occur in the Anderson and Chisel sequences. Cu-Zn-rich deposits occur in the Anderson sequence, while Zn-Cu-rich deposits occur in the Chisel sequence. The primitive arc VMS deposits of the Anderson sequence have distinct sulfide lenses and disconformable alteration zones that are composed mainly of sericite-kyanite-chlorite-rich mineral assemblages. In contrast, the mature arc VMS deposits of the Chisel sequence have flat-lying sulfide lenses and extensive, disconformable alteration zones characterized by metamorphic assemblages of biotite-garnet, chlorite-staurolite, sericite-kyanite, and carbonate (Bailes and Galley, 1996).

The Lalor Zn-Cu-Au deposit is located within the Chisel sequence. The deposit occurs at a depth of approximately 800 m compared to approximately 400 m for other nearby deposits (Chisel, Chisel North, Lost, Ghost). It consists of base metal-rich and gold-rich zones. The gold grades are 1.53 g/t (proven mineral reserves 1 332 000 tonnes; 1.56 g/t probable reserves 11 334 000 tonnes) in the base metal zones and 4.28 g/t (probable reserves 2 530 000 tonnes) in the gold zones (Hudbay website, published January 1, 2014). In comparison, most other deposits in the area have gold grades up to 1.77 g/t (Hudbay unpublished data; Galley et al., 2007). The Chisel area deposits are interpreted to overlie the Powderhouse dacite unit (Figure 2b) at the contact between the Lower and Upper Chisel sequence. The only Au-rich VMS deposit in the Snow Lake camp was Photo Lake. It is a small tonnage, high grade Cu-Au deposit, with gold grades of 4.87 g/t (689 885 tonnes; Galley et al., 2007). As seen in Figure 2, it is hosted in a rhyolite but occurs at the same Upper and Lower Chisel contact (Stewart et al., 2018).

The geology of the Lalor deposit was established in a study by Caté (2016). It is hosted in the 30° ENE dipping Lalor volcanic succession, which is part of the lower Chisel sequence. It is comprised of: 1) Upper Moore mafic unit, 2) “Lalor” Powderhouse dacite, 3) Lalor rhyolite, 4) Moore basalt, and 5) Footwall volcaniclastic unit (Caté, 2016). The Lalor volcanic succession is intruded by mafic, intermediate, and felsic dykes and overlain by steeply dipping Balloch volcanic succession with a 15° NE dipping structural contact. The Balloch volcanic succession at Lalor consists of the Threehouse mafic unit, North Chisel dacite, and Upper Threehouse mafic unit (Caté, 2016).

Chapter 3

3.0 Results

The Lalor deposit is composed of massive to semi-massive base metal sulfide, gold-enriched base metal sulfide and low sulfide gold zones (Figures 5-7). The host rocks are dominantly mafic in composition with intervals of felsic and intermediate volcanic rocks as well as intrusive rocks. In the footwall of the deposit, there is an extensive alteration system that has been metamorphosed and contains calc-silicate to carbonate silicates, Fe-Mg altered rocks, and Ky/Sil-Ms-Bt schists and gneisses. The base metal massive sulfide zones include the 10, 20, 30, and 40 lenses, the massive to semi-massive base metal (Cu-Rich) zones include the 27 and 28 lenses, while the low sulfide gold zones include the 21, 24, 25, and 26 lenses, as illustrated in Figures 5-7. The low-sulfide gold zones are the focus of the thesis.

The observed features of the gold mineralization are presented in three stages: primary rock types and basic geochemical units hosting the gold mineralization; altered rock types associated with gold and base metals areas defined according to their characteristic metamorphic mineral assemblages; and gold associations are described in terms of host rock types, textures, and metal associations. These observations are followed by a discussion of the metamorphic reaction history as it relates to gold mineralization.

3.1 Primary rock types

Much of the Lalor deposit lies within metamorphosed hydrothermally altered rocks. Least altered primary rock types were locally recognized in core from the upper portions of drill holes, within the stratigraphic hanging wall to massive sulfide of the 10 and/or 20 lens ore zones (Figures 5-7). The primary least altered rock types include mafic volcanic rocks with local domains of felsic

and intermediate volcanic rocks with rare occurrences of mafic intrusive rocks (Figure 8a-c). The protolith (felsic, intermediate and mafic) for strongly altered rocks was determined by means of geochemical discrimination diagrams utilizing element ratios of immobile trace elements.

Identifiable, least altered rocks are predominantly volcaniclastic and less commonly coherent volcanic rocks. They range from felsic to mafic in composition, with mafic volcanic rocks the most abundant, followed by rocks of intermediate composition, and felsic volcanic rocks to a lesser extent (Figure 8a-c). The least altered rocks may contain garnet porphyroblasts or small domains with quartz-epidote-rich mineral assemblages. The mineralogy of least altered rocks is typically biotite-hornblende-plagioclase-quartz ± garnet, with variations in modal abundance depending on composition (more plagioclase-quartz in the felsic rocks vs. more biotite-hornblende in the mafic rocks). In the least altered rocks, late buff-coloured carbonate occurs in fractures. This occurs primarily in structural hanging wall rocks.

The least altered rocks occur primarily in the structural hanging wall of the Lalor deposit. Along the 5200N section (Figure 5), they occur at the beginning of the logged sections of the drill holes, but also sporadically within the altered rocks. In the 5400N section (Figure 6), there are less altered rocks at the top of the drill holes and fewer sporadic occurrences within the altered rocks. Along the 5600N section, less altered rocks occur largely on the southwest side of the deposit with localized occurrences within the deeper altered rocks (Figure 7).

The dominant least altered rock types are illustrated in drill hole DUB191 in Figure 9. This drill hole is located along the 5400N section (Figure 6) and contains many of rock types observed in the Lalor deposit and displays the typical succession in which they occur (see discussion of the altered rock types is in the next section). Less altered intermediate volcanic rocks occur near the top of the logged section of DUB191, with short intervals of felsic to mafic

composition rocks (Figure 9). The less altered rocks are sporadic between ~840m-870m and disappear below ~870m in DUB191.

Five units identified using whole rock geochemistry from logged drill holes (Hudbay and JLSL/samples taken for this study) and observations in drill core are: F1, F2, M1, M2, and M3 (Figures 10-17). Initially, the units were identified by samples that grouped/clustered on Zr/TiO_2 versus Nb/Y discriminant plot (using the Winchester and Floyd (1977) diagram) that are based on "alteration resistant" ratios of immobile trace elements. The geochemical groups were further refined using the Primitive Mantle normalized spider diagrams to determine if they had similar overall trace element abundances. Outliers from the Winchester & Floyd (1977) plots were resolved after the initial groups were identified and their spatial context was used to place them into existing units.

F1, F2, and M2 correlate across the three sections (Figures 10-12). M1 is restricted to sections 5200N and 5400N, whereas M3 occurs on sections 5400N and 5600N. Felsic units F1 and F2 plot in the rhyodacite/dacite field of the Winchester and Floyd (1977) diagram. The F1 group forms a cluster in the upper rhyodacite/dacite field (Figure 13) and occurs spatially lower in the footwall of the altered rocks, below the 10, 20, and 21 lenses (Figures 10-12). The F2 unit plots in the lower portion of the rhyodacite/dacite field (Figure 14) and occurs in the altered rocks predominantly in the "middle" of the deposit below the 10 lens (Figures 10-12). Both felsic units have negative Nb and Ti anomalies. There is some variation within this unit along the 5400N section. Due to its spatial occurrence within the deposit and lateral continuity, F2 is considered to be a potential correlative of the Powderhouse dacite unit that typically occurs in the immediate footwall to all VMS deposits located at the Lower-Upper Chisel sequence contact (Stewart et al., 2018).

Based on the Winchester & Floyd (1977) diagram, mafic volcanic rocks are the main host rocks for the Lalor deposit. The mafic volcanic units are subdivided into M1, M2, and M3 on the basis of lithogeochemistry and spatial distribution of main units. M1 plots in the subalkaline basalt field of the Winchester & Floyd (1977) diagram and has a negative Nb anomaly (Figure 15). It occurs on sections 5200N and 5400N, on the SW side of the deposit in the less altered rocks (Figures 10-12). Unit M2 is the most extensive unit in the deposit with less altered to strongly altered varieties (Figures 10-12). There is some variation within M2, but it predominantly clusters in the lower andesite to upper subalkaline basalt fields (Figure 16). The M3 unit occurs on sections 5400N (spatially higher up) and 5600N (spatially lower) as sporadic small intervals (Figures 10-12). It clusters in the middle of the andesite/basalt field (Figure 17). It is separated from M2 based on its distinct cluster on the Winchester & Floyd (1977) diagram and different REE profile (shallower slope than M2 due to generally lower trace element abundances).

3.2 Altered rock types

The Lalor deposit is primarily hosted by altered rocks that are sub-divided into three alteration assemblage associations detailed in Table 2, which include: Ca-Fe-Mg association (Chl-Crb-Tlc-Tr bearing assemblages), Fe-Mg association (Fe-Mg silicate minerals), and K-Al_2SiO_5 association (Ms-Bt-Qz, Bt-Al_2SiO_5, Ms-Al_2SiO_5). Thick quartz veins (>20 cm) occur locally within the altered rocks but are not extensive at the deposit scale, nor do they contain economic mineralization.

The Ca-Fe-Mg association consists of actinolite/tremolite-calcite-chlorite ± diopside ± talc assemblages and actinolite-epidote ± calcite (Figure 8e) that developed within calc-silicate to

carbonate silicate rocks. The dominant assemblage association is Act/Tr-Cc-Chl ± Di ± Tlc, while Act-Ep ± Cc is less common. Calcite in the Act/Tr-Cc-Chl ± Di ± Tlc assemblage association is typically mottled in appearance.

The Fe-Mg association consists of garnet-staurolite-chlorite ± biotite (Grt-St-Chl ± Bt) and anthophyllite-cordierite ± garnet (Ath-Crd ± Grt; Figure 8f). The Fe-Mg assemblage association equates to chlorite-rich VMS alteration (Galley et al., 2007). These assemblages are derived from the chlorite-rich altered Fe-Mg rocks to strongly altered Fe-Mg rocks (anthophyllite-rich and cordierite-rich), with transitional, moderately altered Fe-Mg rocks (containing garnet and staurolite).

The K-Al_2SiO_5 association consists of kyanite/sillimanite-muscovite-biotite (Ky/Sil-Ms-Bt) schists and gneisses (Figure 8g-i). Within this association, the assemblages can be further divided into 1) biotite-muscovite-quartz (Bt-Ms-Qz), 2) biotite-kyanite/sillimanite (Bt-Al_2SiO_5), and 3) muscovite-kyanite/sillimanite (Ms-Al_2SiO_5). These are the metamorphosed equivalent of VMS sericite alteration (Galley et al., 2007).

The spatial distribution of the three alteration assemblage associations varies across the deposit (Figures 5-7). Overall, both alteration intensity and continuity of alteration assemblages increases with depth. In section 5200N, the Fe-Mg association is dominant with intermittent units of K-Al_2SiO_5 alteration and the occurrence of Ca-Fe-Mg alteration on the southwest side of the deposit (Figure 5). The 5400N section shares some similarities with 5200N (Figure 6); however, only two holes logged were on section 5400N. Section 5200N contains more continuous Fe-Mg alteration at depth with sporadic K-Al_2SiO_5 alteration to the northeast, as well as local Ca-Fe-Mg alteration to the southwest. On the 5600N section (Figure 7), the Fe-Mg

association comprises the bulk of the section, with minor occurrences of Ca-Fe-Mg and K-Al_2SiO_5 alteration association.

The graphic log of drill hole DUB191 in Figure 9 is an example of alteration distribution at the Lalor deposit. The Fe-Mg alteration association constitutes a thick interval below 960 m depth as well as in localized intervals from ~860 m to ~880 m. The Ca-Fe-Mg and K-Al_2SiO_5 alteration association occurs intermittently from ~850 m to ~950 m. This is a typical distribution of altered rocks at the Lalor deposit.

3.3 Characterization of gold environments

Gold at the Lalor deposit is associated with massive sulfide and with low (<15%) sulfide zones. Based on core logging observations, petrography and Hudbay assay data, the dominant environments in which gold occurs include massive sulfides, calc-silicate to carbonate silicate rocks, and Fe-Mg altered rocks (Tables 5-6; Figure 20). These gold environments are defined by host rock type (including assemblage association) and mineralization style. Other environments in which gold occurs include: unaltered to weakly altered mafic rocks, Ky/Sil-Ms-Bt schists and gneisses, variable silica-rich rocks (>50% quartz), and plagioclase pegmatite (Tables 5-6; Figure 21). The gold zones at the Lalor deposit delineated by Hudbay are shown in Figures 5-7.

Gold occurs in and proximal to the massive sulfides as electrum (Au and Ag in varying amounts), often in close proximity to hessite (Ag_2Te; Figure 23a). The host massive sulfide consists of euhedral to subhedral pyrite with interstitial sphalerite and chalcopyrite as well as blebby pyrrhotite and galena. Gold occurs in the 10, 20, 30, and 40 massive sulfide lenses (Figures 5-6). In the 10 lens, gold occurs with Cu and Zn, proximal (within 10 metres) to Fe-Mg altered rocks and Ky/Sil-Ms-Bt schists/gneisses as seen in drill holes DUB172, DUB205,

LP0017 (Figure 5) and DUB 191 (Figure 6). Gold mineralization in the 20 lens occurs where it is has been projected by Hudbay to overlap with the 21 gold lens, and proximal to predominantly calc-silicate to carbonate silicate rocks (drill holes DUB204 in Figure 6 and DUB 195 in Figure 7). The 30 and 40 lenses contain Au mineralization proximal to calc-silicate to carbonate silicate rocks (Figures 6-7).

Gold occurs in the calc-silicate to carbonate silicate rocks (Figure 20b) with disseminated to stringer chalcopyrite, disseminated to blebby pyrrhotite, disseminated galena, and the sulfosalts hessite (Ag_2Te), aurostibite ($AuSb_2$), and boulangerite ($Pb_5Sb_4S_{11}$). It also occurs in the footwall of the 10 lens, close to where the 20 lens appears and down-section until the footwall of 40 lens (Figure 5: DUB250, LP0016, LP0017; Figure 6: DUB204; Figure 7). The metamorphic minerals comprising the calc-silicate to carbonate silicate rocks are calcite-tremolite-chlorite ± diopside ± epidote. These rocks can be quite variable in mineral modes, ranging from tremolite-rich to chlorite-rich.

Gold, in Fe-Mg altered rocks (Figure 20c), occurs with disseminated to blebby chalcopyrite and pyrrhotite, disseminated to stringer pyrite and sphalerite, and the sulfosalts petzite (Ag_3AuTe_2), hessite (Ag_2Te), and altaite (PbTe). The metamorphic mineral assemblage association comprising the Fe-Mg altered rocks is garnet-staurolite-chlorite-biotite-anthophyllite-cordierite ± kyanite/sillimanite, with varying degrees of mineralogical differences (i.e. strongly altered Fe-Mg rocks are anthophyllite-cordierite rich and do not contain chlorite). The Fe-Mg altered rocks that contain gold mineralization occur proximal to massive sulfides typically associated with the 10 and 20 lenses (Figure 5-6). Au also occurs in the distal Fe-Mg altered rocks (from approximately 1000-1200m in DUB 191 in Figure 6 and DUB245 and DUB252W01 in Figure 7).

Gold occurs less often (based on assays through intervals of logged drill holes) in the unaltered to weakly altered mafic rocks, Ky/Sil-Ms-Bt schists and gneisses, silica-rich rocks, and plagioclase pegmatite. The unaltered to weakly altered mafic rocks (Figure 21a) contain gold mineralization often contain Pb; these rocks may also contain Cu and/or As. Gold also occurs in an altered mafic volcaniclastic unit in the hanging wall of #10 base metal lens (Figure 5: DUB172, 3-5% sulfides) as well as in base metal lens 20 (Figure 6: DUB204, 2% sulfides; Figure 7: DUB252W01, 2% sulfides). Gold mineralization is also found in a mafic intrusion below the 20-31 base metal lens in LP0016 associated with Cu-Pb-As (Figure 5; 2-3% sulfides).

In the Ky/Sil-Ms-Bt schists and gneisses (Figure 21b), gold occurs with Pb and/or Cu. These rocks, which are found throughout the deposit, are most abundant on its northeast side (Figure 5: DUB205, DUB172; Figure 6: DUB191). The majority of Ky/Sil-Ms-Bt schists and gneisses, however, do not contain Au mineralization. Along the 5200N section, gold occurs in the Ky/Sil-Ms-Bt rocks where they are proximal to10 lens (Figure 5, 5-10% sulfides). Cu is also associated with gold in Ky/Sil-Ms-Bt rocks where massive sulfide is absent (Figure 5, 3-5% sulfides).

Three occurrences of Au mineralization in silica-rich rocks (Figure 21c) were observed, and all are associated with Cu and some with Zn. One is an altered felsic rock and two are quartz-rich, occurring in intervals proximal to massive sulfides (<10 m). The weakly altered felsic rock is strongly foliated and contains biotite, chlorite, quartz veins and gahnite-sulfide stringers (Figure 7: DUB 195, 3% sulfides). Quartz-rich rocks are likely zones of silicification and not original quartz veins as they contain a weak foliation. One of the quartz-rich rocks contains minor biotite (weakly foliated) and sulfides (Figure 5: DUB205, 10% sulfides). The other quartz-rich rock is weakly foliated and contains biotite-pyrite bands with local zones of

sphalerite-chalcopyrite (Figure 6: DUB204, 8% sulfides). One occurrence of Au in a plagioclase pegmatite (Figure 21d; Figure 5: DUB172, 5% sulfides) was observed in association with interstitial biotite and pyrite-galena.

3.3.1 Gold textures

Gold, which was observed in massive sulfides, calc-silicate to carbonate silicate rocks, Fe-Mg altered rocks, and weakly altered mafic rocks, is typically associated with sulfides and sulfosalts. It occurs primarily as electrum and to a lesser extent, in phases such as aurostibite ($AuSb_2$) and petzite (Ag_3AuTe_2). Texturally, gold and gold-bearing minerals occur as discrete inclusions in silicates such as tremolite or sulfides (i.e. pyrite) or along grain boundaries, cleavages and fractures. Gold was identified in 11 of the 18 samples analyzed using the scanning electron microscope (SEM). SEM samples were selected from the different gold environments using assay data to identify those samples with elevated Au concentrations. The results of SEM analysis are summarized in Table 7.

Examples of gold in massive sulfides are shown in Figure 22a-f (samples JLSL-27094 and JLSL-26037). JLSL-26037 is a massive sulfide sample (Po-Py-Cpy-Sph with 7% Act/Tr-Qz-Cc) from the 20 base metal lens in an area overlapping the 21 gold lens (Figure 22a-c). JLSL-27094 is a massive sulfide sample (Aspy-Sph-Po-Py-Cpy with 42% St-Ghn-Bt-Qz) from the 10 base metal lens (Figure 22d-f). The gold in both these samples occurs as electrum in fractures and grain boundaries of sulfides, carbonate, fluorite, and silicates. In JLSL-26037, electrum occurs in contact with sulfides (sphalerite and chalcopyrite) and within fluorite and scapolite (Figure 22b-c). In JLSL-27094, electrum occurs at the contact of sphalerite and arsenopyrite with

biotite and anorthite (Figure 22e-f). Ag occurs in electrum, but it is also present as hessite in JLSL-27094 (Figure 22f).

In a Fe-Mg altered rock (Ghn-Ath-Bt), an electrum inclusion is associated with ilmenite and hessite within a gahnite porphyroblast (Figure 23a; sample JLSL-27090). Gahnite likely formed from the breakdown of sphalerite during prograde to peak metamorphism. In a calc-silicate to carbonate silicate rock (Cc-Chl-Tr), discrete inclusions of aurostibite occur within peak metamorphic tremolite porphyroblasts (Figure 23b; sample JLSL-27056) associated with 19% sulfides (Py-Po-Gal-Cpy). In a weakly altered mafic volcaniclastic rock containing 8% sulfides (Aspy-Cpy-Po-Gal), inclusions of electrum occur within a euhedral and oscillatory zoned anorthite crystal interpreted to be an igneous phenocryst (Figure 23c; sample JLSL-27002).

Gold also occurs along grain boundaries, cleavages, and fractures in calc-silicate to carbonate silicates, Fe-Mg altered rocks, and weakly altered mafic volcanic rocks. There are four examples of gold along fractures and grain boundaries/cleavages in calc-silicate to carbonate silicates: 1) in sample JLSL-26019 (13% Py-Sph-Po-Cpy) electrum occurs with chalcopyrite stringers along cleavages in clinochore (metamorphic chlorite) and in fractures within post-tectonic diopside porphyroblasts (Figure 24a); 2) in sample JLSL-26025 (Anh-Di-Chl-Cal-Ep, 5% Po-Sph-Cpy) electrum occurs with hessite, galena, chalcopyrite, and sphalerite along grain boundaries, fractures and cleavages in carbonate, amphiboles (tremolite-actinolite), and clinopyroxene (esseneite) (Table 7); 3) in sample JLSL-27056 (19% Py-Po-Gal-Cpy, Cc-Chl-Tr) electrum occurs with hessite, galena, and chalcopyrite as disseminated patches and inclusions along the edge of a tremolite grain (Figure 24c); and 4) in sample JLSL-26047 (Chl-Tr-Cc) gold

occurs as petzite along grain boundaries of tremolite, with hessite veinlets, and as aurostibite in a fracture-filling veinlets with hessite and galena within dolomite and tremolite (Table 7).

In a Fe-Mg altered rock (sample JLSL-26079: St-Ath-Grt-Bt gneiss with 7% sulfides (Gal-Py-Cpy-Po)), gold occurs as electrum and petzite and sulfosalts (altaite, PbTe) between grain boundaries of metamorphic biotite (Figure 24b) and as petzite inclusions in pyrite associated with pyrrhotite (Figure 24b).

In the two examples of weakly altered mafic rocks, gold occurs spatially associated with silicate minerals (mainly amphibole). In sample JLSL-27002, which contains 8% sulfides overall (Aspy-Cpy-Po-Gal), gold occurs as electrum with chalcopyrite and galena in fractures and grain boundaries of quartz and actinolite (Figure 24d). In sample JLSL-27181, which contains 8% sulfides overall (Aspy-Cpy-Gal), gold occurs as electrum associated with hessite, arsenopyrite, galena, and pyrite along grain boundaries in amphiboles (Table 7).

3.3.2 Metal associations

As illustrated in Figures 25 to 31, the dominant metal associations for Au at the Lalor deposit are Pb-Au and Cu-Au. In Figure 25, binary plots of Pb vs. Cu at different Au tenor cut-offs indicate Pb-Au and Cu-Au association at gold grades >20 g/t. Lithology data is also included in the symbols to determine if specific rock types are preferential hosts for gold. The host rock type varies overall, but when Au is >20 g/t, there is a Pb-Au association in the mafic volcanic and calc-silicate to carbonate silicate rocks, while there is a Cu-Au association in the Fe-Mg altered rocks.

To further investigate potential Pb-Au and Cu-Au trends, a cutoff grade of 10 000 ppm for Cu and Pb was applied in Figures 26 and 27 respectively, and the figures were further

subdivided by gold tenor (<0.9 g/t, 0.9-5 g/t, 5-10 g/t, 10-20 g/t, and >20 g/t). For comparison and completeness, the gold assays that contained below 10 000 ppm Cu and Pb were plotted in Figure 28. Using the >10 000 ppm Pb, and <10 000 ppm Cu cutoffs, there is a Pb-Au association when Au grades are greater than 5 g/t (Figure 26), but when gold tenor is less than 5 g/t (lower detection limit of Au 0.034 g/t) there is no obvious trend (Figure 28). In the Pb-Au association (Pb >10 000 ppm), Cu concentration is variable from 400-9200 ppm (Figure 26). There is a small cluster when Au is 5-10 g/t, and a weakly positive linear trend when Au is >20 g/t, especially in the mafic rocks (Figure 26). In contrast, using >10 000 ppm Cu and <10 000 Pb pm cutoffs, there is a decrease in the Pb-Au association and an increase in the Cu-Au association as Au tenor increases (Figure 27).

The spatial distribution of the samples within the Cu-Au and Pb-Au groups is illustrated along the three sections in Figures 29-31. Across all three sections, there is a strong spatial correlation of the Pb-Au association with calc-silicate and carbonate silicate rocks. The Cu-Au group occurs throughout the deposit in various rock types, but it is mainly associated with massive sulfides and Fe-Mg altered rocks. The Pb-Au and Cu-Au associations are independent of primary rock type, as groupings are not constrained to any geochemical map units (Figures 29-31).

A subset of samples (using JLSL geochemistry) from the Pb-Au and Cu-Au groups were plotted against a subset of the low-melting point chalcophile elements (LMCE) As, Bi, Hg, Sb, Se, and Te in Figures 32 and 33 (Phillips and Powell, 2010). These elements were chosen as they exhibit similar chemical behavior as gold (Phillips and Powell, 2010). Plots of Pb vs. LMCE in Figure 32 indicate a weak linear trend between Pb-Se, and there is high Sb (over the upper

detection limit) in the presence of Pb. Plots of Cu vs. LMCE in Figure 33 indicate a strong linear trend between Cu-Se, while the other elements are variable with Cu content.

In Figures 34 and 35, Au and Ag are plotted against As, Bi, Hg, Sb, Se, and Te, respectively. Au and Ag display similar trends with weak linear correlations with Se and Te as well as with As and Sb content above the upper detection limits (Figures 34-35). An Ag vs. Au plot yielded no trends, as the Ag content is independent of Au grade.

Chapter 4

4.0 Discussion

The Lalor deposit is a large gold-enriched base metal deposit, which is part of a metamorphically recrystallized VMS system. Metamorphism to high pressure and temperature has formed a variety of middle amphibolite facies mineral assemblages in hydrothermally altered rocks associated with the base metal and gold mineralization. The metamorphic grade affecting the Lalor deposit is high enough for low-temperature sulfide and/or bismuth-telluride melting that elsewhere has been shown to affect gold concentrations, and is also high enough to have produced significant H_2O and CO_2 fluids during dehydration and decarbonation reactions. These processes of low-temperature melting and complicated fluid history during metamorphism necessitates the Lalor gold mineralization be evaluated for the degree to which these processes could have led to Au remobilization and concentration.

The Au-Ag-Cu-Pb-Zn mineralization at the Lalor deposit can be subdivided into two groups – base metal-rich and gold-rich. The base metal lenses are massive to semi massive sulfides that are Zn-Cu-rich and contain minor Pb and Au. The gold zones primarily occur in altered rocks characterized by calc-silicates to carbonate silicate assemblages and Fe-Mg mineral assemblages (Figure 20b-c). Sericite-rich alteration (e.g., Ky/Sil-Ms-Bt assemblages; Figure 21b) does not host significant Au mineralization.

A Pb-Au association occurs in calc-silicate to carbonate silicate rocks (Figures 29-31). The presence of carbonate (in calc-silicates and carbonate silicates) with the Pb-Au association suggests syn-metamorphic remobilization of metals within the deposit.

The Cu-Au association occurs in both massive sulfide and Fe-Mg altered rocks (Figures 29-31), and is interpreted to have developed prior to the main regional metamorphism. This pre-

peak metamorphic Cu-Au association is proximal (within metres) to massive sulfide lenses, and this relationship is commonly related to zone refining during synvolcanic evolution of the VMS system and massive sulfide lenses (Lydon, 1988). Zone refining can also explain Cu-Au associations in Fe-Mg altered rocks that are more distal (>10 m) to the massive sulfide lenses as it could be part of the stockwork of the VMS system. This Cu-Au mineralization is low-sulfide and is found in 'deposit-distal' disseminated to stringer sulfides.

Three mechanisms that could mobilize gold at the Lalor deposit are: 1) mechanical mobilization, 2) mobilization in a melt phase, and 3) mobilization via a fluid phase. These are discussed below.

4.1 Alteration

Three stages of alteration were identified at the Lalor deposit: pre-metamorphic, syn-metamorphic, and post-metamorphic. Pre-metamorphic alteration at Lalor is based on alteration associations that have compositional variations that match those normally attributed to VMS sericite and chlorite alteration (Galley et al., 2007). During metamorphism, sericite altered rocks formed Ky/Sil-Ms-Bt assemblages (Figure 8g-i) and chlorite altered rocks are now expressed as Fe-Mg altered rocks that developed Grt-St-Chl-Bt-Ath-Crd bearing assemblages (Figure 8f) (Tinkham, 2013). Syn-metamorphic alteration represented by the calc-silicate and carbonate silicate assemblages formed in response to the devolatilization of pre-metamorphic carbonate (dolomite in Figure 39) during prograde metamorphism. Post-metamorphic alteration consists of overprinting epidote alteration and buff-coloured carbonate alteration mainly occurring in late crosscutting fractures in the less altered rocks.

4.1.1 Alteration indices

Alteration indices were evaluated to determine alteration trends for the alteration associations. The advanced argillic alteration index (AAAI; Williams and Davidson, 2004), Ishikawa alteration index (AI; Ishikawa et al., 1976), aluminum saturation index (ASI; Zen, 1986), and the chlorite-carbonate pyrite index (CCPI; Large et al., 2001) were all calculated (Table 3) from whole rock geochemical analyses. The JLSL geochemistry samples were separated into two compositional groups (felsic and mafic) prior to evaluation of alteration indices using the Winchester and Floyd (1977) diagram (Figure 18). The least altered samples from the Hudbay dataset (selected from the least altered sections of drill holes logged for this study) were used to compare with the JLSL altered rock geochemistry.

The alteration box plot combines the Ishikawa alteration index and the chlorite-carbonate-pyrite index. The Ishikawa alteration index measures chlorite and sericite alteration, but it cannot discern between the two and it also does not consider carbonate, which can be an important alteration component of VMS deposits. Thus, the CCPI was used to determine the extent of Fe-Mg chlorite alteration and Fe-Mg carbonate, as well as pyrite, all of which are commonly observed in alteration zones proximal to VMS deposits (Large et al., 2001). One major limitation of the alteration box plot is that it does not take into account SiO_2 content. Silica alteration, which can be important in some VMS deposits (Large et al., 2001), was evaluated using the advanced argillic alteration index (AAAI).

In the alteration box plot (Figure 19ab), very few samples from the Lalor deposit plot in the least altered box indicating that most rocks, even the least altered, have seen alteration. One caveat on this is that the alteration box plot is better suited for studies in felsic rocks because many unaltered mafic samples do plot along the “chl-carb” axis (Figure 19ab). The calc-silicate

to carbonate silicate rocks primarily plot along the "chl-carb" axis of the alteration box plot (Figure 19ab). The Fe-Mg altered rocks cluster in the chlorite-pyrite "ore centre" (Large et al., 2001) of the alteration box plot (Figure 19ab). In Figure 19a, there are two samples with a felsic protolith (Ky/Sil-Bt) that plot along the "ser-chl-py" axis. In Figure 19b, there are two samples (Ky-Pl-Bt and Ky-Bt-Ms) with a mafic protolith that plot along the "chl-py-(ser)" and "ser-chl-py" axis.

The advanced argillic alteration index measures the degree of silicification in rocks. At the Lalor deposit, it was important to determine if there was advanced argillic alteration, as this is an important alteration accompanying some Au-rich VMS deposits. An AAAI vs. SiO_2 plot was used to test a subset of samples with high AAAI (>70). The only trend was that SiO_2 increases as AAAI increases, which is to be expected since AAAI is dependent on SiO_2 content. The AAAI vs. AI plot does not show any obvious trends relating AAAI and SiO_2 content. The lack of a silicification/argillic alteration trend is consistent with the lack of mineral assemblages that match those of advanced argillic alteration (i.e., Al_2SiO_5 and quartz). The occurrence of Fe-Mg minerals such as biotite within Lalor deposit assemblages containing Al_2SiO_5 and quartz indicates that these rocks did not undergo advanced argillic alteration (AAAI requires assemblages with very low to absent biotite and sericite content).

The aluminum saturation index (ASI, also commonly referred to as ACNK) was also assessed (Table 3). It is the molar ratio of $Al_2O_3/(CaO+Na_2O+K_2O)$. Feldspars have an ASI of 1. The typical range for unaltered mafic to felsic volcaniclastic rocks is 0.7 to 1.4. The ASI for the weakly altered mafic volcanic rocks is approximately 1 (Table 4). The degree of chlorite alteration can be determined from the cumulative loss of $CaO+Na_2O+K_2O$, which would be reflected in an increase in ASI (if Al_2O_3 is immobile). The calc-silicate to carbonate silicate rocks

generally have a low ASI (< 1) due to higher CaO relative to Al_2O_3 and Na_2O+K_2O (Table 4). In contrast, the FeMg altered rocks predominately have a high ASI (>> 1, ranging from ~ 4-29) since there was a loss of $CaO+Na_2O+K_2O$ relative to Al_2O_3, which confirms strong chlorite alteration (Table 4). The Ky/Sil-Ms-Bt schists/gneisses have moderate ASI values (ranging from ~ 2-8) indicating that they have experienced some sericite alteration but not as much loss of $CaO+Na_2O+K_2O$ as in the FeMg altered rocks (Table 4).

4.2 Metamorphic reaction history

The Snow Lake area, including the Lalor deposit, experienced middle amphibolite facies metamorphism at 1.81 Ga (metamorphic titanite ages, Machado & David, 1992). Froese and Gasparrini (1975) mapped three isograds at Snow Lake based on reactions in pelitic rocks. From south to north, these include: biotite-staurolite, biotite-sillimanite, and biotite-sillimanite-almandine isograds, which separate four metamorphic zones of chlorite-biotite, chlorite-biotite-staurolite, biotite-staurolite-sillimanite, and biotite-sillimanite-almandine (Froese and Gasparrini, 1975). The estimated peak P-T conditions for the Snow Lake arc assemblage are 5 kbar and 550°C, based on thermobarometry studies of a sample from the metamorphosed alteration zones around the Photo Lake deposit, approximately 3 km from the Lalor deposit (Grt + Bt + Pl + Qz + ilmenite + Po + Cpy + Sph + Chl assemblage; Menard & Gordon, 1997). The peak metamorphic assemblages in the altered volcanic rocks at the Photo deposit include staurolite-garnet-biotite and kyanite-chlorite (Menard & Gordon, 1997). At the Lalor deposit, the hydrothermally altered rocks contain the metamorphic mineral associations Sil-Bt ± Ms, Grt-Ath-Crd, and Cc-Tr-Chl ± Di ± Tlc (Table 2). The presence of sillimanite in assemblages suggest

the peak metamorphic temperatures at the Lalor deposit were slightly higher than at the Photo deposit, or that metamorphic pressures were lower.

Sericite altered rocks in the primary VMS system are now represented by kyanite/sillimanite-muscovite-biotite ± staurolite rocks (Figure 36). The peak metamorphic Al_2SiO_5 polymorph is Sil replacing Ky in some rocks (Figure 36c). Staurolite is a prograde mineral and appears to be reacting out to form Ky when it occurs in this assemblage (Figure 36d).

Chlorite alteration associated with the original VMS system has undergone dehydration during metamorphism to form the Fe-Mg assemblages that are now present (Figure 37a). The composition of Fe-Mg-Al chlorite lies between the composition of Fe-Mg cordierite and Fe-Mg orthoamphibole. The formation of the cordierite + anthophyllite association in rocks that are dominated by both phases therefore resulted from the breakdown of chlorite during prograde metamorphism at temperatures below the peak metamorphism. The peak "transitional" Fe-Mg assemblage is Grt-St-Bt-Chl (Figure 37b). The most strongly Fe-Mg altered part of the hydrothermal system has a peak assemblage of Grt-Ath-Crd (Figure 37c).

The calc-silicate to carbonate silicate rocks have an assemblage association of calcite-actinolite/tremolite-chlorite ± talc ± diopside ± epidote. The peak metamorphic assemblages are Cc-Tr-Chl ± Di ± Tlc (Figure 38a-b) and minor Act-Ep (Figure 38c-d). Remnant dolomite, which is also present in altered rocks at the Lalor deposit (Figure 39), is crosscut by peak metamorphic tremolite. Primary dolomite and the lack of quartz present in the same sample indicate that decarbonation reactions (Eqn. 2, Eqn. 3) have likely occurred (Tinkham, 2013).

(Eqn. 2) $5\ \text{dolomite} + 8\ \text{quartz} + H_2O = \text{tremolite} + 3\ \text{calcite} + 7\ CO_2$

(Eqn. 3) $\text{tremolite} + 3\ \text{calcite} + 2\ \text{quartz} = 5\ \text{diopside} + H_2O + 3\ CO_2$

Dehydration of chlorite rich rocks during prograde metamorphism can release H_2O into the system and drive reactions such as Eqn. 2 that require an input of H_2O. The presence of calcic amphibole (actinolite) in very chlorite-rich rocks (Figure 40) suggests that either Fe-Mg alteration did not lead to complete calcium loss, or that a calcium carbonate alteration overprinted intense Fe-Mg altered rocks. Anhydrite also occurs in the rocks, indicating the presence of a S-bearing oxidizing fluid phase present during metamorphism (Figure 41).

4.2.1 Sulfide/metal reactions

The variable occurrence (mineral association, textures, etc.) of gold can be related to potential reactions that occurred during metamorphism. The peak metamorphic P-T conditions of 5 kbar, 550°C (Menard & Gordon, 1997) are conducive to sulfide reactions that could result in mobilizing metals, especially in the presence of sulfosalts and tellurides. Along with galena, these phases can lower the melting temperature of other sulfide minerals (Tomkins et al., 2007).

The main sulfide phases present at Lalor are pyrite, pyrrhotite, chalcopyrite, sphalerite, galena, and arsenopyrite (Figure 42); gold occurs with sulfides such as chalcopyrite and galena. Disseminated to stringer chalcopyrite occurs with Au in a variety of rock types, including massive sulfides and Fe-Mg altered rocks. Galena occurs with Au primarily in the calc-silicates to carbonate silicates. Arsenopyrite occurs locally with Au in primarily unaltered mafic volcanic rocks.

At the Lalor deposit, there is significantly more pyrrhotite than pyrite. It is likely the pyrrhotite is a product of pyrite break down during prograde metamorphism, such as in the desulfidation reaction of Eqn. 4 (Toulmin and Barton, 1964; Craig and Vokes, 1993):

(Eqn. 4) $2\ FeS_2 = 2\ FeS + S_2$

Gold can be mobilized during sulfide/metal reactions, where the desulfidation of pyrite to form pyrrhotite (Eqn. 4) can result in gold complexing with bisulfide (Eqn. 5) (Tomkins, 2007):

(Eqn. 5) $5\ FeS_2 + 2\ Au + 2\ H_2O = 5\ FeS + 2\ Au(HS)_2^- + SO_2$

The gold bisulfide complex can subsequently be mobilized during progressive metamorphism. Alternatively, changes in sulfur fugacity can result in sulfidation of wall rocks that forms chalcopyrite and allows for the deposition of gold.

Gold can also precipitate from a fluid phase during the desulfidation of sphalerite to form the Zn-spinel gahnite as in Eqn. 6 (Figure 43a). For example, electrum inclusions were observed in a gahnite porphyroblast within a Fe-Mg altered rock (Figure 23a).

(Eqn. 6) $ZnS + 2\ Al + 2\ O_2 = ZnAl_2O_4 + ½\ S_2$

Eqn. 6 is a general reaction for sphalerite breaking down to form gahnite. Gahnite often occurs with sphalerite and locally concentrated with sphalerite stringers. Gahnite can also form from the breakdown of staurolite, but at a lesser extent in sulfide-poor rocks (Figure 43b). It can derive Al from staurolite, but typically Al is available from other aluminous phases (chlorite, mica, kyanite, garnet, etc.) and these aluminous minerals can also supply the required O_2.

4.3 Mechanical mobilization

Mechanical mobilization can occur through deformation. Pre-D_1/D_2 structures likely exist at the Lalor deposit, but have been subsequently overprinted by deformation and metamorphism (S_i was observed locally in garnet porphyroblasts). A mafic intrusion that occurs at the base of the 20 & 31 massive sulfide lenses (Figure 5; LP0016) contains gold mineralization. The occurrence of intrusive rocks can introduce gold into a VMS system, but at the Lalor deposit, this Au

association is local and may be a product of ductility differences between a competent least altered intrusion and altered host rocks.

4.4 Mobilization of metals in a melt phase

At the Lalor deposit, sulfide melting is a possible but an unlikely mechanism for mobilization of metals. The coexistence of kyanite and sillimanite indicates that metamorphic conditions have reached at least ~500°C and ~4 kbar. The local presence of sillimanite on its own indicates that P-T conditions may have been higher. Peak metamorphic conditions at the nearby Photo Lake deposit (approximately 5 kbar, 550°C; Menard and Gordon, 1997) indicate that the pressure and temperatures at which pyrite desulfidation can occur to initiate arsenopyrite melting have been met (560°C and 5 kbar; Tomkins et al., 2007). However, arsenopyrite melting is an unlikely mechanism for gold transport at Lalor since arsenopyrite only occurs locally in some rock types: mafic intrusion, altered mafic volcaniclastic rocks, massive sulfide (10 lens), and Cc-Act-Qtz alteration assemblage proximal to calc-silicates and carbonate silicate rocks. The nature of the arsenopyrite mineralization varies within different lithologies and the lack of spatial continuity between them indicates that they are unrelated; however, arsenopyrite melting could have occurred locally. Gold textures at the microscopic scale do not show a common association with arsenopyrite, as they do at some other deposits (e.g. Challenger, Hemlo, Montauban; Tomkins and Mavrogenes, 2002; Tomkins et al., 2004; Tomkins, 2007) where arsenopyrite melting has been proposed.

Galena melting is another possible mechanism but unlikely a significant mechanism for widespread mobilization of gold at the Lalor deposit. Galena is often present within massive sulfides as well as disseminated chalcopyrite and to a lesser extent, disseminated sphalerite.

Galena can lower the melting temperature for other ore minerals (such as sphalerite, and chalcopyrite) within an assemblage (Tomkins et al., 2007). However, the variation in sulfide assemblages suggests that sulfide melting could have occurred only locally. Gold mineralization occurs with low melting point chalcophile elements (Figures 32-35), indicating that it was likely mobilized with these elements.

4.5 Mobilization of metals in a fluid phase

The mobilization of metals in a metamorphic fluid phase at the Lalor deposit is likely, and the evidence that supports this is discussed. Literature often indicates that metamorphism and deformation are concurrent (e.g. Tomkins et al., 2007; Phillips and Powell, 2010), and this is likely to be the situation in the Snow Lake arc assemblage, which underwent metamorphism synchronous with the F_2 event (Menard and Gordon, 1997).

During metamorphism, fluid is released at the greenschist to amphibolite facies transition due to devolatilization reactions. A metamorphic "devolatilization" model has been proposed for the formation of gold-only deposits (Phillips and Powell, 1993, 2010), and although the Lalor deposit is a gold-enriched VMS deposit, some concepts from that model can potentially be applicable to gold mobilization in VMS deposits. Dehydration reactions release H_2O to generate or contribute to an existing fluid phase. Similarly, desulfidation of pyrite can release sulfur into the system, and decarbonation reactions release CO_2. Some of these reactions require H_2O to proceed, which can be sourced from the dehydration of hydrous minerals such as chlorite.

A low salinity fluid is a viable method for the transport of gold and explains the low concentration of other metals such as Pb and Cu (Phillips and Powell, 2010). Gold was likely transported as a sulfur complex as the desulfidation of pyrite to form pyrrhotite (Eqn. 4) releases

sulfur to the fluid phase. The dominant sulfur species in aqueous solutions >250°C and >5 kbar is the trisulfur ion (Pokrovski and Dubrovinsky, 2011), which occurs in magmatic, epithermal and orogenic systems. The S_3^- ion has a high affinity for gold and can selectively extract it from Cu, Zn, and Pb in a fluid phase, forming an $Au(HS)S_3^-$ complex. The trisulfur ion is efficient at concentrating gold, but it is also sensitive to changes that can result in its precipitation, such as lowering temperature can convert S_3^- into sulfate and sulfide. (Pokrovski et al., 2015)

Disseminated to stringer sulfides are typically associated with the presence of gold, indicating that wall rock sulfidation may have played a role in the precipitation of gold. At the Montauban deposit, Tomkins (2007) showed that sulfidation of wall rocks resulted in the gold deposition (Eqn. 7):

(Eqn. 7) $Au(HS)_2^-{}_{(aq)} + Fe,Mg\text{-amphibole} = Au_{(s)} + FeS + Mg\text{-amphibole} + H_2S$

At the Lalor deposit, the diverse metamorphic mineral assemblages indicate a complex fluid evolution. Desulfidation, decarbonation, and dehydration reactions all occurred in the Lalor deposit system and released S_2, CO_2, and H_2O into a fluid phase. The desulfidation of pyrite and sphalerite formed pyrrhotite and gahnite, respectively, and released sulfur into the system. At the Lalor deposit, the required P-T conditions have been met for the trisulfur ion as the dominant sulfur phase in the fluid phase, which is effective at concentrating gold.

Pre-metamorphic carbonate (dolomite, as in Figure 39) experienced decarbonation during prograde metamorphism, resulting in some of the assemblages observed in the calc-silicates to carbonate silicates (Eqn. 2-3) that contain tremolite and calcite (Tinkham, 2013). In these calc-silicate and carbonate silicate rocks, decarbonation reactions contributed CO_2 to the fluid phase to act as a buffer to locally mobilize metals such as gold until it eventually precipitates from the C-O-H-S fluid. Gold occurs in and around peak metamorphic minerals like

tremolite (Figure 24c) and diopside (Figure 24a) in calc-silicate rocks interpreted to have contained carbonate during prograde metamorphism, and carbonate-silicate rocks that still contain carbonate (calcite).

At Lalor, the presence of auriferous phases within the Fe-Mg altered rocks is interpreted to be the result from fluid-assisted sulfidation of wall rocks. Gold mobilization in the Fe-Mg altered rocks, which lack primary carbonate, was likely transported and deposited by a CO_2-free fluid phase, thus the Cu-Au occurrences are more widespread and at overall lower concentrations. Cu associated with the gold mineralization is consistent with limited Cu remobilization as a sulfide complex such as $Cu(HS)^{2-}$during regional metamorphism. The primary Cu-Au enrichment of the Lalor stringer mineralization within Fe-Mg altered rocks accounts for the bulk of the Cu and Au in the footwall Fe-Mg altered rocks. However, in Fe-Mg rocks proximal (within metres) to massive sulfides, both sulfide melting and fluid mobilization locally remobilized and concentrated gold, whereas in Fe-Mg rocks distal (>10 m) to massive sulfides, Cu and Au was remobilized and concentrated by local fluid-dominated transport.

4.6 Timing of gold emplacement and remobilization

Gold at Lalor was initially emplaced by zone refining processes during deposit formation and its primary distribution was locally modified by Au-base metal remobilization during subsequent metamorphism and deformation. Syn-metamorphic Au remobilization into low-sulfide Au zones has resulted in a new “ore type” for the Snow Lake district and may eventually enhance the economic return on the Lalor deposit.

Gold mineralization is observed, at the microscale, as inclusions within peak metamorphic tremolite (Figure 23b) and in gahnite within a Fe-Mg altered rock (Figure 23a),

indicating it was present prior to the final stage of porphyroblast growth. Gold is also found along grain boundaries, fractures, and cleavages of peak metamorphic chlorite, diopside, and biotite (Figure 24ab), indicating that it was at least locally remobilized and emplaced at this scale. In some samples, gold occurs as both inclusions in peak metamorphic porphyroblasts (Figure 23b) and along grain boundaries (Figure 24c).

Gold mineralization in the mafic volcanic rocks is separate from the VMS-forming event. Gold in the mafic volcaniclastic rocks (Figure 23c) is present due to a magmatic input, as inclusions of electrum occur within a euhedral and oscillatory-zoned anorthite (igneous plagioclase). Gold mineralization within the mafic intrusive unit at the base of the 20-31 is also likely from a similar source, as it shares the Cu-Pb-As-Au metal association with the mafic volcaniclastic rocks.

Gold distribution and the Cu-Au association within the massive sulfides are more likely related to zone refining processes (Lydon et al., 1986). The preferential association of Pb-Au in calc-silicates and carbonate silicates, and Cu-Au in massive sulfides and Fe-Mg altered rocks suggest the Au distribution is more constrained by alteration assemblages and that a single process, such as sulfide melting, is an unlikely mechanism for to explain Au distribution.

Chapter 5

5.0 Conclusions

1. At the Lalor deposit, gold mineralization occurs in massive sulfides, calc-silicates to carbonate silicates, and Fe-Mg altered rocks. In the massive sulfides, gold content and its distribution are dominantly a function of primary VMS zone refining processes with only local and minor Au remobilization during metamorphism. In calc-silicates to carbonate silicate rocks, gold mineralization has been concentrated primarily through syn-metamorphic remobilization processes. In the Fe-Mg altered rocks proximal to massive sulfides, the distribution and tenor of Au reflects primary zone refining in a VMS system with local remobilization during metamorphism and deformation. Gold in Fe-Mg altered rocks distal to massive sulfide is largely a product of local metamorphic remobilization of primary VMS stringer gold via fluid-dominated transportation.

2. The two dominant metal associations of gold mineralization are Cu-Au and Pb-Au. The Cu-Au association is volumetrically greater, more significant and occurs in a variety of rock types. The Pb-Au association occurs primarily in altered rocks characterized by calc-silicates to carbonate silicate. The Pb-Au association is considered to be a product of a syn-metamorphic remobilization of gold by a fluid phase.

3. Gold mineralization occurs primarily as electrum. It also occurs as sulfosalt phases (ie. aurostibite, petzite). Texturally, gold occurs along fractures, grain boundaries, and cleavages, and to a lesser extent, as discrete inclusions.

4. Metamorphic devolatilization is responsible for adding components such as H_2O, CO_2 and S_2 into a fluid phase that remobilized Au and some metals (e.g. Cu, Pb) locally in the Lalor deposit. This occurs in altered rocks located proximal and distal to the massive sulfide lenses. Gold was mobilized and transported as a sulfur complex, with CO_2 acting as a buffer for a low salinity fluid phase such that it could maintain an elevated gold content for transport and deposition. The result of this mobilization is clearly responsible for the Pb-Au association in calc-silicate to carbonate silicate altered rocks.

References

Ashton, K.E., Lewry, J.F., Heaman, L.M., Hartlaub, R.P., Stauffer, M.R. and Tran, H.T. 2005: The Pelican Thrust Zone: basal detachment between the Archaean Sask Craton and Palaeoproterozoic Flin Flon–Glennie Complex, western Trans-Hudson Orogen. Canadian Journal Of Earth Sciences, 42: 685-706.

Bailes, A.H. 2012: Preliminary Report on the Stratigraphic and Structural Controls on Mineralization at the Lalor Lake mine, Internal report for HudBay Minerals Limited; 50p.

Bailes, A.H. and Galley, A.G. 1996: Setting of Paleoproterozoic volcanic-hosted massive sulphide deposits, Snow Lake; in EXTECH I, A multidisciplinary approach to massive sulphide research: Rusty Lake-Snow Lake greenstone belt, Manitoba, (ed.) G.F. Bonham-Carter, A.G. Galley and G.E.M. Hall: Geological Survey of Canada Bulletin, 426, 105-138.

Bailes, A. H., and Galley, A.G. 1999: Evolution of the Paleoproterozoic Snow Lake arc assemblage and geodynamic setting for associated volcanic-hosted massive sulphide 88 deposits, Flin Flon Belt, Manitoba, Canada: Canadian Journal of Earth Sciences, 36, 1789-1805.

Bailes, A.H. and Galley, A.G. 2007: Geology of the Chisel–Anderson lakes area, Snow Lake, Manitoba (NTS areas 63K16SW and west half of 63J13SE); Manitoba Science, Technology, Energy and Mines, Manitoba Geological Survey, MAP Geoscientific map 2007-1, 1 colour map with accompanying notes. scale 1:20 000.

Bailes, A.H., Galley, A.G., Paradis, S. and Taylor, B.T. 2016: Variations in Large Synvolcanic Alteration Zones at Snow Lake, Manitoba, Canada, with Proximity to Associated VMS Deposits; Economic Geology, v.111, pp. 933-962.

Bailes, A.H., Gordon, T.M., and Hunt, P.A., 1988, U-Pb geochronology of the Richard Lake tonalite, a possible synvolcanic pluton in the Snow Lake area: Manitoba Energy and Mines, Minerals Division, 1998 Report of Field Activities, p. 63–65.

Bailes, A.H., Hunt, P.A., and Gordon, T.M., 1991, U-Pb zircon dating of possible synvolcanic plutons in the Flin Flon belt at Snow Lake, Manitoba: Geological Survey of Canada, Radiogenic age and isotopic studies, Report 4, p. 35–43.

Basu, K., Bortnikov, N.S., Mookherjee, A., Mozgova, N.N. and Tsepin, A.I. 1981: Rare minerals from Rajpura-Dariba, Rajasthan, India. II. Intermetallic compound $Ag_{74.2}Au_{16.4}Hg_{9.4}$. Neue Jahrburch fur Mineralogie and Petrologie Abh, 141: 217-223.

Basu, K., Bortnikov, N.S., Mookherjee, A., Mozgova, N.N., Tsepin, A.I. and Vyalsov, L.N. 1983: Rare minerals from Rajpura-Dariba, Rajasthan, India. IV. A new Pb-Ag-Tl-Sb sulphosalt, rayite. Neus Jahrbuch fur Mineralogie and Petrologie, Monatsheft, H.7: 296-304.

Caté, A. 2016: Geology of the Paleoproterozoic Zn-Cu-Au Lalor volcanogenic massive sulphide deposit and its gold-rich lenses, Snow Lake, Manitoba. Ph.D. thesis, Institut national de la recherche scientifique, Université du Québec, Québec, Que. 430 pp.

Caté, A., Mercier-Langevin, P., Ross, P.-S., and Simms, D. 2014. Structural controls on geometry and ore distribution in the Lalor auriferous VMS deposit, Snow Lake, west-central Manitoba (part of NTS 63K16): preliminary results from underground mapping. Report of activities 2014. Manitoba Mineral Resources, Manitoba Geological Survey. pp. 104–155.

Connors, K.A., Ansdell, K.M. and Lucas, S.B. 1999: Coeval sedimentation, magmatism and fold-thrust development in the Trans-Hudson Orogen: propogation of deformation into an active continental arc setting, Wekusko Lake area, Manitoba; Canadian Journal of Earth Sciences, v. 36. no. 11, p. 275-291.

Cook, N.J. 1996: Mineralogy of the sulphide deposits at Sulitjelma, northern Norway. Ore Geology Reviews, 11: 303-338.

Corrigan, D., Pehrsson, S., Wodicka, N. and de Kemp, E. 2009: The Palaeoproterozoic Trans-Hudson Orogen: a prototype of modern accretionary processes. Geological Society, London, Special Publications, 327, 457-479.

Craig, J.R. and Vokes, F.M. 1993: The metamorphism of pyrite and pyritic ores: an overview. Mineralogical Magazine, 57: 3-18.

David, J., Bailes, A.H. and Machado, N. 1996: Evolution of the Snow Lake portion of the Paleoproterozoic Flin Flon and Kisseynew belts, Trans-Hudson Orogen, Manitoba, Canada; Precambrian Research, 80, 107-124.

Dubé, B., Gosselin, P., Mercier-Langevin, P., Hannington, M., Galley, A. 2007a: Gold-rich volcanogenic massive sulphide deposits. In Goodfellow WD (ed) Mineral deposits of Canada: a synthesis of major deposit-types, disctict metallogeny, the evolution of geological provinces, and exploration methods, Geological Association of Canada, Mineral Deposits Division, Special Publication 5, pp 75–94.

Froese, E. and Gasparrini, E. 1975: Metamorphic Zones in the Snow Lake area, Manitoba. Canadian Mineralogist 13: 162-167.

Frost, B.R., Mavrogenes, J.A. and Tomkins, A.G. 2002: Partial melting of sulfide ore deposits during medium- and high-grade metamorphism. Canadian Mineralogist 40: 1-18.

Galley, A.G., Syme, E.C., and Bailes, A.H., 2007, Metallogeny of the Paleoproterozoic Flin Flon Belt, Manitoba and Saskatchewan, in Goodfellow, W.D., ed., Mineral Deposits of Canada: A Synthesis of Major Deposit Types, District Metallogeny, the Evolution of Geological Provinces, and Exploration Methods: Geological Association of Canada, Mineral Deposits Division, Special Publication No. 5, p. 509-531.

Gibson, H.L., Allen, R.L., Riverin, G. and Lane, T. E. 2007: The VMS Model: Advances and Application to Exploration Targeting. In "Proceedings of Exploration 07: Fifth Decennial International Conference on Mineral Exploration" edited by B. Milkereit, p. 713-730.

Hofmann, B.A. 1994: Formation of a sulfide melt during Alpine metamorphism of the Lengenbach polymetallic sulfide mineralization, Binntal, Switzerland. Mineralium Deposita, 29: 439-442.

Hudbay Minerals: Our Business - Our Development - Lalor. Accessed 29 August 2014.

Ishikawa, Y., Sawaguchi, T., Iwaya, S., and Horiuchi, M. 1976: Delineation of prospecting targets for Kuroko deposits based on modes of volcanism of underlying dacite and alteration halos. Mining Geology, 26: 105–117 (in Japanese with English abs.).

Krause, J. and Williams, P.F. 1999: Structural development of the Snow Lake allochthon and its role in the evolution of the southeastern Trans-Hudson Orogen in Manitoba, central Canada; Canadian Journal of Earth Sciences, v. 36. no. 11, p. 1881–1899.

Kretz, R. (1983): Symbols of rock-forming minerals. American Mineralogist, 68, 277–279.

Lewry, J.F. and Collerson, K.D. 1990: The Trans-Hudson Orogen: extent, subdivisions and problems. In: Lewry, J.F. and Stauffer, M.R. (eds) The Early Proterozoic Trans-Hudson Orogen of North America. Geological Association of Canada, Special Paper, 37, 1–14.

Lucas, S.B., Stern, R.A. and Syme, E.C. 1996: Flin Flon greenstone belt: intraoceanic tectonics and the development of continental crust (1.92-1.84 Ga); Geological Society of America Bulletin, 108, 602-629.
Lydon, J.W., 1984: Volcanogenic massive sulphide deposits, Part 1--A descriptive model: Geoscience Canada, v. 11, p. 195-202.
Lydon, J.W., 1988: Volcanogenic massive sulfide deposits, II: Genetic models. Geoscience Canada, vol.15, p. 43-65.
Marshall, B., Vokes, F.M. and Larocque, A.C.L. 2000: Regional metamorphic remobilization: upgrading and formation of ore deposits. In Spry, P.G., Marshall, B. and Vokes, F.M. (eds) Metamorphosed and metamorphogenic ore deposits. Reviews in Economic Geology, v. 11, p. 19-38.
Machado, N. and David, J. 1992: Geochronology of the Reindeer-Superior transition zone and of the Snow Lake area: preliminary results; in Lithoprobe Trans-Hudson Orogen Transect Workshop No. 2, Report No. 26, p. 40-42.
Menard, T. and Gordon, T.M. 1995: Syntectonic alteration of VMS deposits, Snow Lake, Manitoba. Manitoba Energy & Mines, Rep. Activities 1995, 164-167.
Menard, T. and Gordon, T.M. 1997: Metamorphic P-T paths from the eastern Flin Flon Belt and Kisseynew Domain, Snow Lake, Manitoba. The Canadian Mineralogist, 35: 1093-1115.
Mercier-Langevin, P., Hannington, M.D., Dube, B., Becu, V. 2011: The gold content of volcanogenic massive sulfide deposits. Miner Deposita, 46: 509-539.
Phillips, G.N. and Evans, K.A. 2004: Role of CO_2 in the formation of gold deposits. Nature, 429: 860–863.
Phillips, G.N. and Powell, R. 1993: Link between gold provinces. Economic Geology, 88: 1084–1098.
Phillips, G.N. and Powell, R. 2010: Formation of gold deposits: a metamorphic devolatilization model. Journal of Metamorphic Geology, 28: 689–718.
Pokrovski, G.S. and Dubrovinsky, L.S. 2011: The S_3^- ion is stable in geological fluids at elevated temperatures and pressures. Science, 331: 1052–1054.
Pokrovski, G.S. & Dubessy, J. 2015: Stability and abundance of the trisulfur radical ion S_3^- in hydrothermal fluids. Earth and Planetary Science Letters, 411: 298-309.
Pokrovski G.S., Kokh M.A., Guillaume D., Borisova A.Y., Gisquet P., Hazemann J.L., Lahera E., Del Net W., Proux O., Testemale D., Haigis V., Jonchière R., Seitsonen A.P., Ferlat G., Vuilleumier R., Saitta A.M., Boiron M.C., and Dubessy J. 2015: Sulfur radical species form gold deposits on Earth. Proceedings of the National Academy of Sciences 112 (44): 13484-13489.
Puddephatt, R.J. 1978: The Chemistry of Gold. Elsevier, Amsterdam.
Stern, R.A., Machado, N., Syme, E.C., Lucas, S.B., and David, J. 1999: Chronology of crustal growth and recycling in the Paleoproterozoic Amisk collage (Flin Flon Belt), Trans-Hudson Orogen (Canada). Canadian Journal of Earth Sciences, 36: 1807–1827.
Stewart, M.S., Lafrance, B., Gibson, H.L. 2018: Early thrusting and folding in the Snow Lake camp, Manitoba: tectonic implications and effects on volcanogenic massive sulfide deposits. Canadian Journal of Earth Sciences, 55: 935-957.
Syme, E.C. 1995: 1.9 Ga arc and ocean floor assemblages and their bounding structures in the central Flin Flon Belt; LITHOPROBE Trans-Hudson Orogen Transect, Report of Fifth Transect Meeting, Regina, Saskatchewan, April 3-4, 1995, LITHOPROBE Secretariat, University of British Columbia, Report 48, p. 261-272.

Syme, E.C., Lucas, S.B., Bailes, A.H., and Stern, R.A. 1999: Contrasting arc and MORB-like assemblages in the Paleoproterozoic Flin Flon Belt, Manitoba, and the role of intra-arc extension in localizing volcanic-hosted massive sulphide deposits. Canadian Journal of Earth Sciences, 36: 1767-1788.

Tinkham, D.K. 2013: A model for metamorphic devolatilization in the Lalor deposit alteration system, Snow Lake, MB. Abstract from GAC-MAC 2013 in Winnipeg, MB.

Tomkins, A.G. 2007: Three mechanisms of ore re-mobilisation during amphibolite facies metamorphism at the Montauban Zn-Pb-Au-Ag deposit. Miner Deposita, 42: 627-637.

Tomkins, A.G., Frost, B.R. and Pattison, D.R.M. 2006: Arsenopyrite melting during metamorphism of sulfide ore deposits. Canadian Mineralogist, 44: 1325-1342.

Tomkins, A.G. and Mavrogenes J.A. 2002: Mobilization of gold as a polymetallic melt during pelite anatexis at the Challenger gold deposit, South Australia: a metamorphosed Archean deposit. Economic Geology, 97: 1249-1271.

Tomkins, A.G., Pattison, D.R.M and Frost, B.R. 2007: On the initiation of metamorphic sulfide anatexis. Journal of Petrology, v. 48, No. 3, p. 511-535.

Tomkins, A.G., Pattison D.R.M., and Zaleski, E. 2004: The Hemlo gold deposit, Ontario: an example of melting and mobilization of a precious metal–sulfosalt assemblage during amphibolite facies metamorphism and deformation. Economic Geology, 99: 1063-1084.

Toulmin, P. and Barton, P.B. 1964: A thermodynamic study of pyrite and pyrrhotite. Geochimica et Cosmochimica Acta, 56: 227-243.

Williams, N.C. and Davidson, G.J. 2004: Possible submarine advanced argillic alteration at the Basin Lake prospect, Western Tasmania, Australia. Economic Geology, 99 (5): 987-1002.

Winchester, J.A. and Floyd, P.A. (1977) Geochemical discrimination of different magma series and their differentiation product using immobile elements. Chemical Geology, 20: 325-343.

Zen, E. 1986: Aluminum enrichment in silicate melts by fractional crystallization: Some mineralogic and petrographic constraints. Journal of Petrology, 27 (5): 1095-1117.

Tables

Table 1: Mineral abbreviations used in this thesis (modified from Kretz, 1983)

Mineral	Abbreviation
Actinolite	Act
Albite	Ab
Amphibole	Amph
Anhydrite	Anh
Ankerite	Ank
Anthophyllite	Ath
Anorthite	An
Arsenopyrite	Aspy
Biotite	Bt
Calcite	Cc
Carbonate	Crb
Chalcopyrite	Cpy
Chlorite	Chl
Cordierite	Crd
Diopside	Di
Dolomite	Dol
Epidote	Ep
Gahnite	Ghn
Galena	Gal
Garnet	Grt
Hornblende	Hbl, Hb
Kyanite	Ky
Magnetite	Mt
Muscovite	Ms
Plagioclase	Pl
Pyrite	Py
Pyrrhotite	Po
Quartz	Qz
Sillimanite	Sil
Sphalerite	Sph
Staurolite	St
Talc	Tlc
Tremolite	Tr

Table 2: Mineral assemblages observed at the Lalor deposit

Assemblage	Prograde	Peak	Retrograde
Calc-silicates to carbonate silicates			
Ep-Act ± Qz ± Cc ± Anh ± Bt ± Chl ± Di ± Ghn	x	x	
Tlc-Chl ± Bt ± Ath	x		
Tlc-Act/Tr-Cc-Chl ± Bt ± Mt ± Di ± Ms ± Ghn	x	x	
Bt-Act/Tr ± Chl ± Qz ± Crd ± Cc ± Ghn ± Ms ± Ath ± St	x		
Act/Tr-Chl ± Qz ± Tlc ± Ky/Crd ± Grs/St ± Anh ± Ghn		x	
Act/Tr-Cc ± Qz ± Di		x	
Act/Tr-Cc-Chl ± Qz ± Di		x	
Fe-Mg altered rocks			
Chl ± Bt ± Cc	x		
Bt ± Grt ± St ± Ms ± Sil ± Act ± Ghn	x		
Ath-Crd ± Ghn ± Bt ± Ky/Sil ± Grt ± St		x	
Crd ± Grt ± St ± Bt ± Ms ± Ky ± Tlc	x		
Ath ± Grt ± St ± Bt ± Chl ± Ms ± Ky ± Tlc ± Ghn ± Mt	x		
Chl-Ath-Crd ± Bt ± St ± Grt ± Ms ± Ky/Sil ± Ghn ± Mt	x		x
Chl ± Grt ± St ± Bt ± Ms ± Ky/Sil ± Tlc	x		x
Ky/Sil-Ms-Bt schists & gneisses			
Ms-Bt ± Crd ± Ghn ± Act/Tr			
Bt ± Chl ± Grt ± Ghn ± St ± Ky			
Sil-Ms-Bt ± Qz ± Grt ± St ± Crd ± Chl		x	
Ky-Ms-Bt ± Qz ± Ath ± Grt	x		
Ky/Sil-Bt-Ms ± Qz ± St ± Chl ± Grt	x		x
Ky/Sil-Bt ± Chl ± St ± Ghn ± Grt ± Ath ± Crd			x
Ky-Bt ± Qz ± St ± Grt ± Chl	x		x
Sil-Bt ± Qz ± St ± Ghn		x	

Table 3: VMS alteration indices

Alteration index	Abbreviation	Equation
advanced argillic alteration index (Williams and Davidson, 2004)	AAAI	$\frac{100\ (SiO_2)}{SiO_2 + 10\ MgO + 10\ CaO + 10\ Na_2O}$
Ishikawa alteration index (Ishikawa et al., 1976)	AI	$\frac{100\ (K_2O + MgO)}{K_2O + MgO + Na_2O + CaO}$
aluminum saturation index (Zen, 1986)	ASI	$\frac{Al_2O_3}{Na_2O + K_2O + CaO}$
chlorite-carbonate-pyrite index (Large et al., 2001)	CCPI	$\frac{100\ (FeO + MgO)}{MgO + FeO + Na_2O + K_2O}$

Table 4: Alteration indices (Purple: weakly altered mafic volcaniclastics, Green: Calc-silicate to carbonate silicates, Orange: FeMg altered rocks, Blue: Ky/Sil-Ms-Bt schists/gneisses)

DDH	Depth	Sample ID	SiO_2	Al_2O_3	$Fe_2O_3(t)$	MgO	CaO	Na2O	K2O	AAAI	AI	ASI	CCPI
DUB191	1153.55	JLSL-26002	43.38	8.53	15.65	7.30	0.27	0.04	0.06	36.31	95.96	23.05	99.57
DUB226W02	977.41	JLSL-26019	25.77	14.84	11.92	23.34	5.84	0.01	0.01	8.11	79.98	2.54	99.97
DUB195	816.61	JLSL-26035	76.29	4.24	6.61	2.73	1.05	0.10	0.26	66.29	72.22	3.01	96.29
DUB195	819.27	JLSL-26036	44.49	17.88	17.92	3.44	1.03	0.66	0.67	46.45	70.86	7.58	94.14
DUB195	823.2	JLSL-26037	5.49	0.51	31.91	0.29	6.72	0.01	0.01	7.25	4.20	0.08	99.95
LP0029	56.14	JLSL-26039	11.83	6.59	2.91	23.11	21.81	0.01	0.01	2.57	51.44	0.30	99.94
LP0029	70.1	JLSL-26040	22.88	3.56	10.60	6.12	32.13	0.02	0.01	5.64	16.00	0.11	99.85
LP0029	138.07	JLSL-26047	10.74	0.72	3.75	19.07	27.82	0.04	0.01	2.24	40.64	0.03	99.80
DUB252W01	1024.21	JLSL-26066	38.47	14.19	13.65	8.55	12.50	0.23	0.07	15.31	40.37	1.11	98.67
DUB252W01	1079.88	JLSL-26079	48.72	18.68	15.79	10.66	0.99	0.18	0.90	29.17	90.81	9.02	96.08
DUB252W01	1140.67	JLSL-26086	37.64	4.04	32.95	2.47	3.51	0.20	0.43	37.85	43.87	0.98	98.25
DUB252W01	1147.29	JLSL-26089	47.98	16.05	17.84	14.90	0.65	0.18	0.16	23.37	94.78	16.21	98.97
DUB252W01	1169.82	JLSL-26093	77.19	7.44	8.41	5.05	0.14	0.07	0.04	59.47	96.04	29.76	99.19
DUB172	909.08	JLSL-27003	50.59	13.95	15.04	6.34	6.37	1.26	0.21	26.59	46.19	1.78	93.57
DUB172	928.15	JLSL-27007	46.22	19.27	11.19	2.41	5.16	5.16	1.06	26.64	25.16	1.69	68.62
DUB204	849.06	JLSL-27046	86.30	3.59	4.36	3.33	1.29	0.04	0.20	64.94	72.63	2.35	96.97
DUB204	875.32	JLSL-27056	36.97	4.18	3.92	19.74	18.14	0.13	0.02	8.86	51.96	0.23	99.37
DUB204	844.3	JLSL-27057	52.73	13.07	9.80	6.29	12.23	0.31	0.06	21.88	33.62	1.04	97.75
DUB204	963.3	JLSL-27069	45.10	13.71	7.66	9.47	10.91	1.29	0.09	17.23	43.93	1.12	92.54
DUB204	971.1	JLSL-27073	43.48	14.91	10.42	10.58	12.44	0.57	0.11	15.56	45.11	1.14	96.86
LP0008	4.28	JLSL-27078	33.28	21.52	16.53	8.86	2.48	1.12	4.53	21.08	78.81	2.65	81.80
LP0008	61.36	JLSL-27085	59.28	15.23	10.43	2.41	0.68	0.34	3.72	63.35	85.73	3.21	75.98
LP0008	93.91	JLSL-27089	22.36	18.61	23.23	18.12	1.25	0.07	0.19	10.32	93.28	12.32	99.38
LP0008	105.06	JLSL-27090	25.14	21.58	19.76	12.20	0.38	0.73	1.50	15.89	92.51	8.27	93.48
LP0008	106.52	JLSL-27091	32.86	21.28	29.74	2.35	0.26	0.05	0.74	55.26	90.88	20.27	97.60
LP0008	109.96	JLSL-27092	56.58	19.09	8.92	2.66	7.83	0.66	2.04	33.66	35.63	1.81	81.09
LP0008	111.67	JLSL-27093	80.73	9.32	4.05	0.80	1.79	0.28	0.47	73.77	38.02	3.67	86.61
LP0008	113.17	JLSL-27094	15.01	8.09	39.36	1.63	0.97	0.08	0.63	35.90	68.28	4.82	98.30
LP0008	121.1	JLSL-27097	17.64	10.53	31.40	4.32	0.26	0.14	1.47	27.21	93.54	5.63	95.69
DUB205	804	JLSL-27103	83.39	1.35	6.48	0.72	0.21	0.01	0.43	89.87	83.94	2.08	94.24
DUB250	677.04	JLSL-27118	54.00	15.33	16.15	4.40	3.35	1.46	0.60	36.96	50.97	2.83	90.89
DUB250	712.67	JLSL-27122	45.07	15.86	8.50	4.14	20.52	0.08	0.02	15.41	16.80	0.77	99.22
DUB250	827.25	JLSL-27126	53.08	1.60	2.85	18.00	19.99	0.14	0.03	12.22	47.25	0.08	99.19
DUB250	889.86	JLSL-27132	35.60	16.13	13.25	20.95	3.37	0.08	0.03	12.73	85.88	4.64	99.68
DUB250	896.3	JLSL-27133a	28.01	18.83	14.85	20.29	1.56	0.08	0.02	11.33	92.53	11.34	99.67
DUB250	896.3	JLSL-27133b	49.54	16.23	11.82	15.11	1.94	0.12	0.51	22.39	88.35	6.32	97.56
DUB250	975.35	JLSL-27135	70.69	13.73	6.46	4.05	0.21	0.10	2.53	61.85	95.50	4.83	79.98
DUB250	905.4	JLSL-27140	76.74	7.01	4.51	7.98	1.20	0.08	0.33	45.32	86.65	4.35	96.66
DUB250	904.32	JLSL-27141	45.23	9.21	9.40	14.61	10.87	0.16	0.03	15.00	57.03	0.83	99.21
LP0017	12.65	JLSL-27142	38.96	14.56	10.33	4.26	25.26	0.42	0.06	11.51	14.40	0.57	96.81
LP0017	84.83	JLSL-27148	19.54	6.75	39.87	1.60	0.24	0.05	0.43	50.83	87.50	9.38	98.86
LP0016	137.65	JLSL-27179	22.60	2.09	18.25	2.65	2.45	0.03	0.02	30.58	51.84	0.84	99.76
LP0016	145.24	JLSL-27181	39.91	13.84	8.75	9.91	14.06	1.22	0.28	13.68	40.01	0.89	92.56
DUB191	879.67	JLSL-27190	31.09	19.02	18.53	7.11	8.24	0.59	1.42	16.32	49.14	1.86	92.73
DUB191	1001.43	JLSL-27199	64.75	10.48	11.00	9.72	0.31	0.05	1.21	39.11	96.81	6.68	94.27
DUB191	762.07	JLSL13-004	53.33	14.25	15.70	4.23	6.67	2.27	0.52	28.82	34.70	1.51	87.72
DUB226W06	886.06	JLSL13-017	51.78	3.77	19.12	2.93	2.18	0.04	0.03	50.14	57.14	1.68	99.68
DUB226W06	901.45	JLSL13-020	37.88	1.59	39.28	1.06	2.35	0.02	0.04	52.48	31.70	0.66	99.85
DUB226W06	902.22	JLSL13-021	43.23	16.10	13.17	13.17	4.49	0.13	0.07	19.55	74.13	3.43	99.25
DUB191	1032.84	JLSL13-034	79.91	10.84	2.74	2.38	0.13	0.17	2.32	74.89	94.00	4.14	67.28
DUB172	1088.2	JLSL13-043	51.40	14.24	11.50	9.05	0.32	0.06	0.37	35.28	96.12	18.99	97.95
DUB195	881.45	JLSL13-044	45.77	19.81	10.58	6.07	14.84	1.33	0.08	17.07	27.55	1.22	92.19
DUB245	995.95	JLSL13-081	59.16	11.67	11.38	15.11	0.66	0.05	0.05	27.22	95.53	15.36	99.62
DUB245	1078.31	JLSL13-089	58.29	8.75	16.37	7.70	0.27	0.04	0.04	42.12	96.15	25.00	99.67
DUB245	1146.21	JLSL13-090	50.82	7.93	21.57	7.21	0.46	0.04	0.16	39.73	93.65	12.02	99.31

Table 5: Gold occurrences in rock types by Au tenor, by meter (as per assays), and by percentage in each group (using data from logged drill core).

	Au >2 g/t		Au >5 g/t		Au >10 g/t		Au >15 g/t		Au >20 g/t	
Lithology	*Metres*	*%*	*Metres*	*%*	*Metres*	*%*	*Metres*	*%*	*Metres*	*%*
Felsic volcanics	1	0.43	0	0	0	0	0	0	0	0
Intermediate volcanics	14.32	6.16	11.99	9.67	7.38	10.56	5.34	12.89	2.93	10.49
Mafic volcanics	20.26	8.72	12.48	10.07	10.45	14.95	4.86	11.73	4.76	17.04
Sulfide-rich rocks	27.4	11.79	15.7	12.66	7.63	10.91	3.12	7.53	2	7.16
Calc-silicates/carbonate silicates	47	20.22	21.08	17	9.31	13.32	5.99	14.46	3.22	11.53
Fe-Mg altered rocks	78.34	33.7	36.7	29.6	18.71	26.76	11.97	28.89	7.94	28.43
Ms-Bt-Qz rocks	30.97	13.32	18.44	14.87	12.34	17.65	7.93	19.14	4.86	17.4
Ky/Sil-Bt-Qz rocks	6.22	2.68	3.91	3.15	1	1.43	1	2.41	1	3.58
Ky/Sil-Ms-Qz rocks	6.92	2.98	3.68	2.97	3.09	4.42	1.22	2.94	1.22	4.37
Total	232.43	100	123.98	99.99	69.91	100	41.43	99.99	27.93	100

Table 6: Characterization of gold occurrences at the Lalor deposit

Environment	Assemblage	Protolith	Mineralogy	Mineralization Style	How Au occurs	Location (lenses)	Range of Cu (ppm)	Range of Zn (ppm)	Range of Pb (ppm)
Massive sulfide	Gal-Po-Cpy-Sph-Py	N/A	Qz, Crb, Ghn	Euhedral-subhedral Py, interstitial Sph & Cpy, blebby Po & Gal	In fractures: electrum with hessite	10, 20, 30, 40	600-91800	300-372300	0-75400
Calc-silicate to carbonate silicate	Cc-Act/Tr-Chl ±Di±Ep	varies	Cc, Act/Tr, Chl, Di, Ep	Disseminated-stringer Cpy, disseminated-blebby Po, disseminated Gal	In fractures & as inclusions: electrum & aurostibite with hessite, boulangerite	HW10, 20, 21, 24, 25, 26, 30, 40	0-53200	0-243600	0-129200
Fe-Mg altered rocks	Grt-St-Chl-Bt-Ath-Crd±Ky/Sil	varies	Grt, St, Chl, Bt, Ath, Crd, Ky/Sil	Disseminated-blebby Cpy & Po, disseminated-stringer Py & Sph	In fractures: electrum & petzite with hessite, altaite	10, 20, 21, 25, 26, 27, 28, HW40	0-94500	0-282300	0-26300
Mafic rocks	Bt-Pl/Qz-Act/Hbl±Grt	N/A	Bt, Pl/Qz, Act/Hbl, Grt	Disseminated Cpy, Aspy, Gal	Electrum as inclusions & in fractures	HW10, FW20, HW21	200-7000	0-235100	0-30000
Ky/Sil-Ms-Bt	Ky/Sil-Ms-Bt-Qz	varies	Ky/Sil, Ms, Bt, St	Varies (Py, Cpy, Gal; loc Sph, Po)	Cu-Au	FW10, 20, 21, 25	0-131100	0-315300	0-22800
Silica-rich rocks	varies, but mainly Qz	N/A	Qz & misc.	Blebby Cpy, banded Py & Sph	Cu-Au	FW10, 20/21	N/A	N/A	N/A
Plagioclase pegmatite	Bt-Qz-Pl	N/A	Bt, Qz, Pl	Interstitial Py-Gal	Pb-Au	HW10	500-3500	298-600	800-37100

Table 7: Summary of SEM analyses

Sample	Rock type	Au?	Summary
JLSL-26019	Calc-Crb	Yes	*May 9/13:* bogdanovite, petzite, altaite, diss Gal; electrum associated w/ sulfides in silicates; Ag in Cpy-Po, Crb, silicates
JLSL-26025	Calc-Crb	Yes	*May 1/13:* Au in Cpy; Ag in Cpy-Po, Tr; Gal w/ hessite, electrum, Au *May 9/13:* Electrum, hessite, altaite, Gal, Cpy, Sph along fractures/planes of weakness of silicates
JLSL-26037	Sulfide-rich	Yes	*May 9/13:* Aspy, Cpy, electrum, Crb in fluorite, Gal, Py; altaite with Cpy, Sph, in Po; electrum in silicates
JLSL-26047	Calc-Crb	Yes	*Oct 10/14:* hessite & petzite; Py, Cpy, Aspy, Gal-Po; in Cc-Dol, Tr *Oct 31/14:* hessite & aurostibite in Gal vein in Dol with proximal Tr/Act; gudmundite also present (FeSbS)
JLSL-26069	Calc-Crb	No	*Oct 10/14:* Ag with Gal, Cpy, Sph, Po in Dol-dominantly Tr
JLSL-26079	Fe-Mg	Yes	*May 9/13:* Au with hessite in Po-Py; hessite & electrum inclusion in Po grain; hessite-electrum vein around Qz-apatite; mucho PbTe (altaite), electrum, hessite together along cleavage planes
JLSL-27002	Mafic	Yes	*May 9/13:* Se-Gal, Cpy, Ag, Gal; amphibole-plagioclase matrix *Feb 24/14:* Au with Ag, Cpy, Gal, Aspy and apatite; discrete electrum inclusions in anorthite & proximal to apatite *Oct 31/14:* Act/Hbl & Fe-Ti oxides in Qz & albite-anorthite
JLSL-27007A	Plag peg	No	*Apr 25/13:* Py, Po, Gal, Cpy, Aspy in albite, Cc; Ag in veins with Cc
JLSL-27008	Fe-Mg	No	*May 1/13:* hessite in Cpy, Po in Ath-Chl; Gal veins
JLSL-27037	Mafic	No	*Feb 12/14:* diss Py, Po, Cpy; Gal immiscible texture w/ freibergite
JLSL-27056	Calc-Crb	Yes	*Apr 25/13:* Au, Ag-Te, Cpy, sulfosalts with amphiboles *May 1/13:* Gal, Cpy, hessite veins in fractures, and aurostibite; in Chl-Crb-Tr
JLSL-27057	Mafic	No	*Feb 12/14:* Gal w/ Aspy at edges, Cpy, Po, Sph, Ag-tetrahedrite, meneghinite in fractures/cleavages; in Act/Hbl, Bt, Qz
JLSL-27090	Fe-Mg	Yes	*Feb 12/13:* Cpy, Sph, Gal & Ag with Ghn, amphibole (likely Ath) *Feb 13/13:* Cpy, Po, Ag-Te with Ghn & monzanite *May 1/13:* hessite in Po in Cpy in amphibole; hessite & Gal inclusions in Ghn; electrum & hessite in fractures w/ Gal, Cpy & ilmenite in Ghn
JLSL-27093	Ky/Sil-Bt	No	*Feb 13/13:* Py, Gal, Aspy, Cpy, Po in Qz matrix; interstitial Ag-Te
JLSL-27094	Sulfide-rich	Yes	*Feb 13/13:* Ag-tellurides & Py in fractures; Au associated with Aspy & Sph; Au, Ag with Qz & blebby Cpy; Sph & Au-Ag splays in fractured epidote; massive sulfide associated gold
JLSL-27103	Silica-rich	Yes	*May 9/13:* Gal, Cpy, Sph, hessite; acanthite and electrum within Qz, Bt fractures; primarily Ag-tellurides
JLSL-27181	Mafic	Yes	*Feb 13/13:* Gal, Aspy, Cpy, Ag-Te, Ag with calcic amphiboles Feb 24/14: Lots of Gal; Au-Ag associated w/ Gal+Se; hessite with Gal; Aspy+Py+Gal w/ electrum grain; in Crb & Ca-amph matrix
JLSL-27199	Fe-Mg	No	*Oct 31/14:* Cpy, Sph, Po in Qz, Crd, Ghn, St, with Ath

Figures

Figure 1: Regional geology of the Paleoproterozoic Flin Flon belt, with the Snow Lake assemblage located at its eastern end (red box) (Syme et al., 1995; Bailes and Galley, 2007).

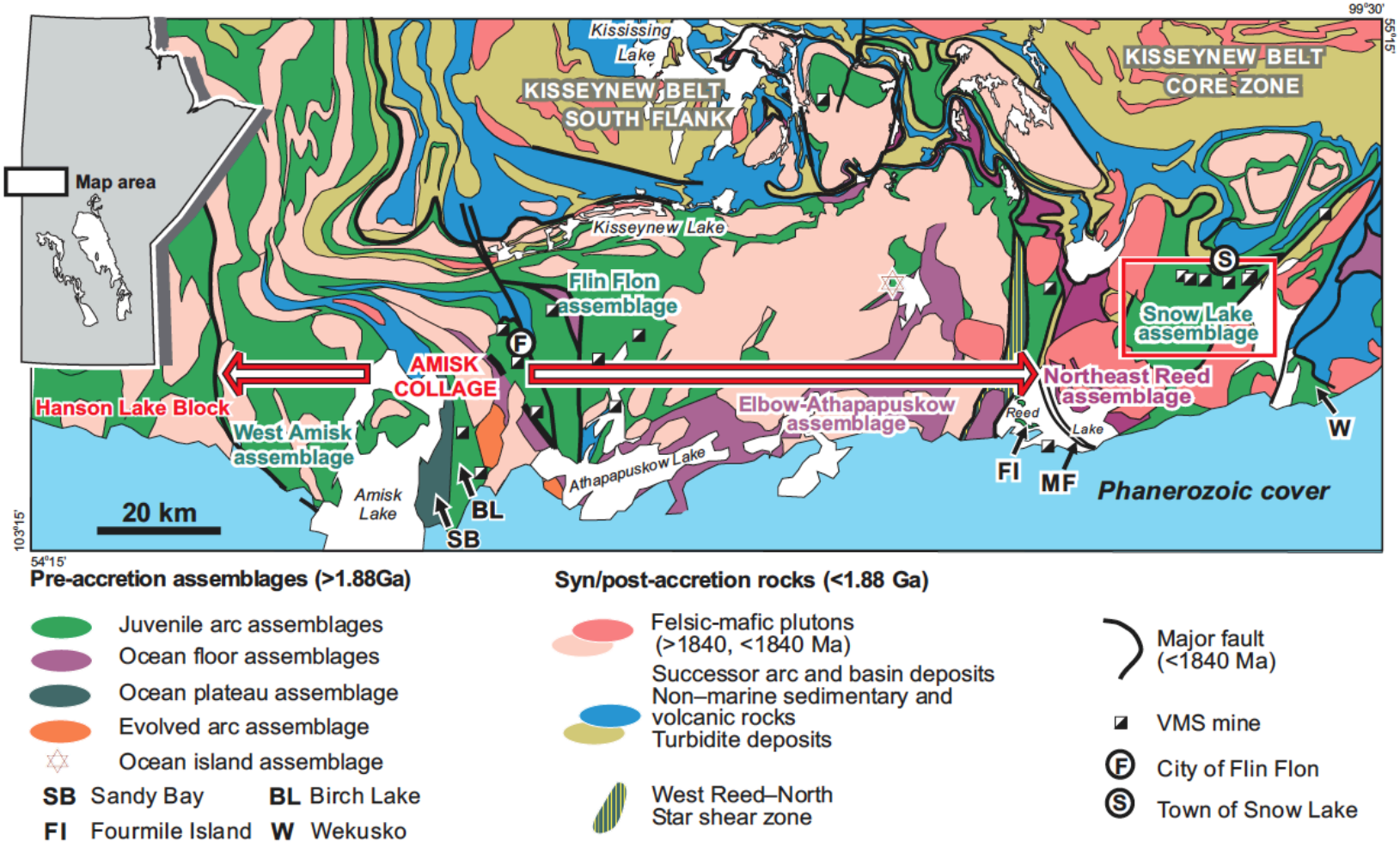

Figure 2: a) Local simplified assemblage map of the Snow Lake arc and b) Idealized cross section of the Snow Lake arc assemblage (Bailes et al., 2016).

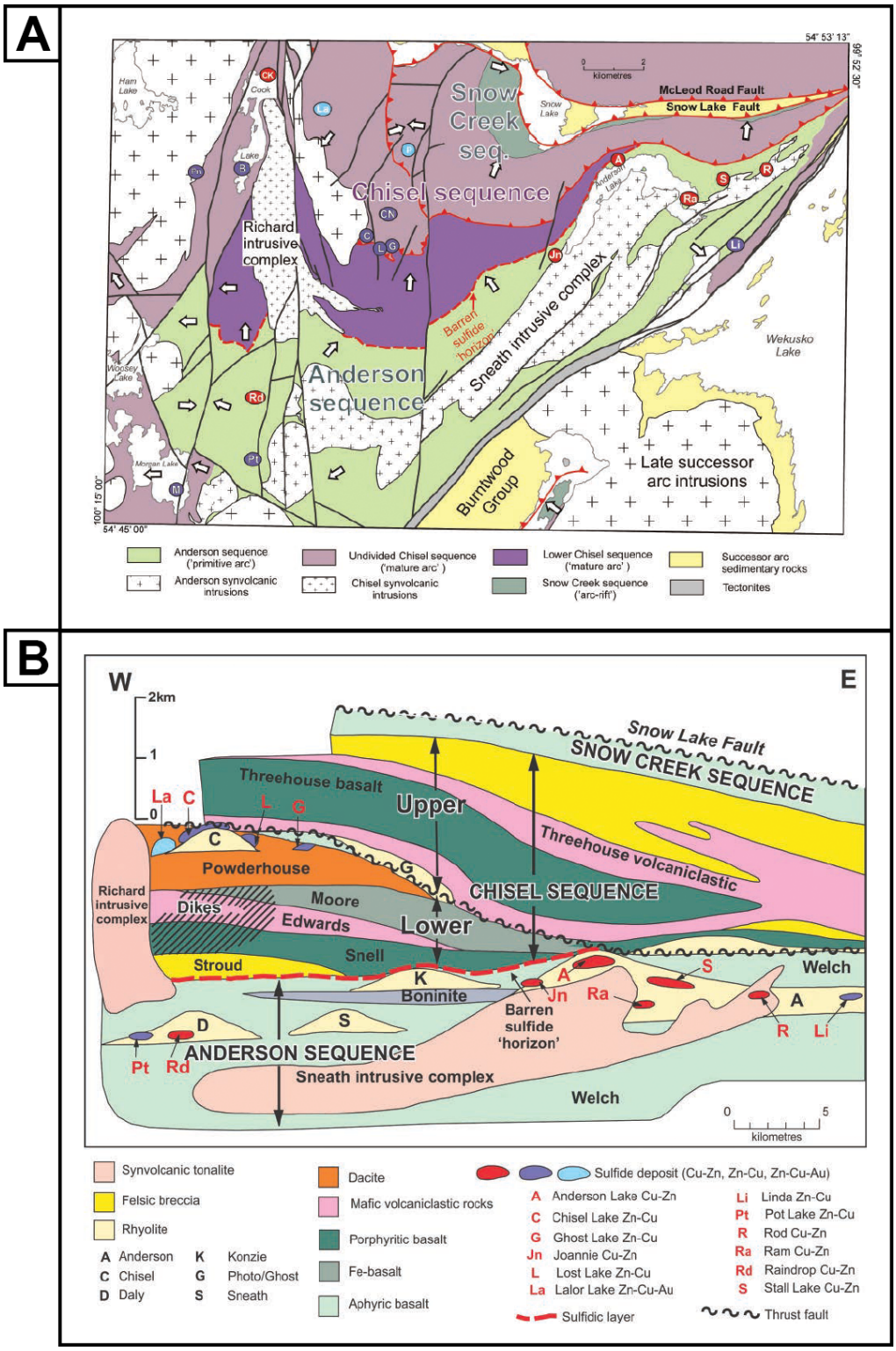

Figure 3: Models of a VMS deposit, showing (A) the metal distribution (Modified from Gibson, 2005) and (B) the associated hydrothermal system (Modified from Franklin, 1996; Franklin et al., 2005).

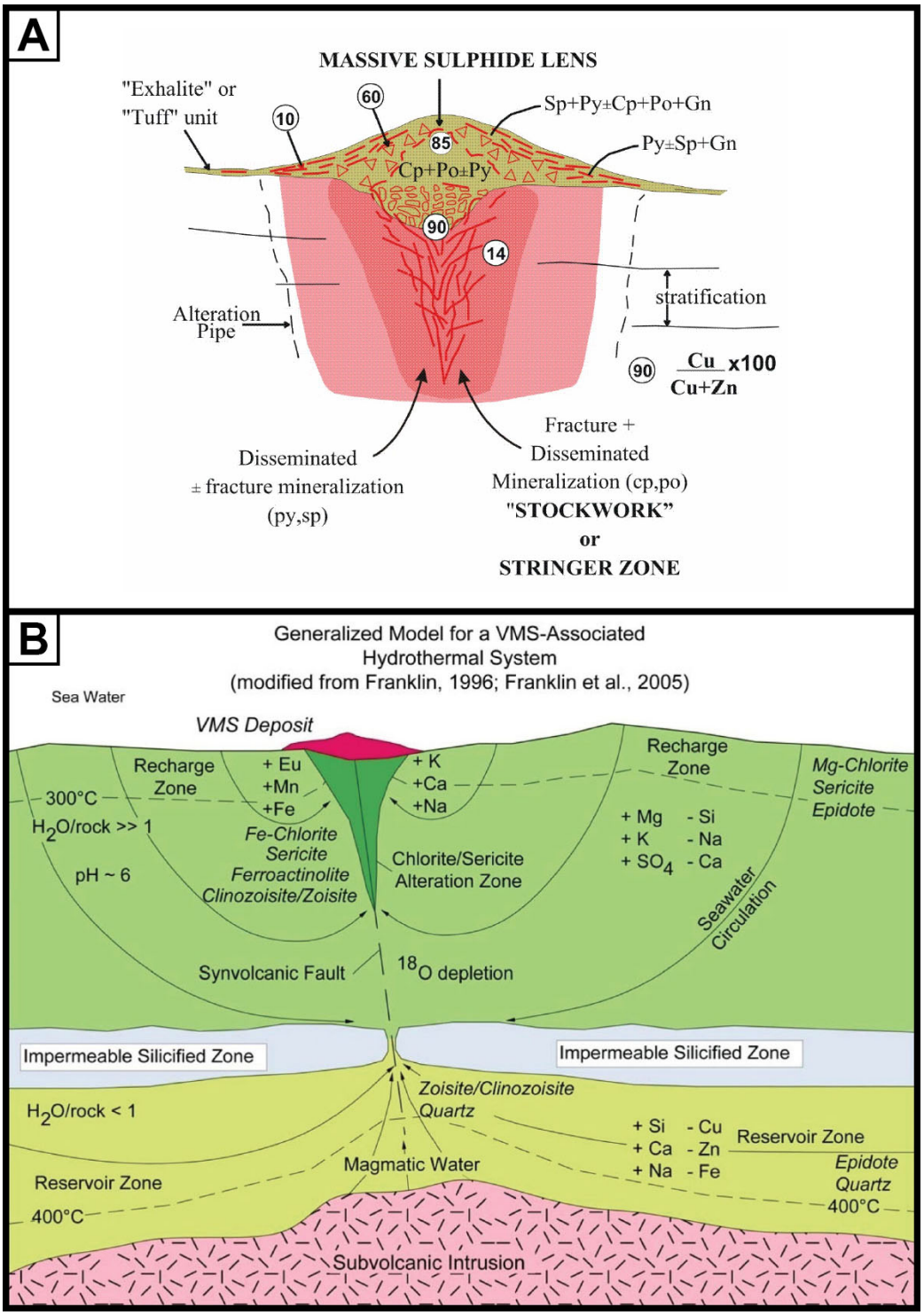

Figure 4: Plan map of the Lalor deposit and sections 5600N, 5400N, 5200N (highlighted in blue) where logging was completed, with surface projections of drill hole traces (underground drill holes omitted) and ore lenses (10 lens in pink, 20 lens in green, 21 lens in orange).

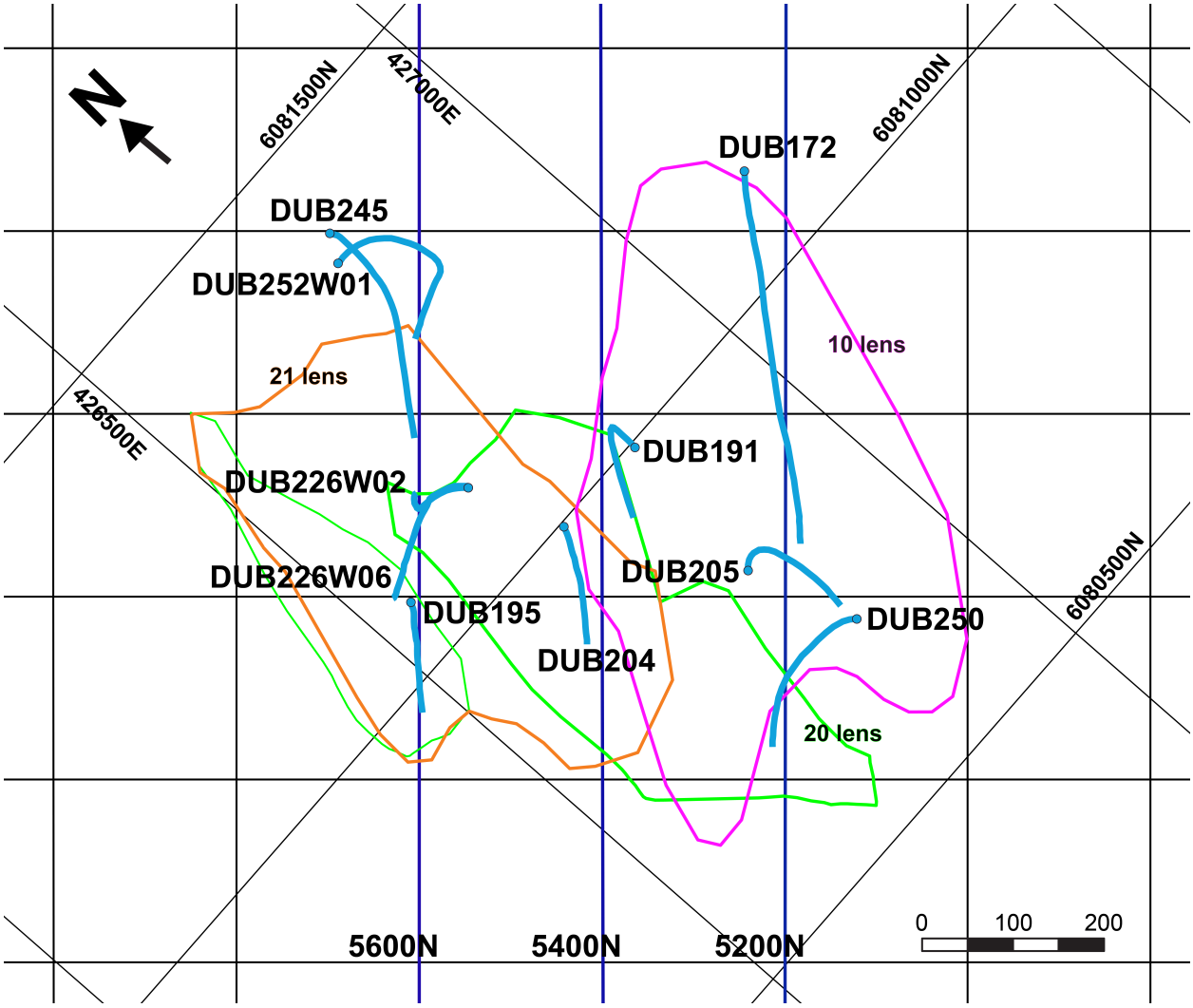

Figure 5: 5200N section with logged drill holes (graphic logs superimposed onto drill hole traces) and ore lenses illustrating the distribution of the different rock types and assemblage associations. (LP0008 is shown as a dashed line since it is ~50 m off section.)

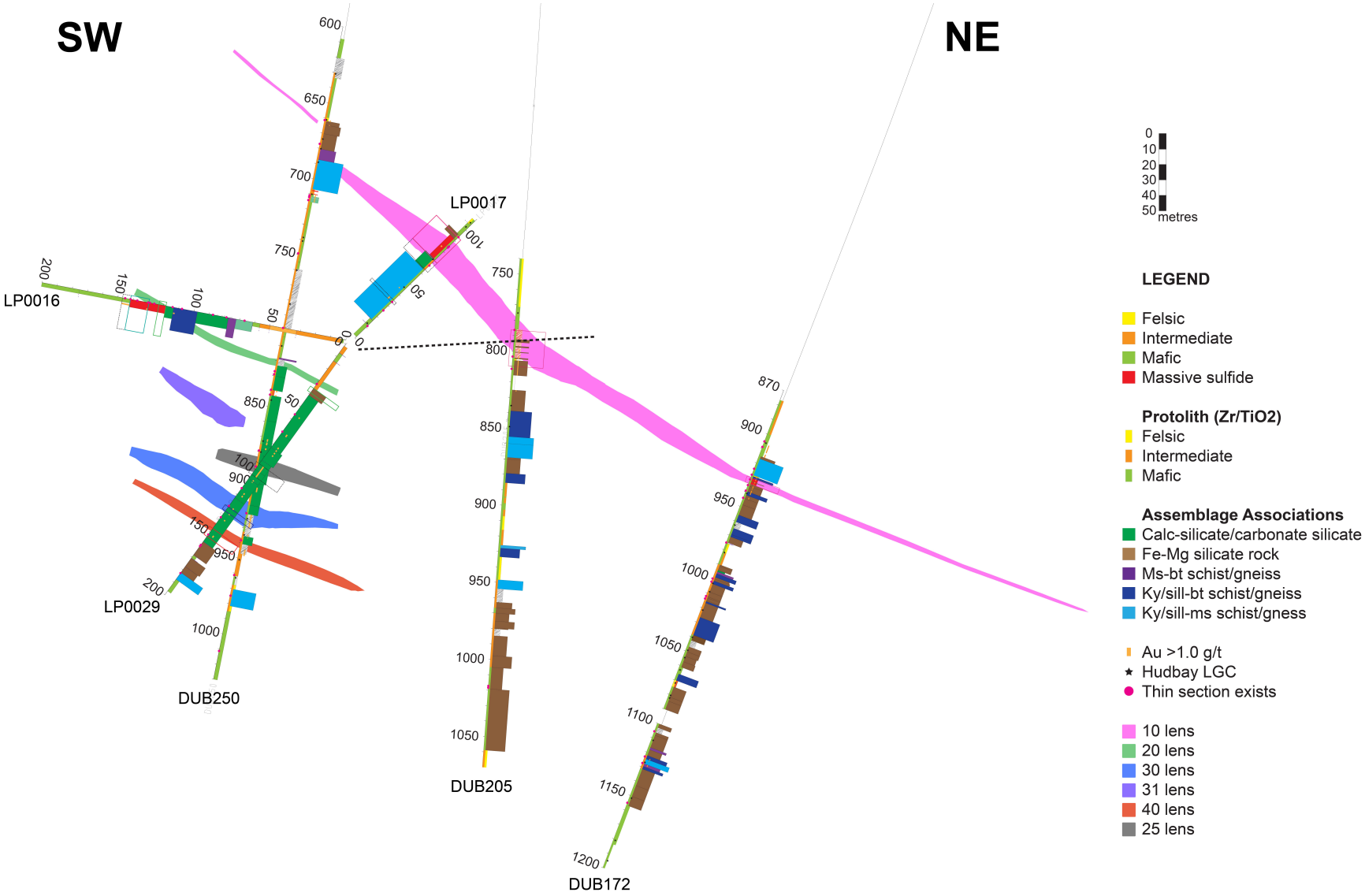

Figure 6: 5400N section with logged drill holes (graphic logs superimposed onto drill hole traces) and ore lenses illustrating the distribution of the different rock types and assemblage associations.

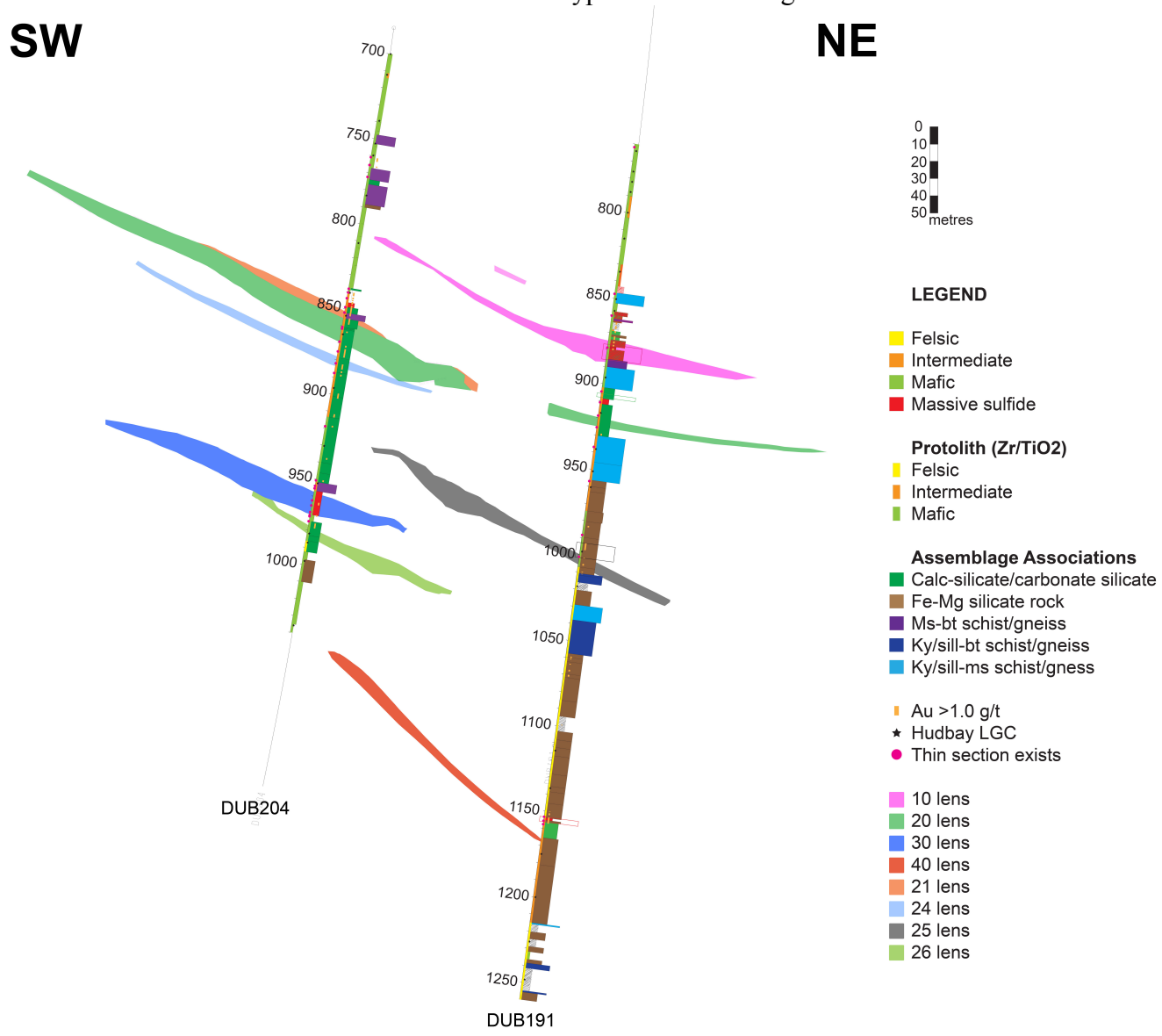

Figure 7: 5600N section with logged drill holes (graphic logs superimposed onto drill hole traces) and ore lenses illustrating the distribution of the different rock types and assemblage associations.

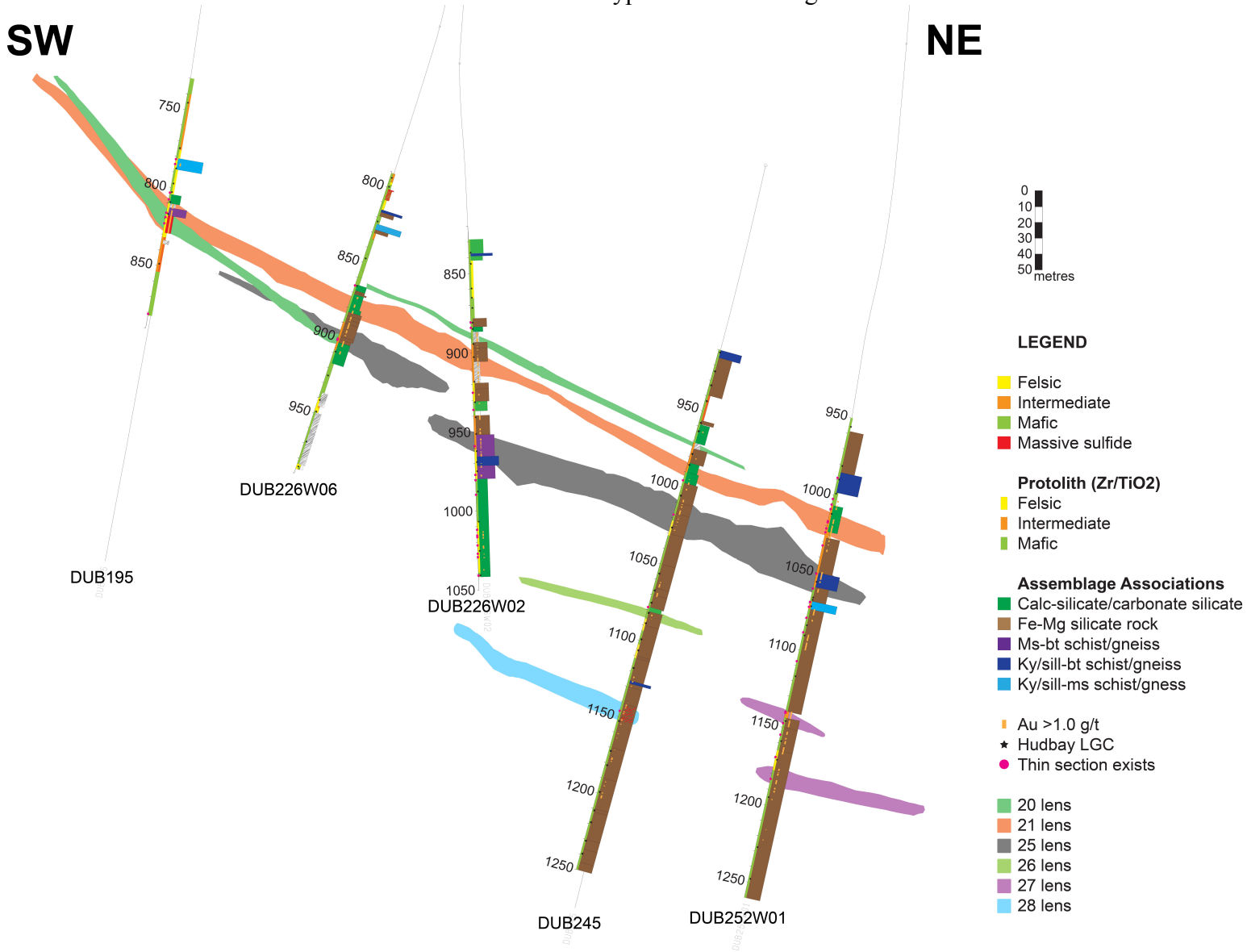

Figure 8: Examples of rock types observed at the Lalor deposit, as shown in graphic logs: A) Felsic volcanic: Grt-Hb-Bt-Pl/Qz in LP0008 ~7.25-13.25 m, B) Intermediate volcanic: sample JLSL-27167 of Grt-Bt-Amph from LP0016 ~41m, C) Mafic volcanic: sample JLSL-27181 of Aspy-Cc-Act from LP0016 ~145m, D) Sulfide-rich: sample JLSL-27179 of Py-Sph-Cc from LP0016 ~137 m, E) Chl-Crb-Tlc-Tr: sample JLSL-27174 of Cc-Chl from LP0016 ~87 m, F) Fe-Mg: sample JLSL-26090 of Grt-Bt-Crd-Chl from DUB252W01 ~1155m, G) Bt-Ms-Qz: Bt-Qz with Cpy-Sph-Py in DUB 204 ~855 m, H) Bt-Al_2SiO_5: sample JLSL-27175 of Py-Sil-Bt-Qz from LP0016 ~108 m, and I) Ms-Al_2SiO_5: JLSL-27085 of Py-Ky-Bt-Ms from LP0008 ~61 m.

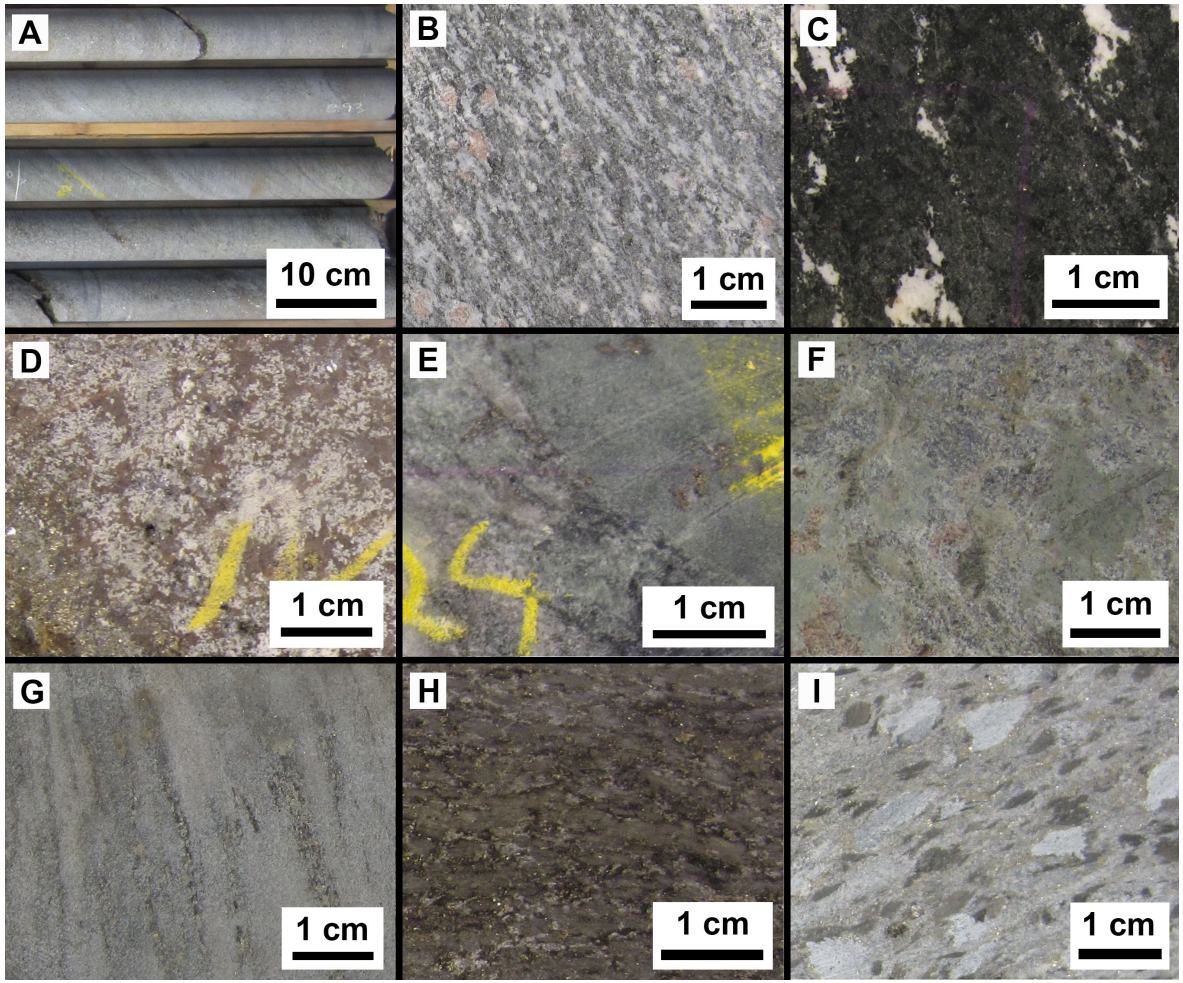

Figure 9: Example of a graphic log used to capture data in this study; DUB191 from the 5400N section. Not shown to scale (originally 1:500). The lithology is logged as an assemblage association (different widths and colours to represent each one), or primary rock type if less altered and able to discern protolith. The sum of alteration mineralogy indicates the "strength" of alteration, while the percentage of alteration minerals is recorded for continuity and level of alteration between units. The general name of each unit is noted in the Notes section.

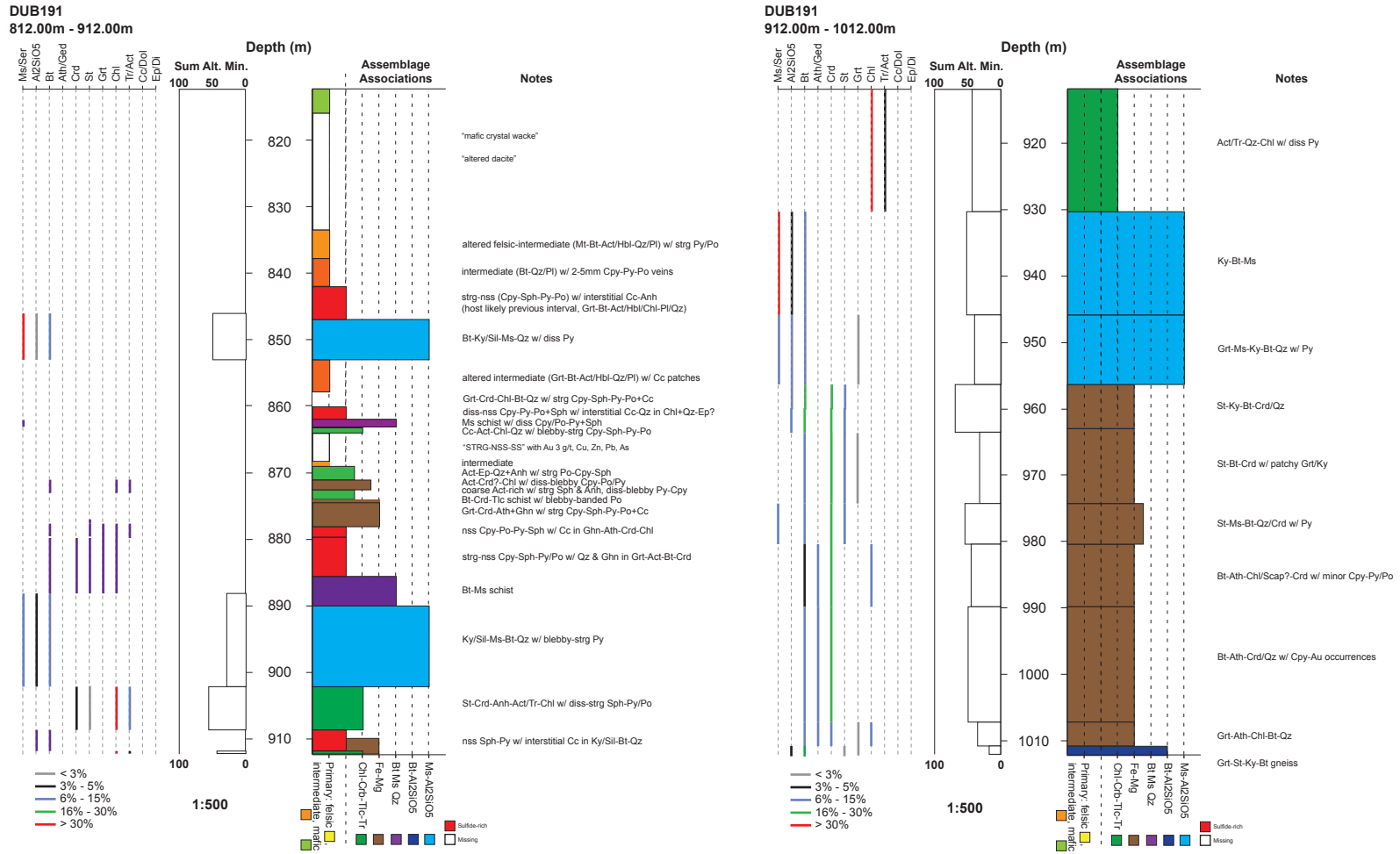

Figure 10: Cross section along 5200N showing geochemical map units delineated using geochemistry from logged drill holes. Outline of ore lenses are also shown.

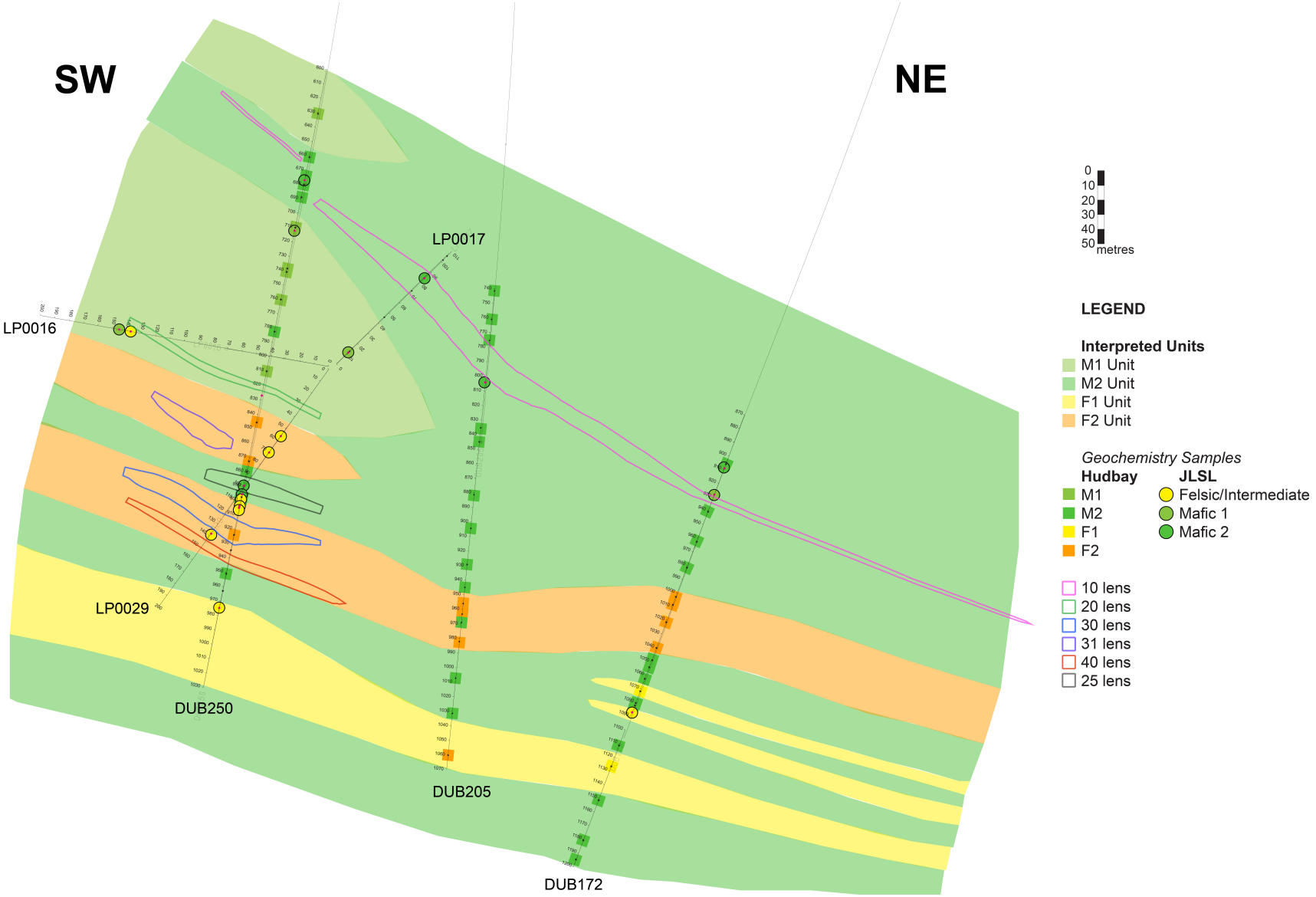

Figure 11: Cross section along 5400N showing geochemical map units delineated using geochemistry from logged drill holes. Outline of ore lenses are also shown.

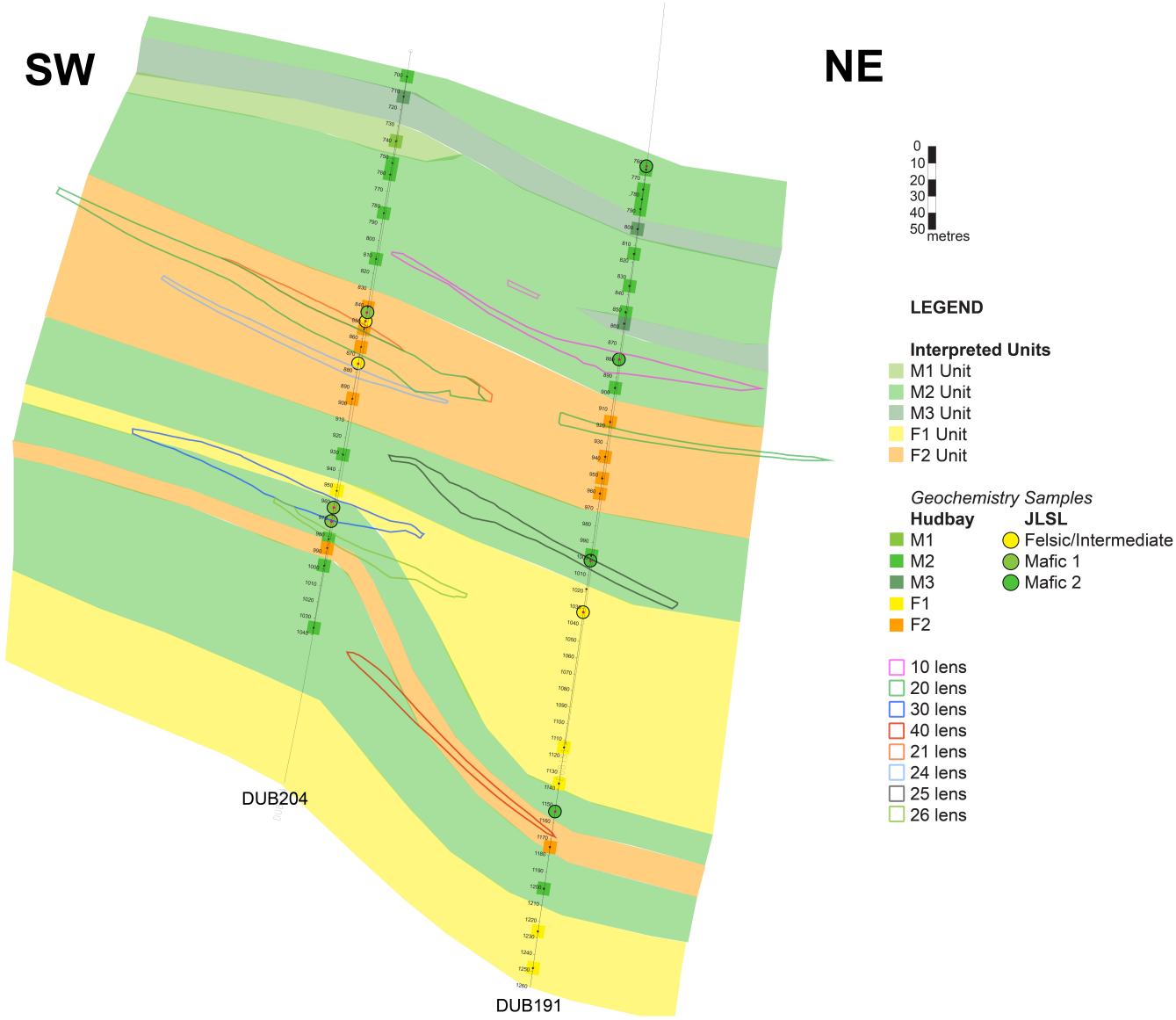

Figure 12: Cross section along 5600N showing geochemical map units delineated using geochemistry from logged drill holes. Outline of ore lenses are also shown.

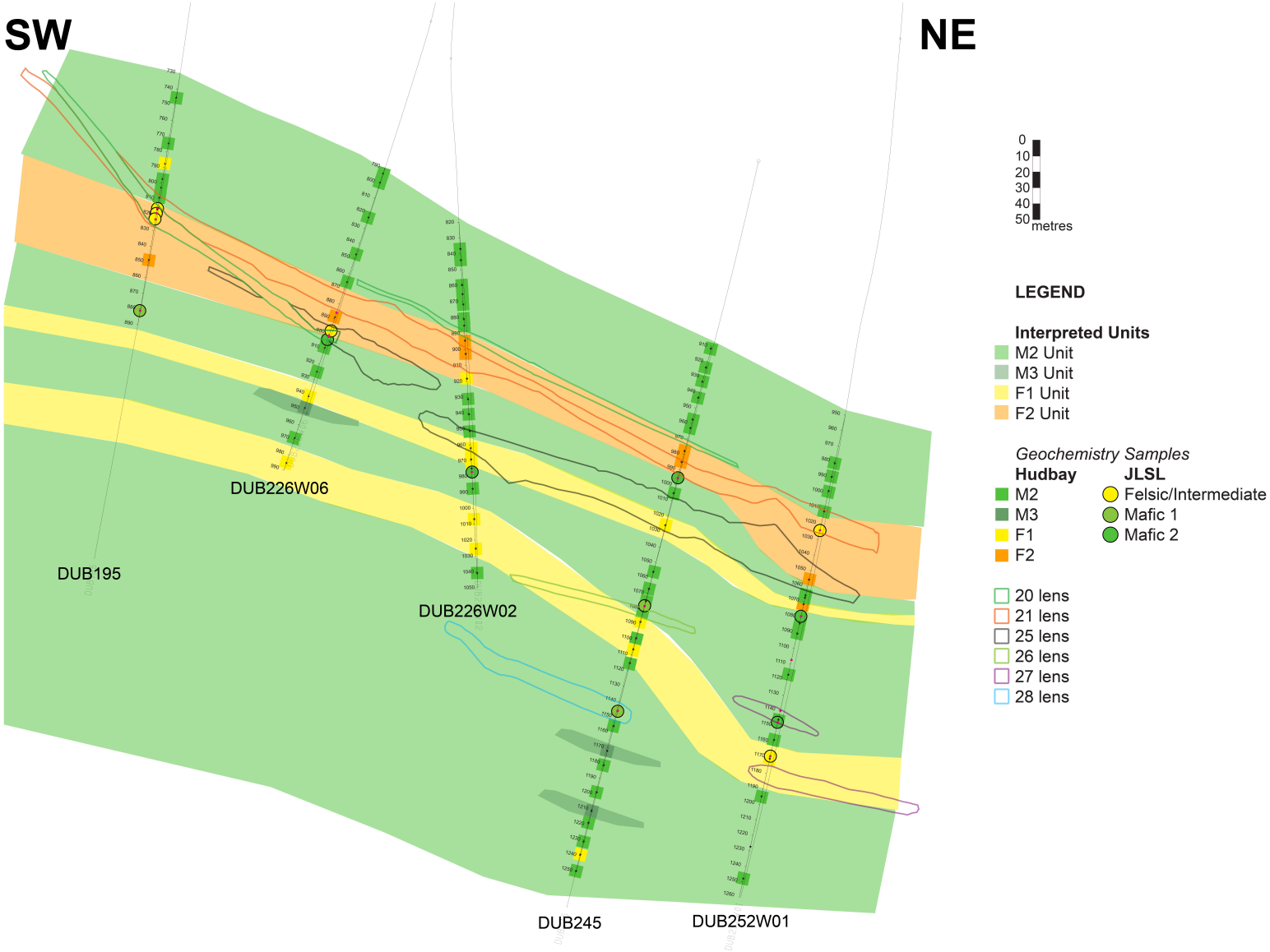

Figure 13: Diagrams showing geochemical protolith for Unit F1 (Winchester & Floyd 1977 and Primitive Mantle normalized spider plots) from each section to compare and confirm traceability of the units between sections.

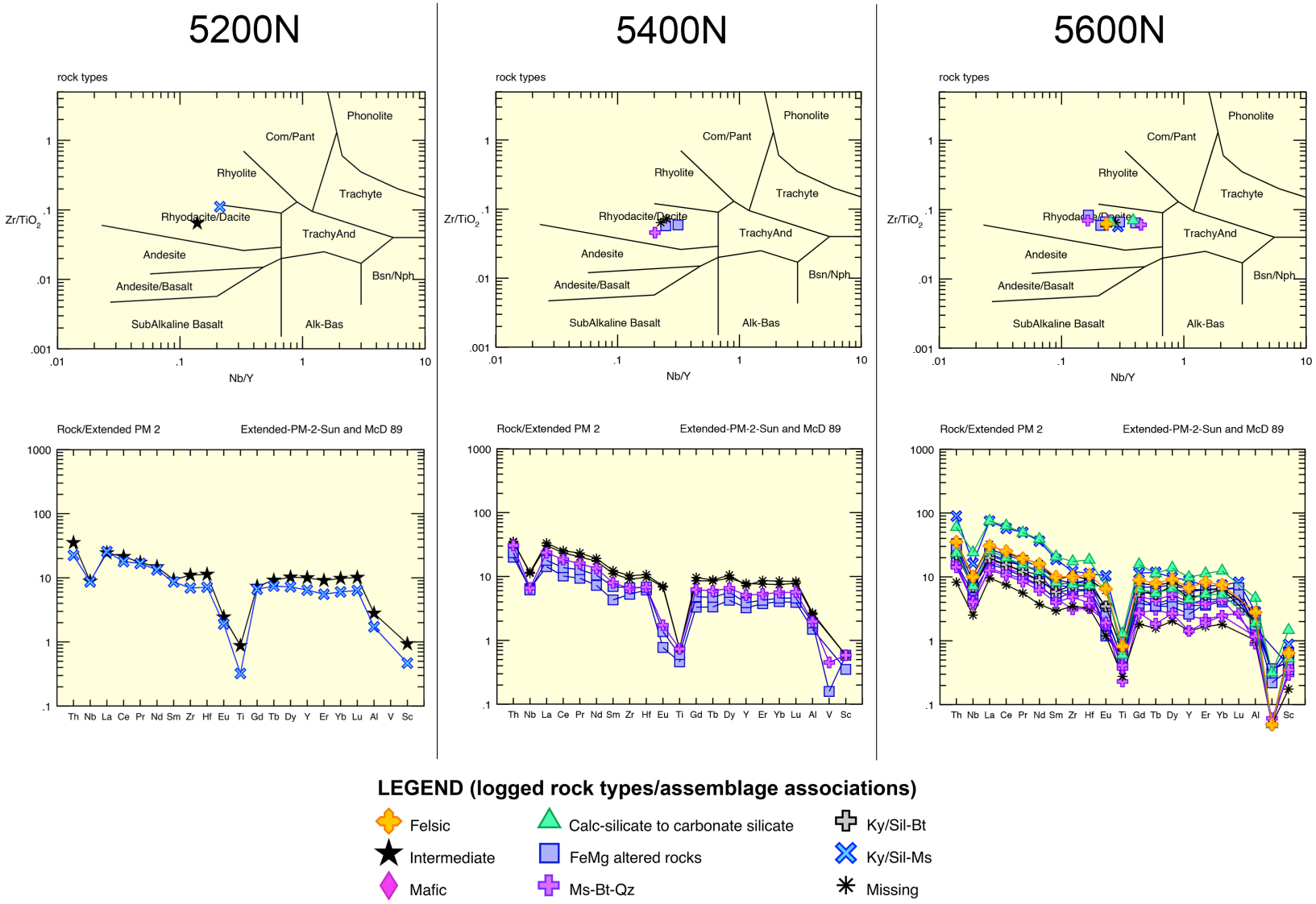

Figure 14: Diagrams showing geochemical protolith for Unit F2 (Winchester & Floyd 1977 and Primitive Mantle normalized spider plots) from each section to compare and confirm traceability of the units between sections.

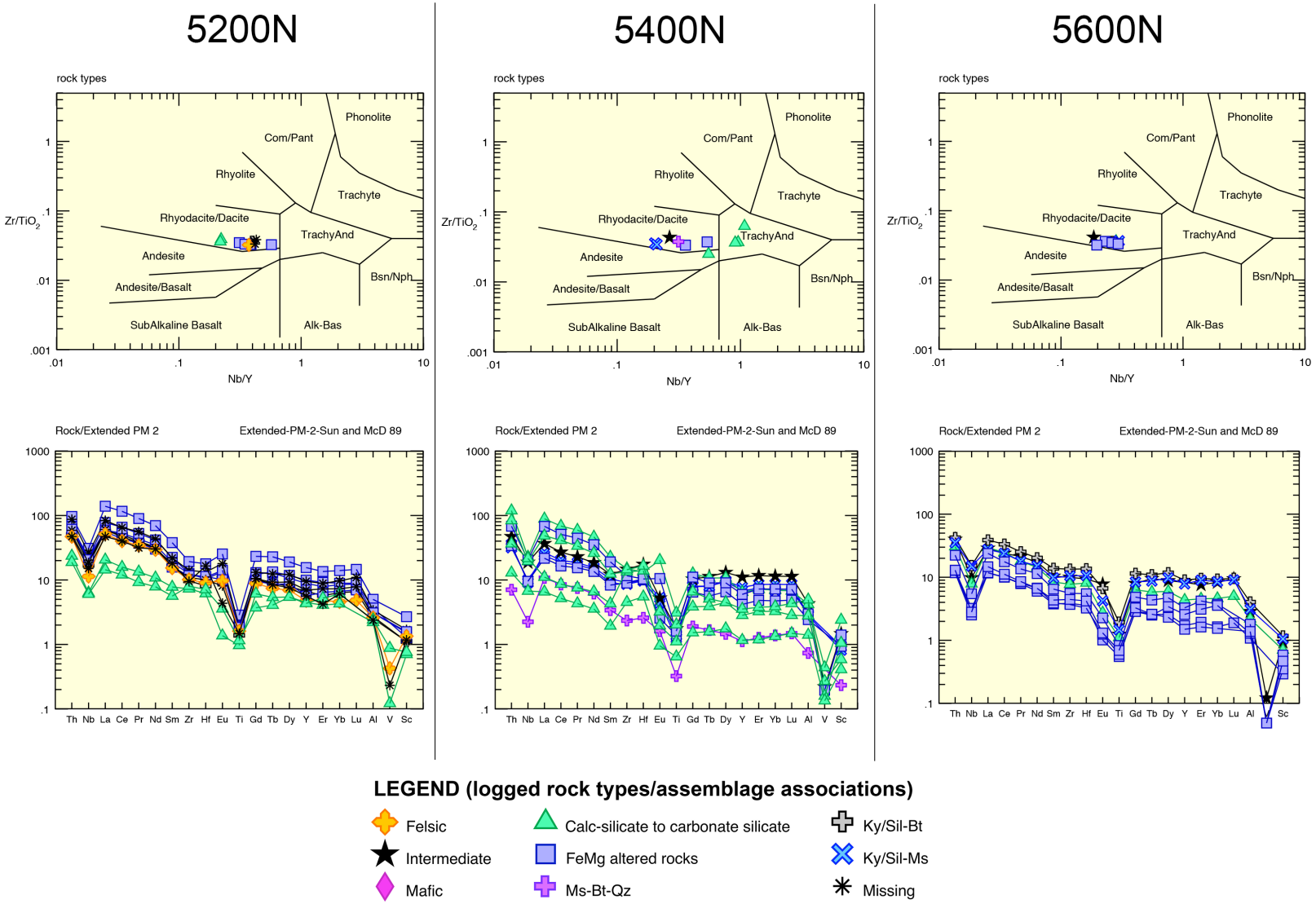

Figure 15: Diagrams showing geochemical protolith for Unit M1 (Winchester & Floyd 1977 and Primitive Mantle normalized spider plots) from each section to compare and confirm traceability of the units between sections.

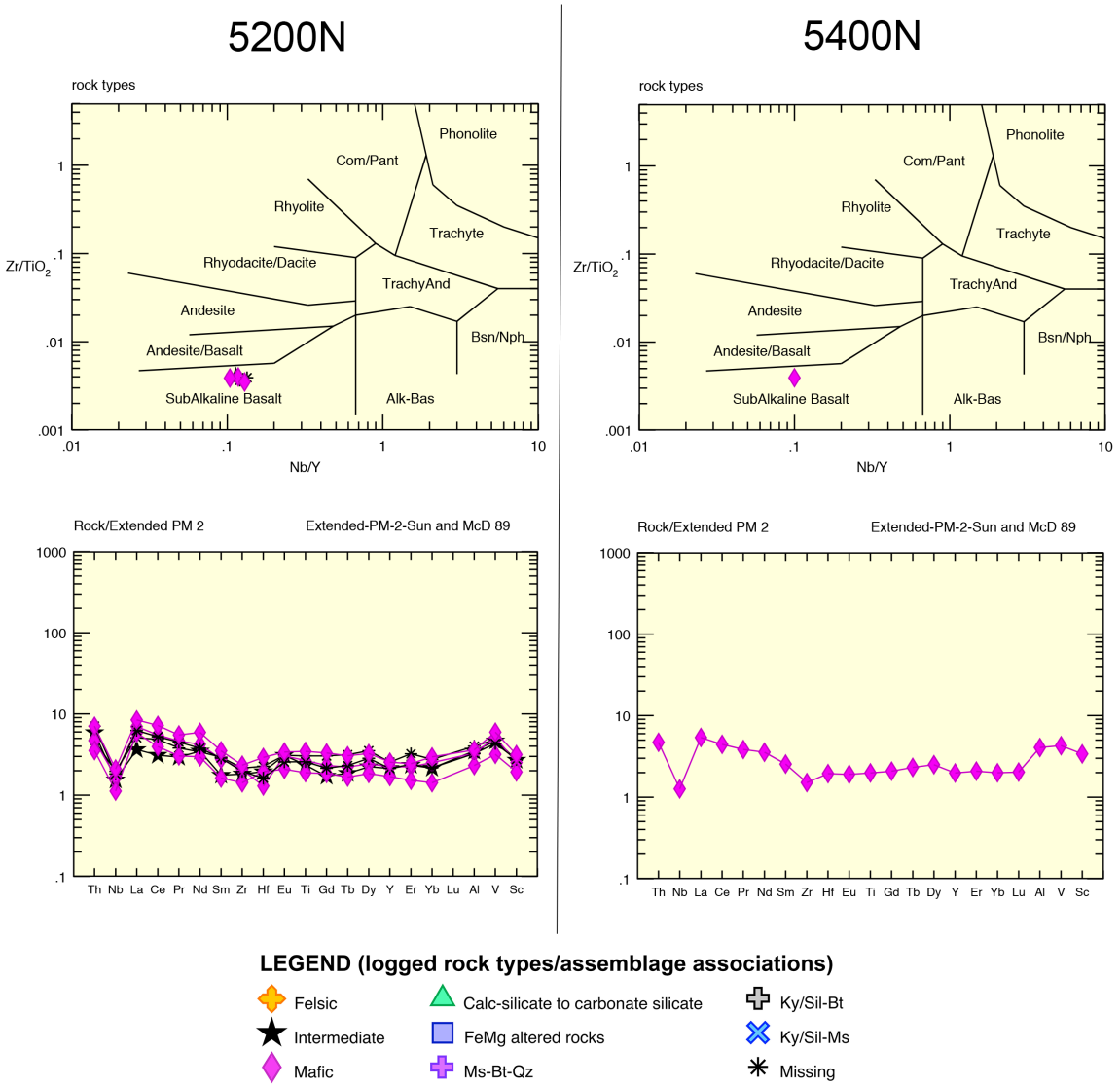

Figure 16: Diagrams showing geochemical protolith for Unit M2 (Winchester & Floyd 1977 and Primitive Mantle normalized spider plots) from each section to compare and confirm traceability of the units between sections.

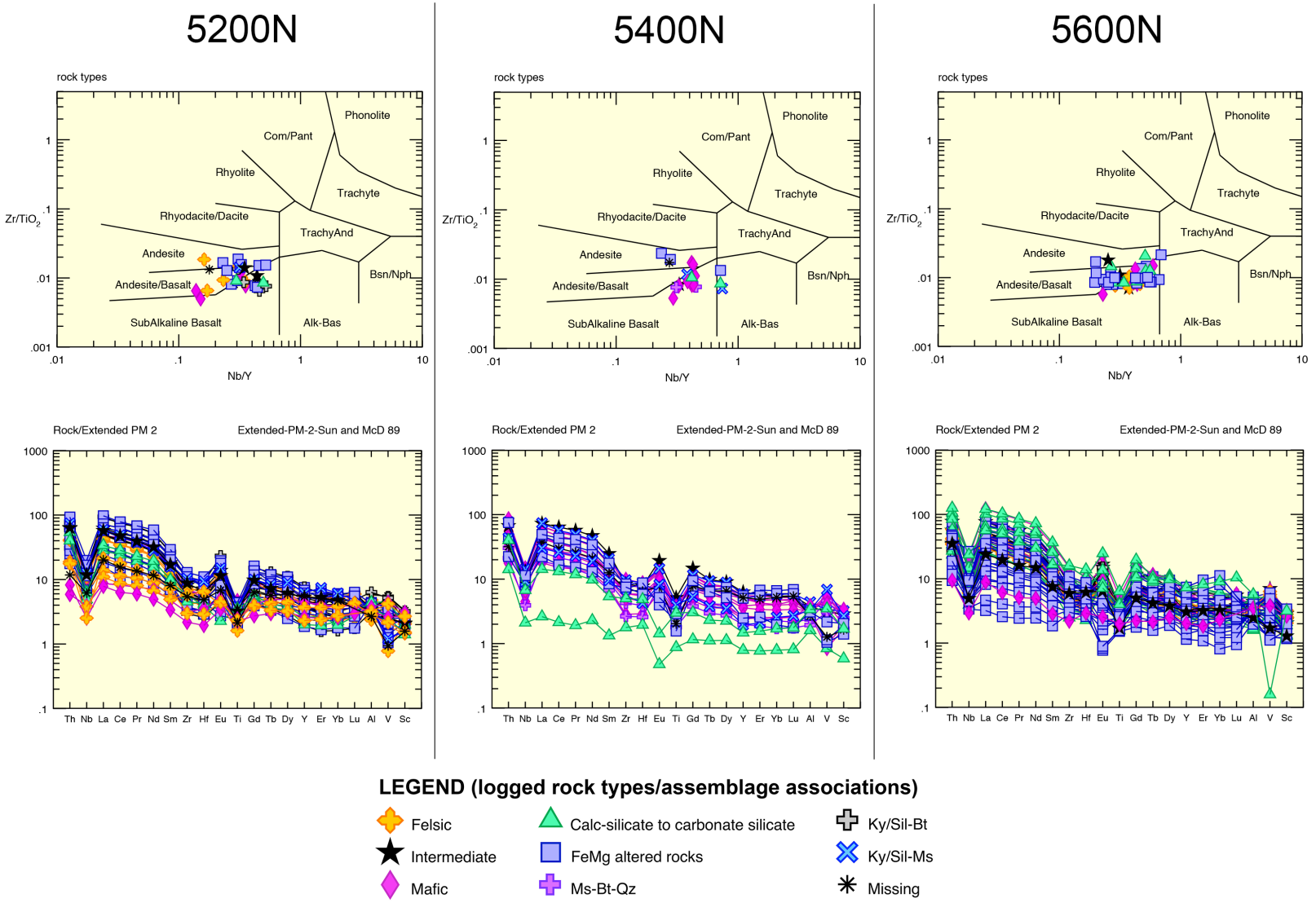

Figure 17: Diagrams showing geochemical protolith for Unit M3 (Winchester & Floyd 1977 and Primitive Mantle normalized spider plots) from each section to compare and confirm traceability of the units between sections.

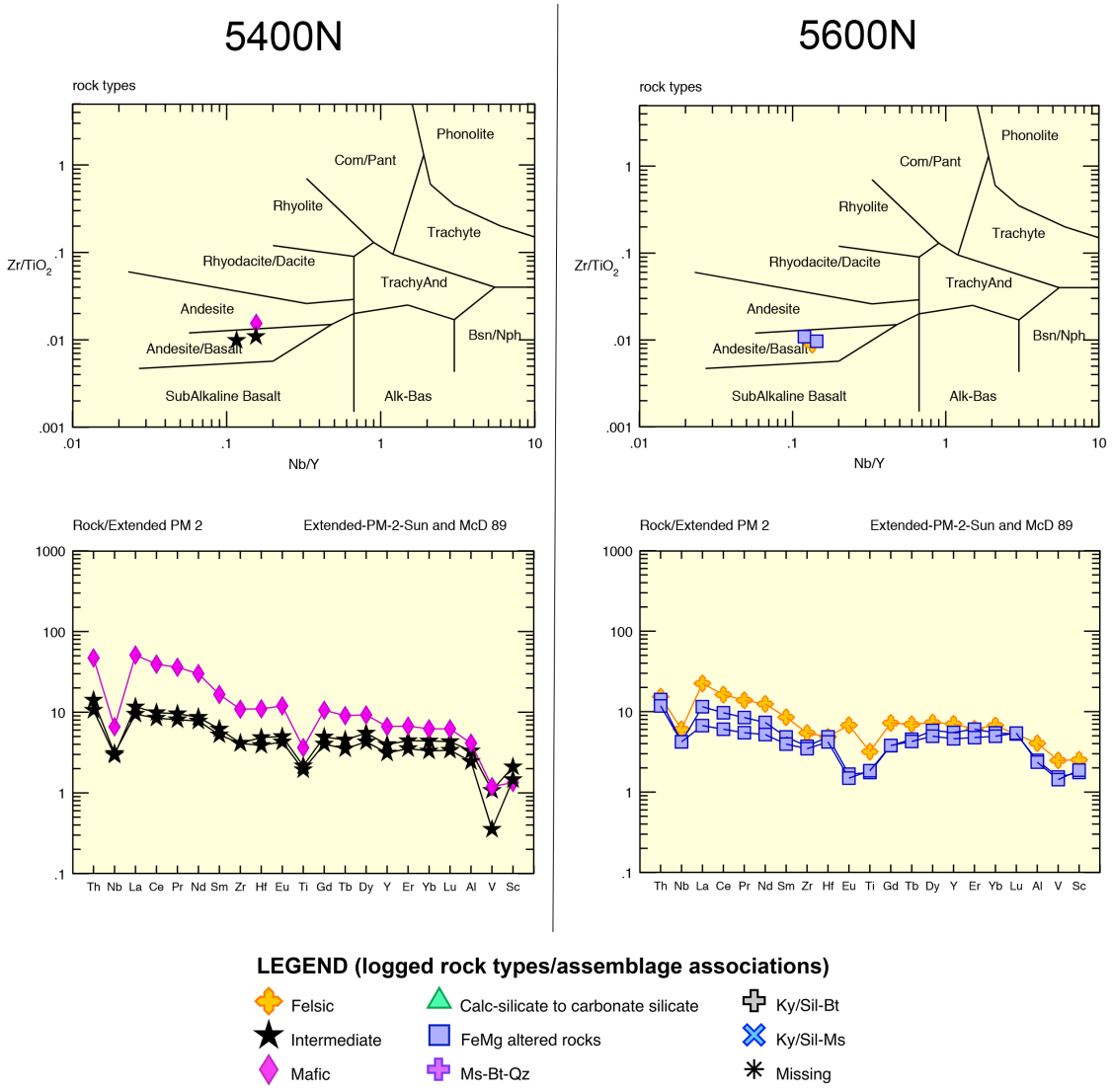

Figure 18: Discrimination of the pre-alteration protolith of JLSL alteration samples using geochemical plots based on ratios of immobile trace element that resist modification by element mobility during alteration and metamorphism (Winchester & Floyd, 1977): A) Felsic and B) Mafic. Symbols in the legend indicate the present rock type or assemblage association logged for each sample.

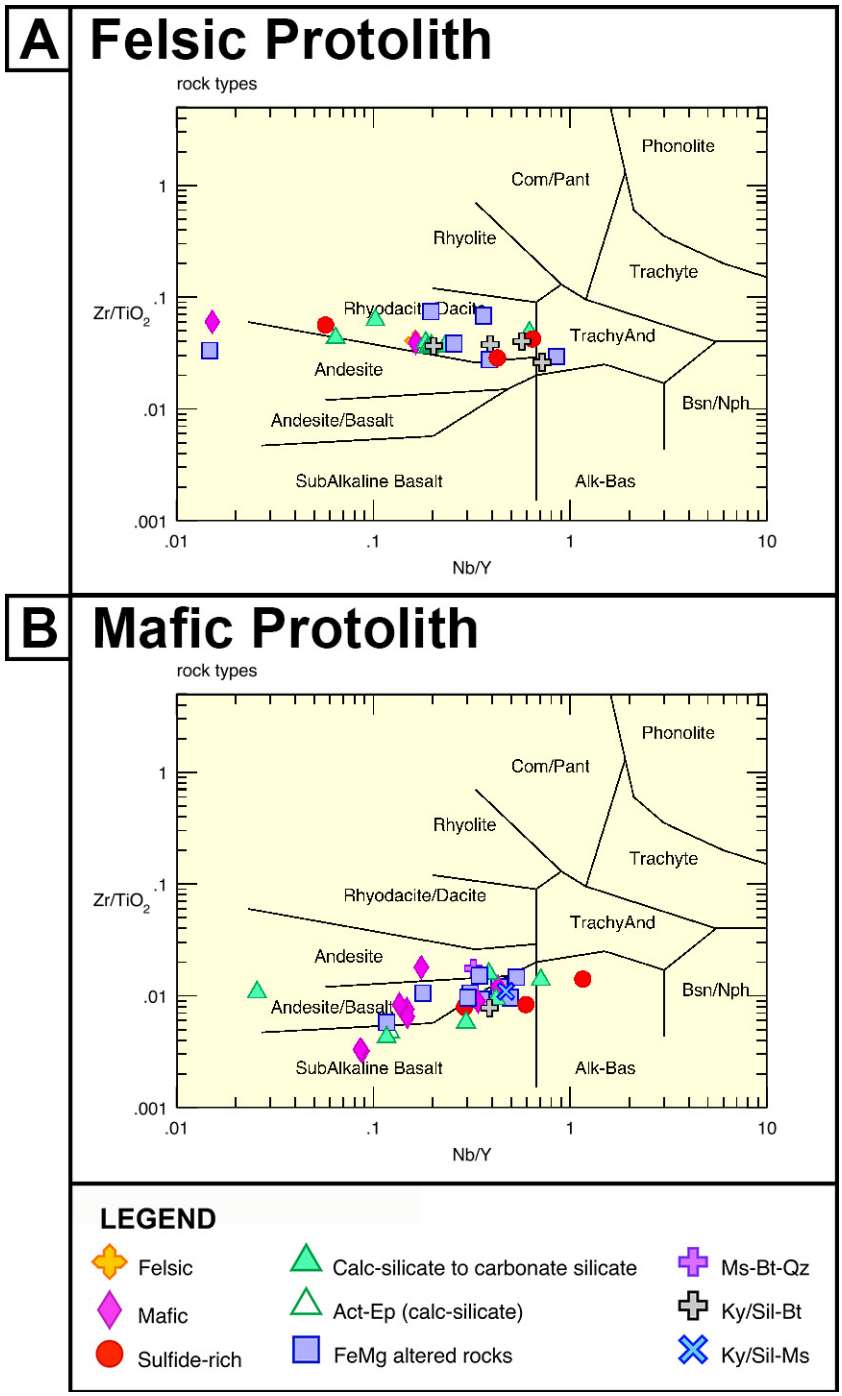

Figure 19: Alteration box plot (Large et al., 2001) showing common trends in hydrothermal alteration with JLSL samples plotted from the A) Felsic Protoliths and B) Mafic Protoliths groups in Figure 18.

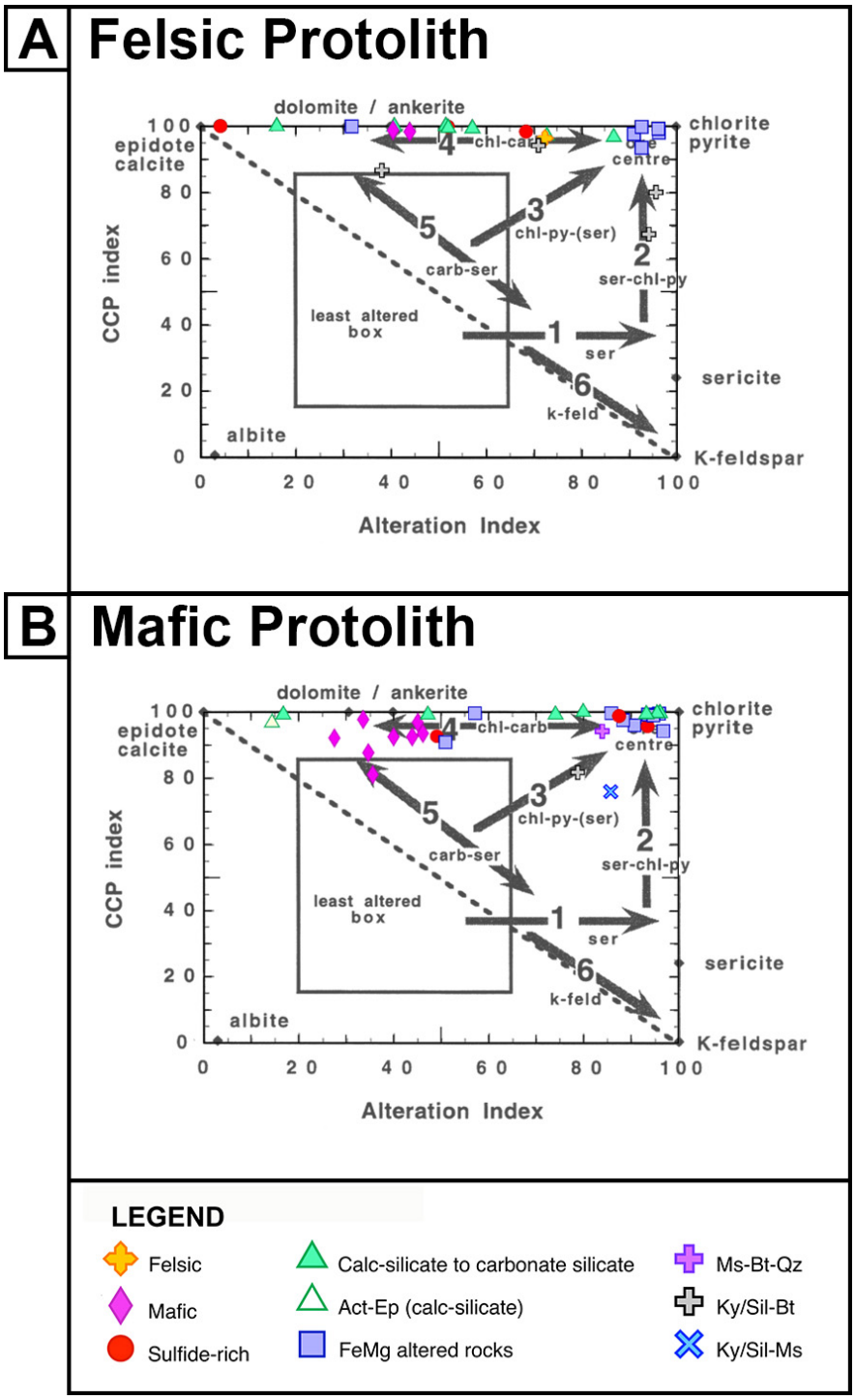

Figure 20: Drill core photos of rock types in which typically have anomalously high Au values: A) Massive sulfide (Cpy-Cc-Sph-Py sample JLSL-26037 from DUB195 ~823 m, ~4.56 g/t, 20 lens), B) Calc-silicates to carbonate silicates (Chl-Cc-Act/Tr sample JLSL-27056 from DUB204 ~875 m, ~3.68 g/t, between 21 and 24 lens), and C) Fe-Mg altered rocks (Grt-Ath-Crd sample JLSL-26079 from DUB252W01 ~1080 m, ~5.69 g/t, below 25 lens)

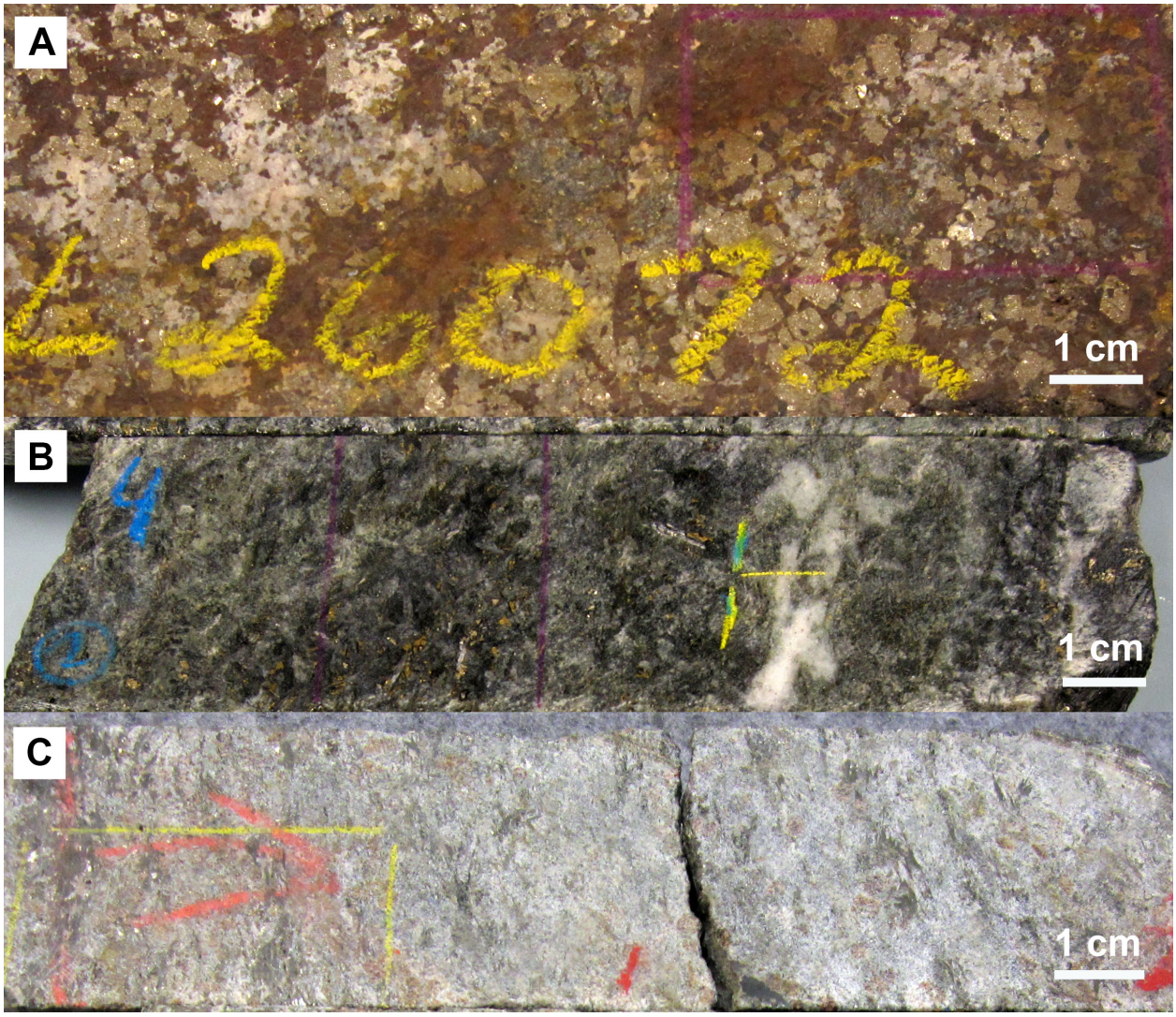

Figure 21: Drill core photos of rock types in which anomalous Au values are sparse. A) Unaltered to weakly altered mafic rocks (Grt-Bt-Hb sample JLSL-27003 from DUB172 ~909 m, 24.4 g/t, above 10 lens), B) Ky/Sil-Ms-Bt schists and gneisses (JLSL-27093 from LP0008 ~111 m, 50 g/t, proximal to 10 lens), C) Silica-rich rocks (Py-Cpy-Ghn-Bt-Qz sample JLSL-27103 from DUB205 ~804 m, 10.4 g/t, below 10 lens), D) Plagioclase pegmatite (Gal-Bt-Pl sample JLSL-27007 from DUB172 ~928 m, 159.3 g/t, above 10 lens)

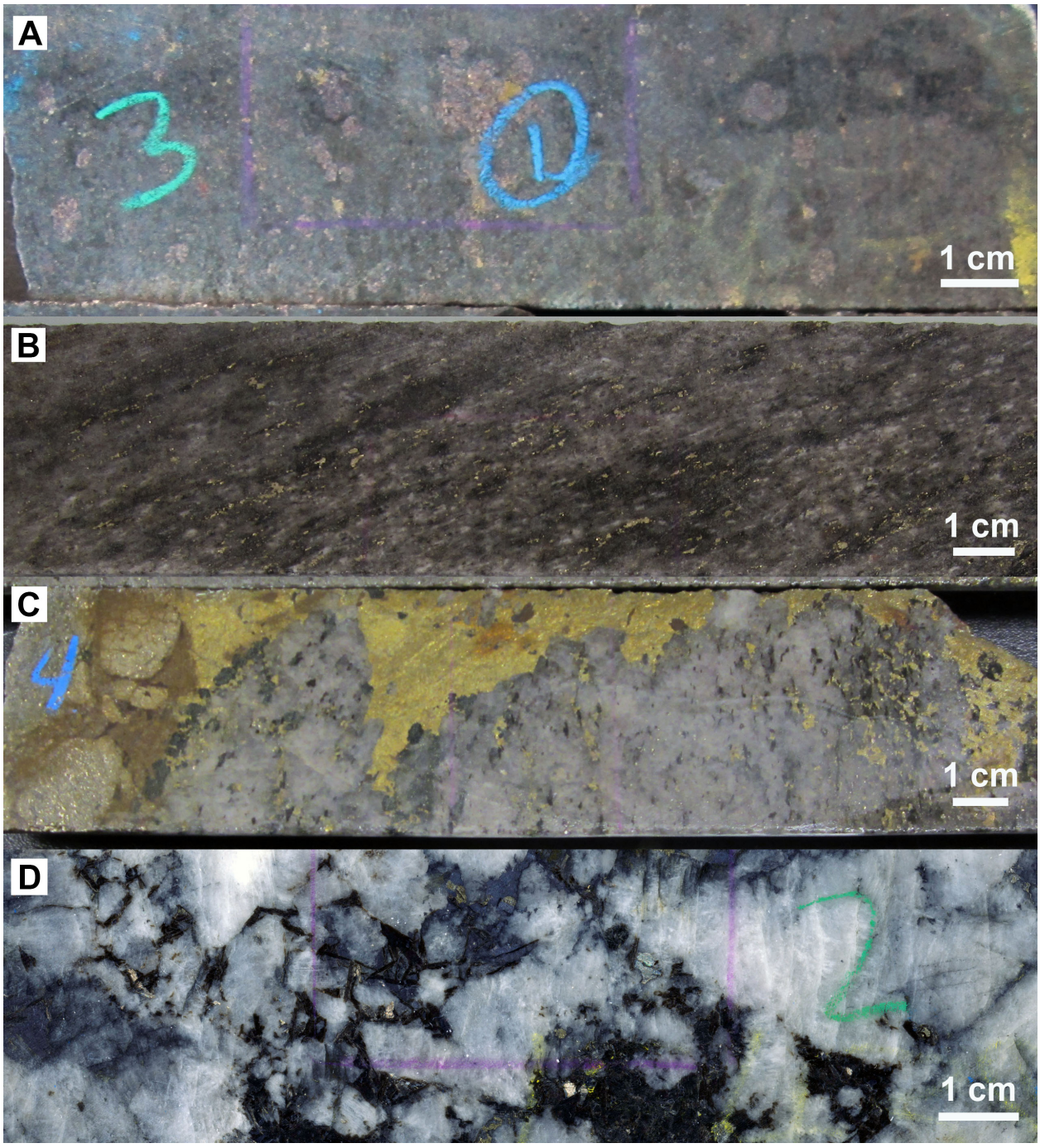

Figure 22: Examples of gold mineralization styles (occurring as electrum) in massive sulfides: Sample JLSL-26037 is from the 20/21 base metal/gold lens (DUB195 ~823 m) in A) drill core, B-C) photomicrograph and accompanying SEM image. Sample JLSL-27094 is from the 10 base metal lens (LP0008 ~113 m) in D) drill core, E-F) photomicrographs and accompanying SEM image.

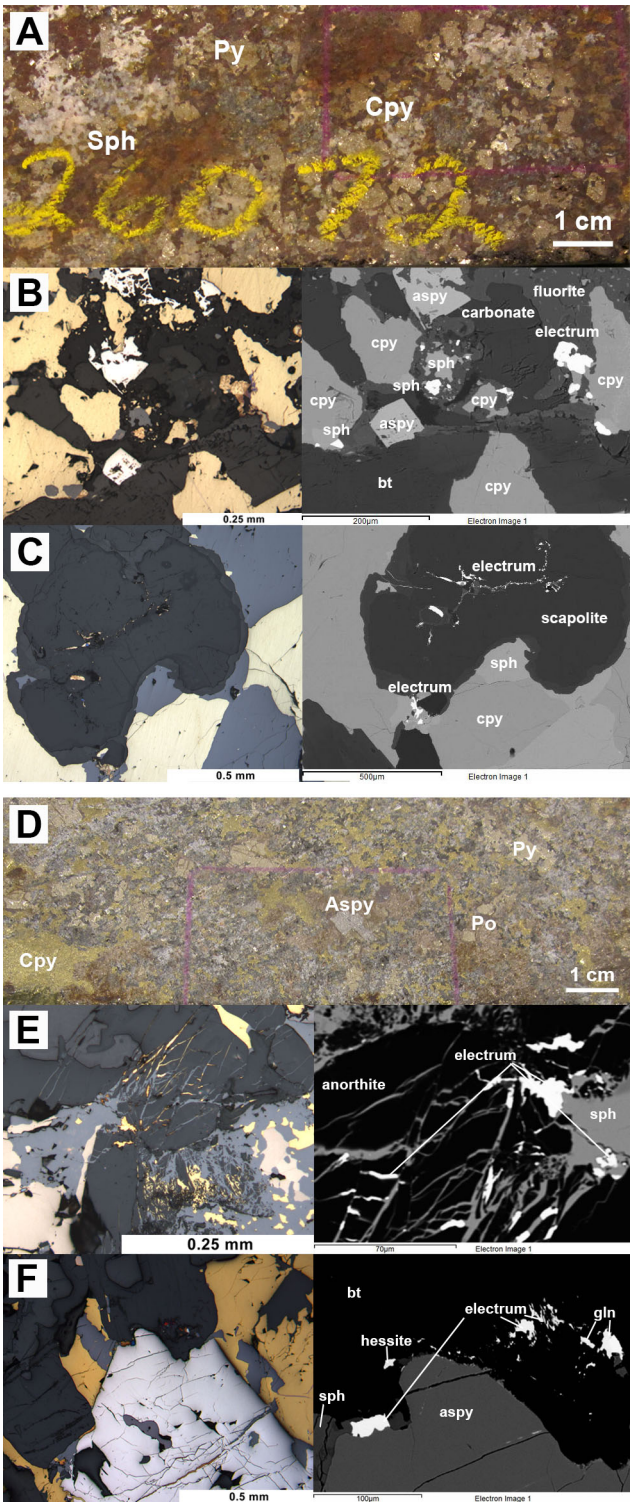

Figure 23: Examples of gold mineralization occurring as discrete inclusions in drill core, photomicrographs (PPL, RFL), and SEM images from samples A) JLSL-27090 showing metamorphic gahnite with electrum and hessite inclusions (from the footwall of 10 lens in LP0008 ~105m), B) JLSL27056 showing aurostibite and boulangerite contained within metamorphic tremolite (from the 24 gold lens in DUB204 ~875m) and C) JLSL-27002 showing inclusions of electrum in anorthite (in the hanging wall to 10 lens in DUB172 ~906m).

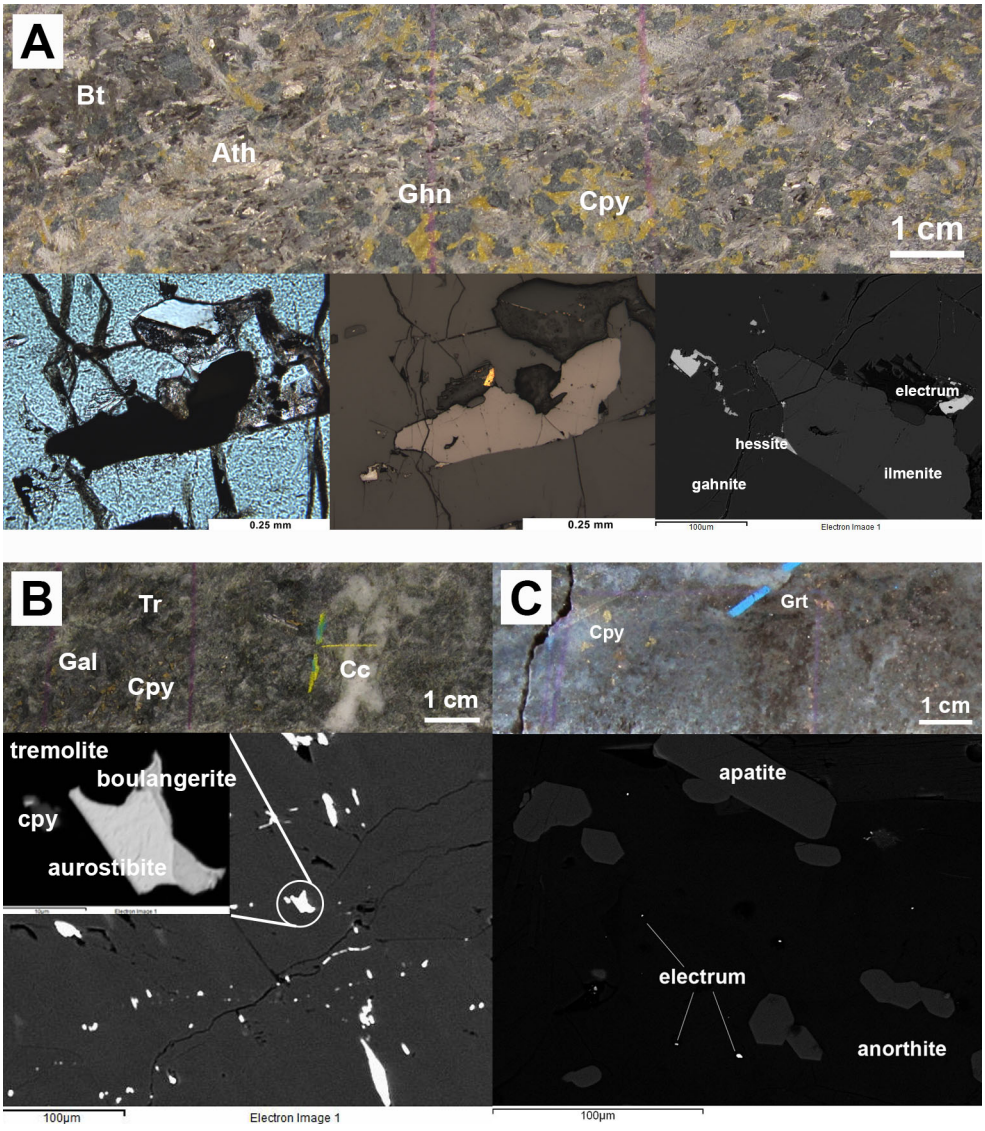

Figure 24: Examples of gold mineralization occurring along grain boundaries, fractures, and cleavages. Drill core and corresponding SEM images for samples A) JLSL-26019 in the footwall of 25 gold lens in DUB226W02 ~977 m (electrum), B) JLSL-26079 in the footwall of 25 gold lens in DUB252W01 ~1079 m (electrum, petzite), C) JLSL-27056 in the 24 gold lens in DUB204 ~875 m (electrum), and D) JLSL-27002 in the hanging wall to the 10 base metal lens in DUB172 ~906 m (electrum).

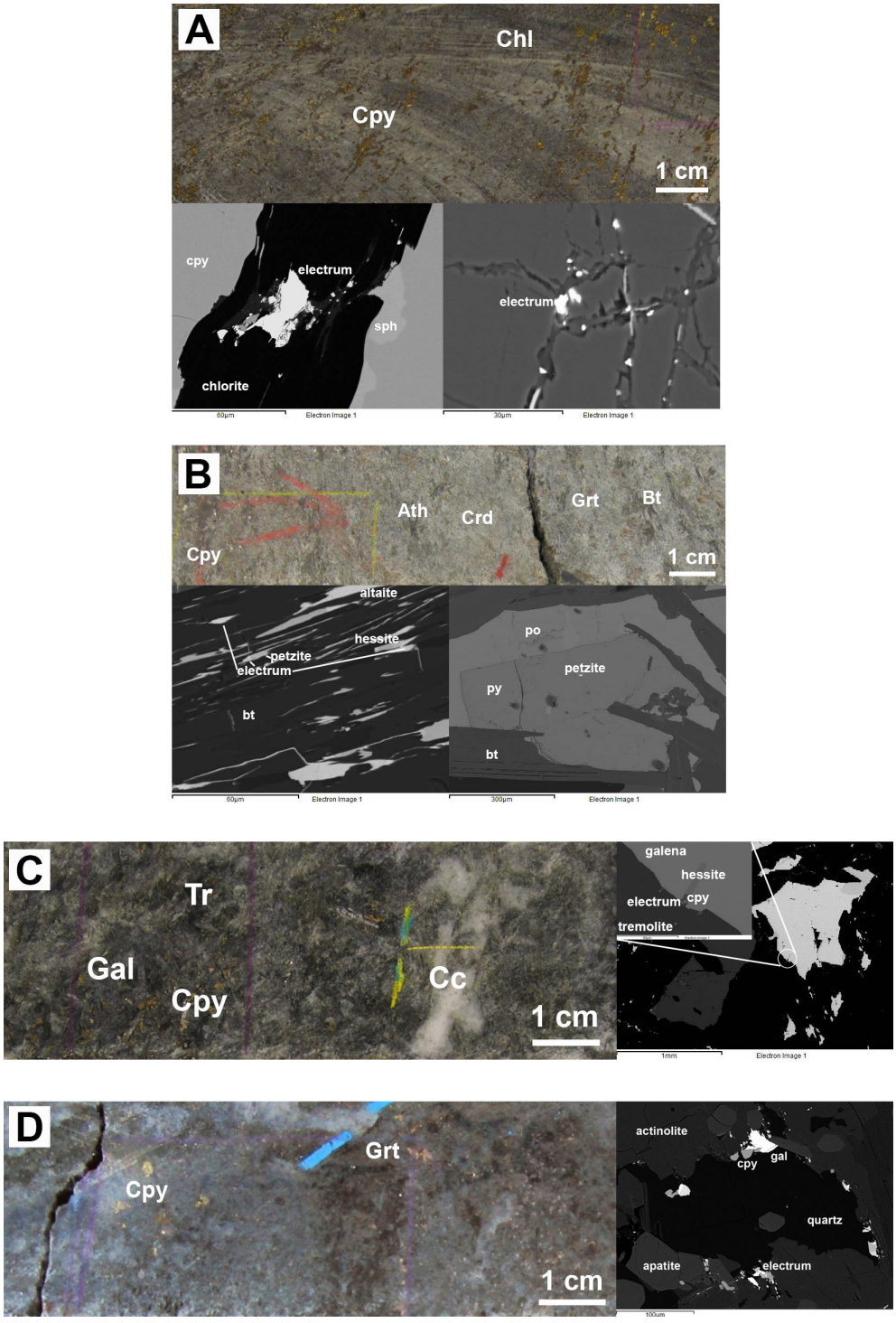

Figure 25: Pb vs. Cu plots by Au tenor, using Hudbay assay data for logged drill holes, to examine the association of Au with Cu and Pb as well as any variations in this association (such as rock type) with different Au tenor.

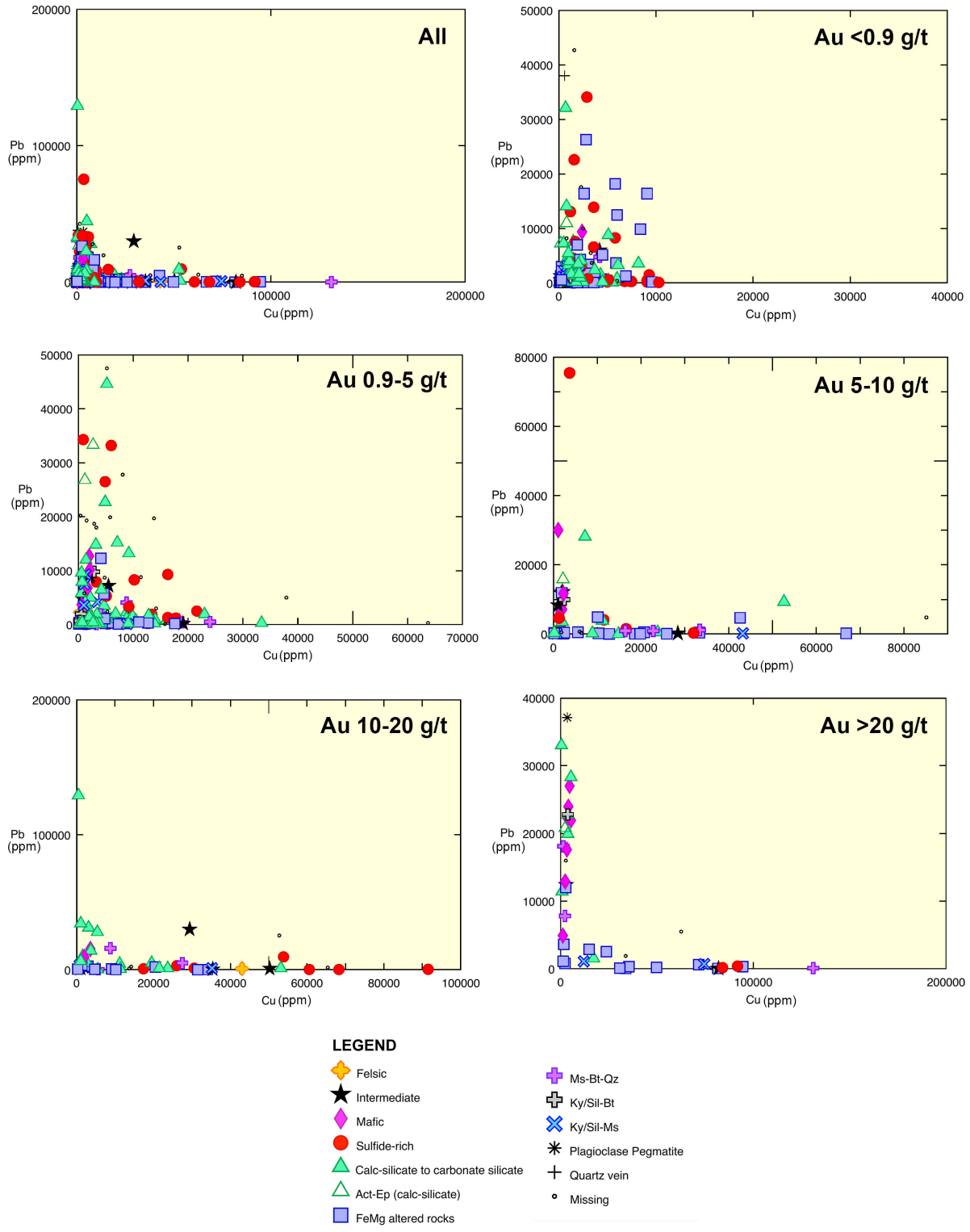

Figure 26: Pb vs. Cu plots by Au tenor; sub-selected from Figure 25 with a cutoff of <10 000 ppm Cu and >10 000 ppm Pb to examine samples with low Cu and high Pb (Pb-Au group) for variations in rock type with different Au tenor.

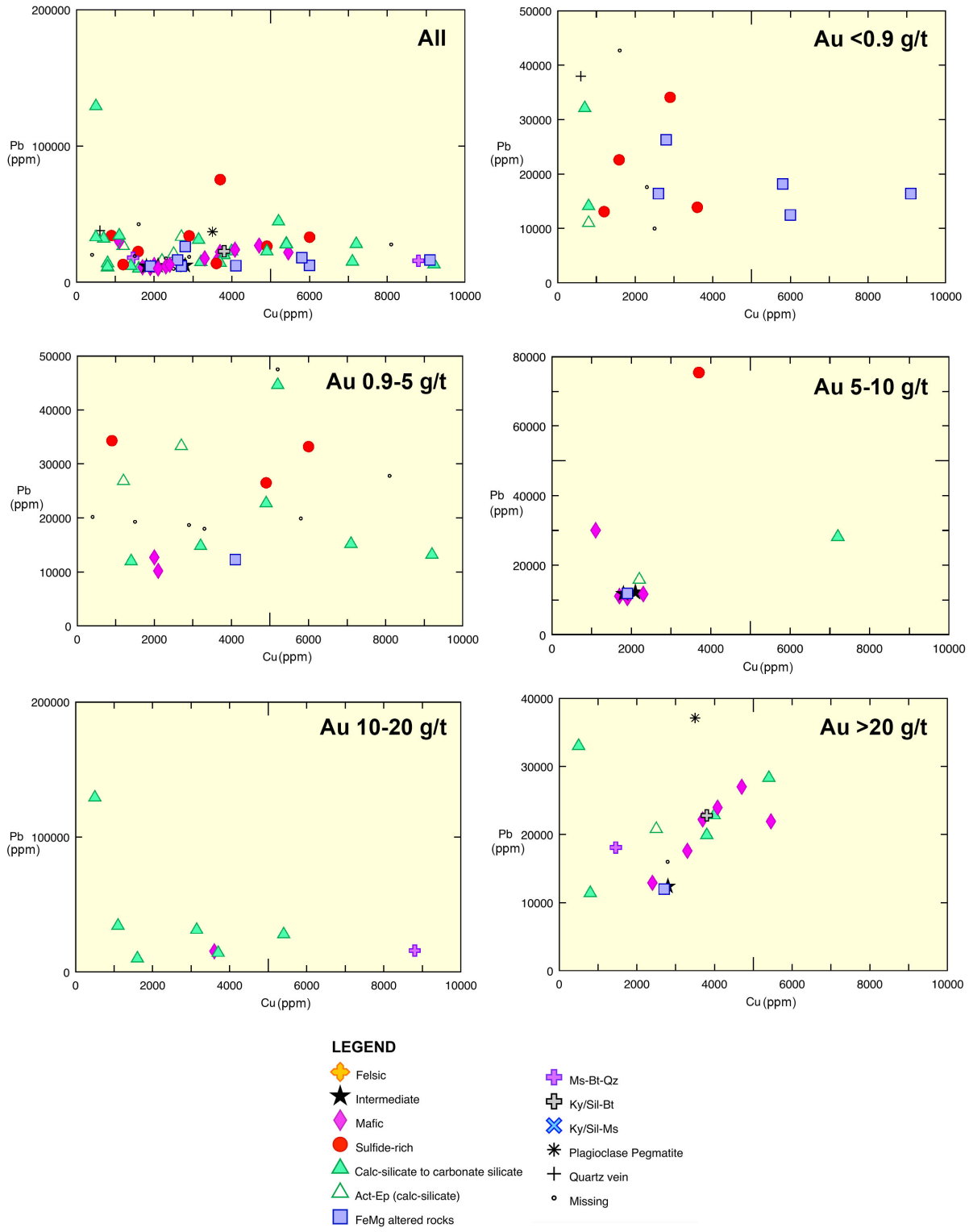

Figure 27: Pb vs. Cu plots by Au tenor; sub-selected from Figure 25 with a cutoff of >10 000 ppm Cu and <10 000 ppm Pb to examine samples with high Cu and low Pb (Cu-Au group) for variations in rock type with different Au tenor.

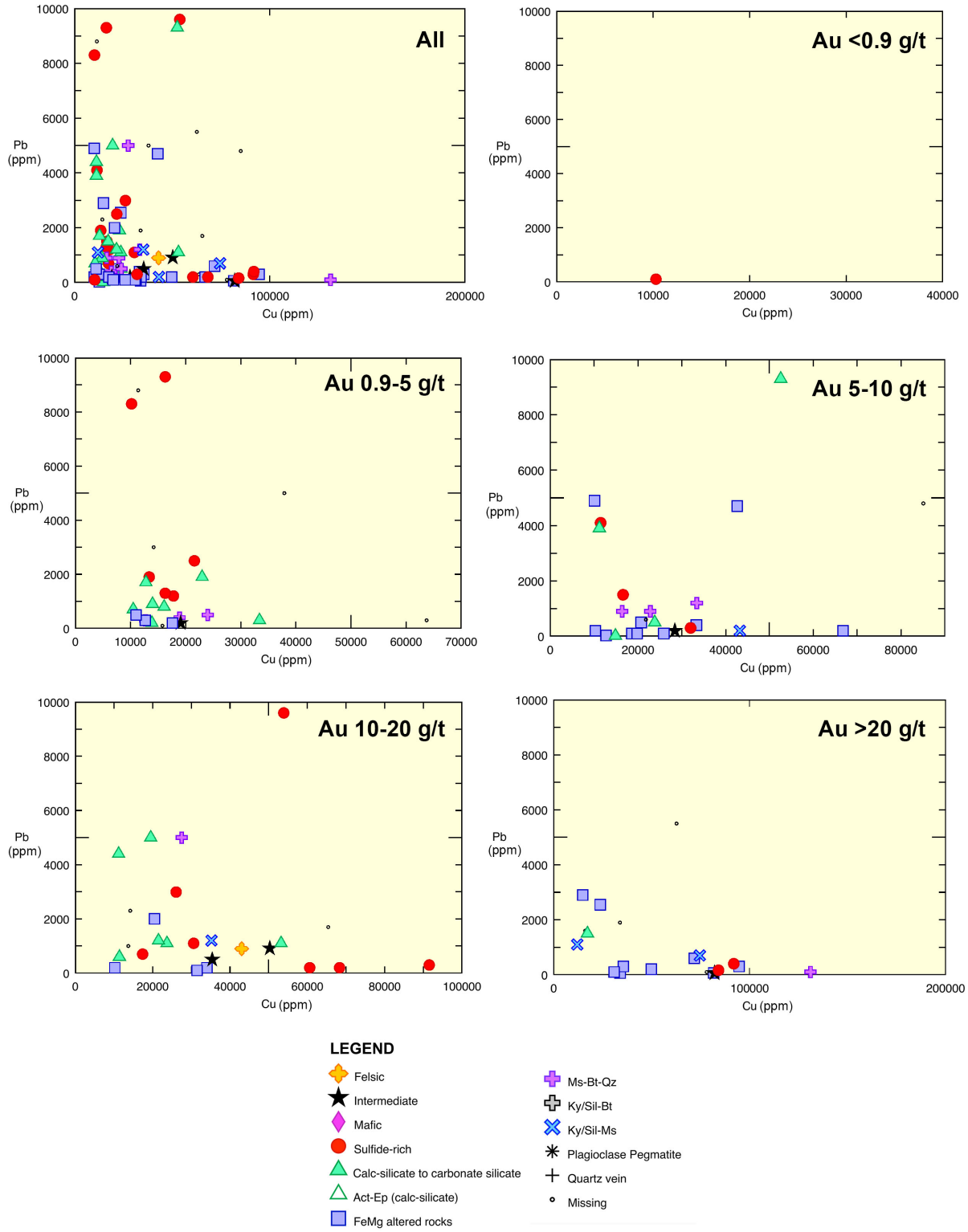

Figure 28: Pb vs. Cu plots by Au tenor; sub-selected from Figure 25 with Cu and Pb values below 10 000 ppm to examine trends in samples with low Cu and low Pb.

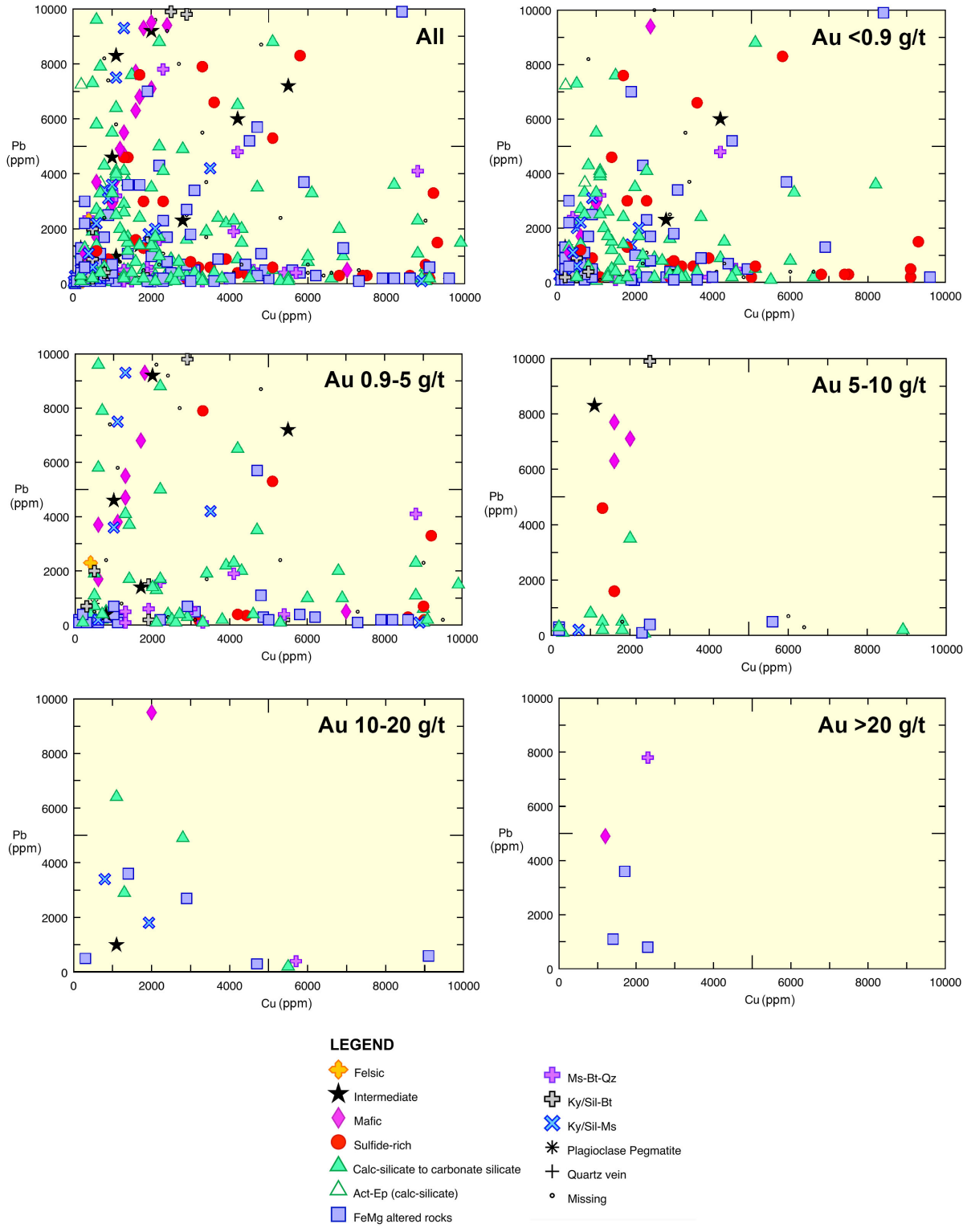

Figure 29: Cross section along 5200N showing the distribution of Pb-Au and Cu-Au groups from Figures 26 and 27 in addition to logged drill holes, ore lenses, and geochemical map units.

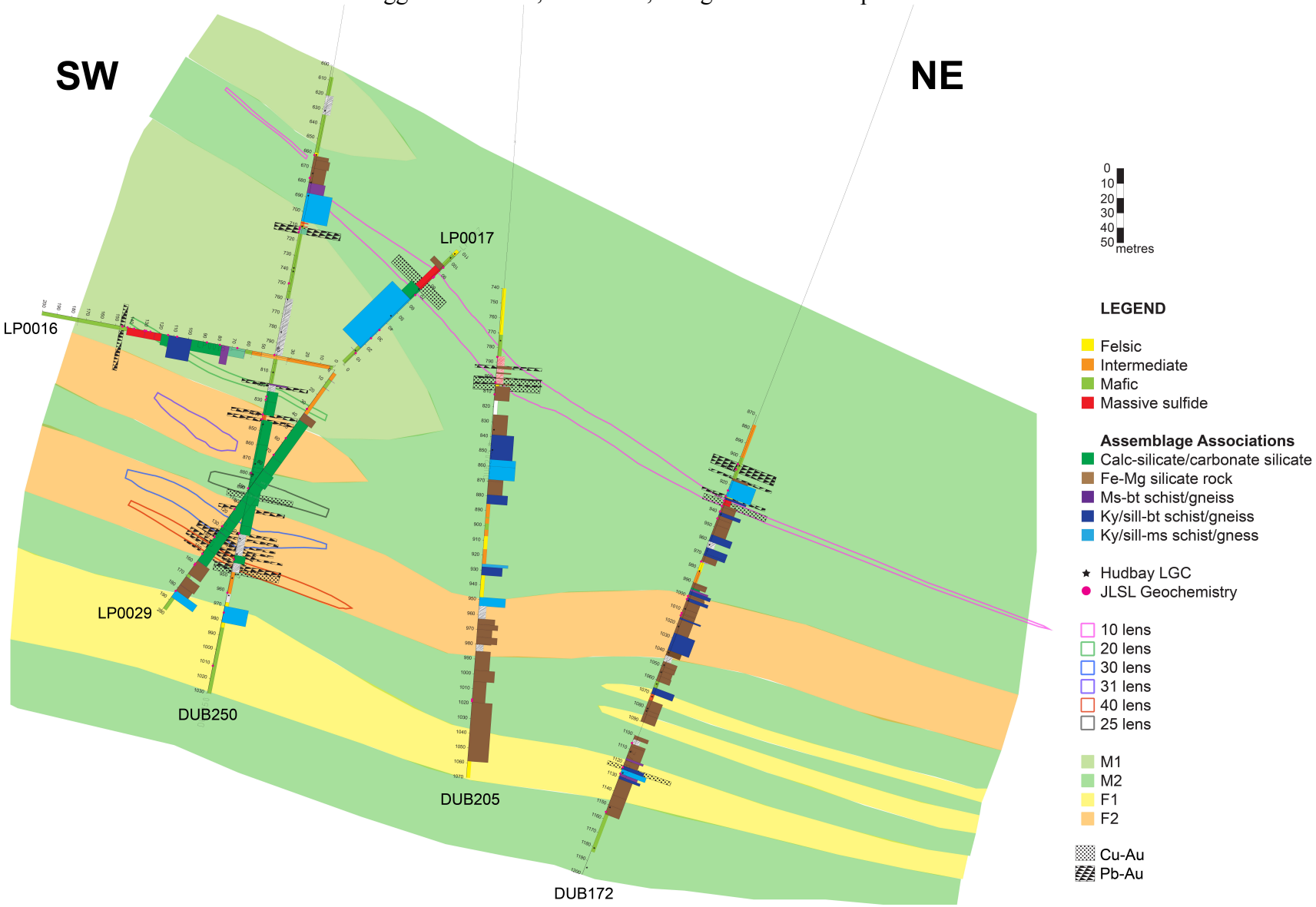

Figure 30: Cross section along 5400N showing the distribution of Pb-Au and Cu-Au groups from Figures 26 and 27 in addition to logged drill holes, ore lenses, and geochemical map units.

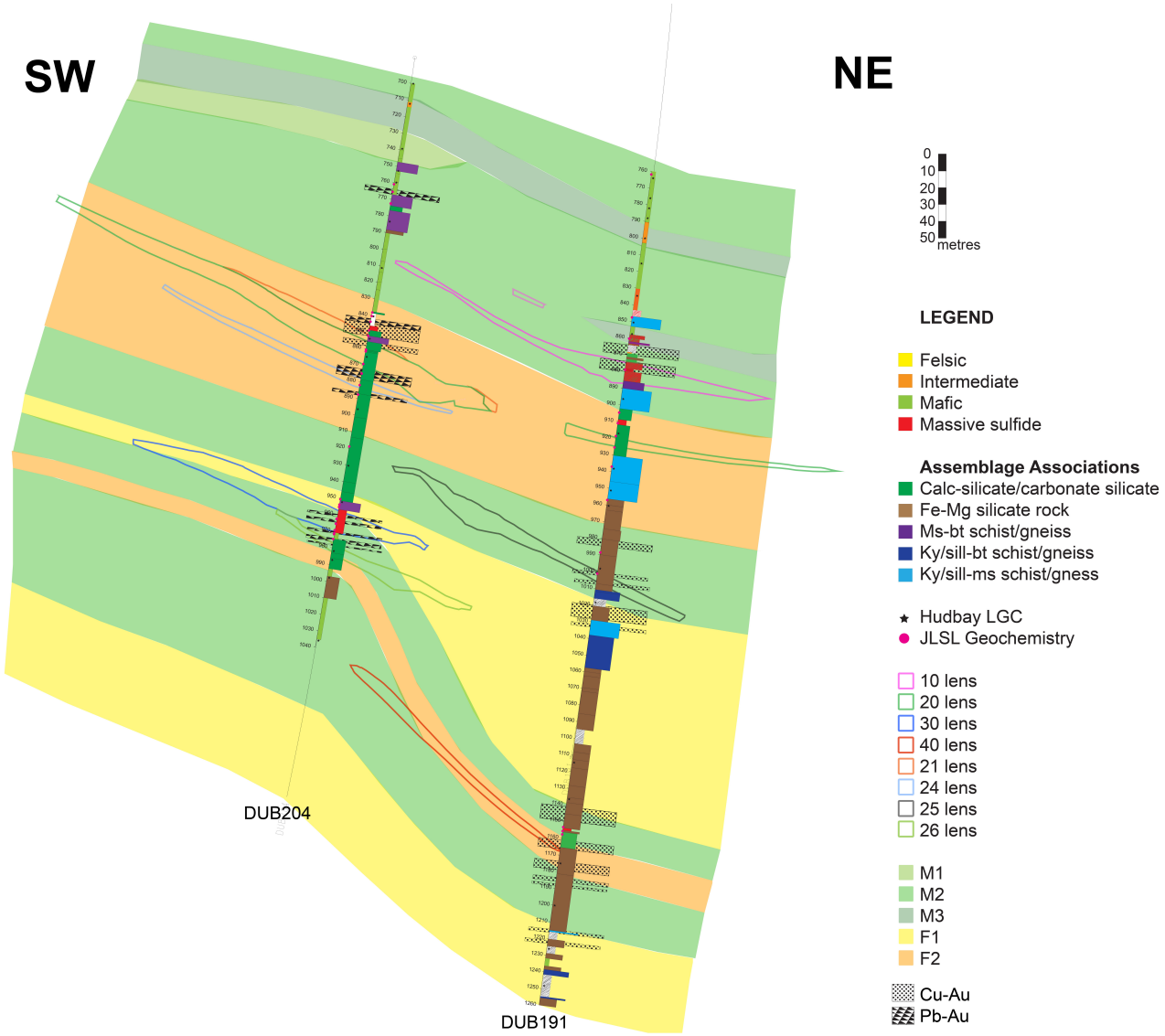

Figure 31: Cross section along 5600N showing the distribution of Pb-Au and Cu-Au groups from Figures 26 and 27 in addition to logged drill holes, ore lenses, and geochemical map units.

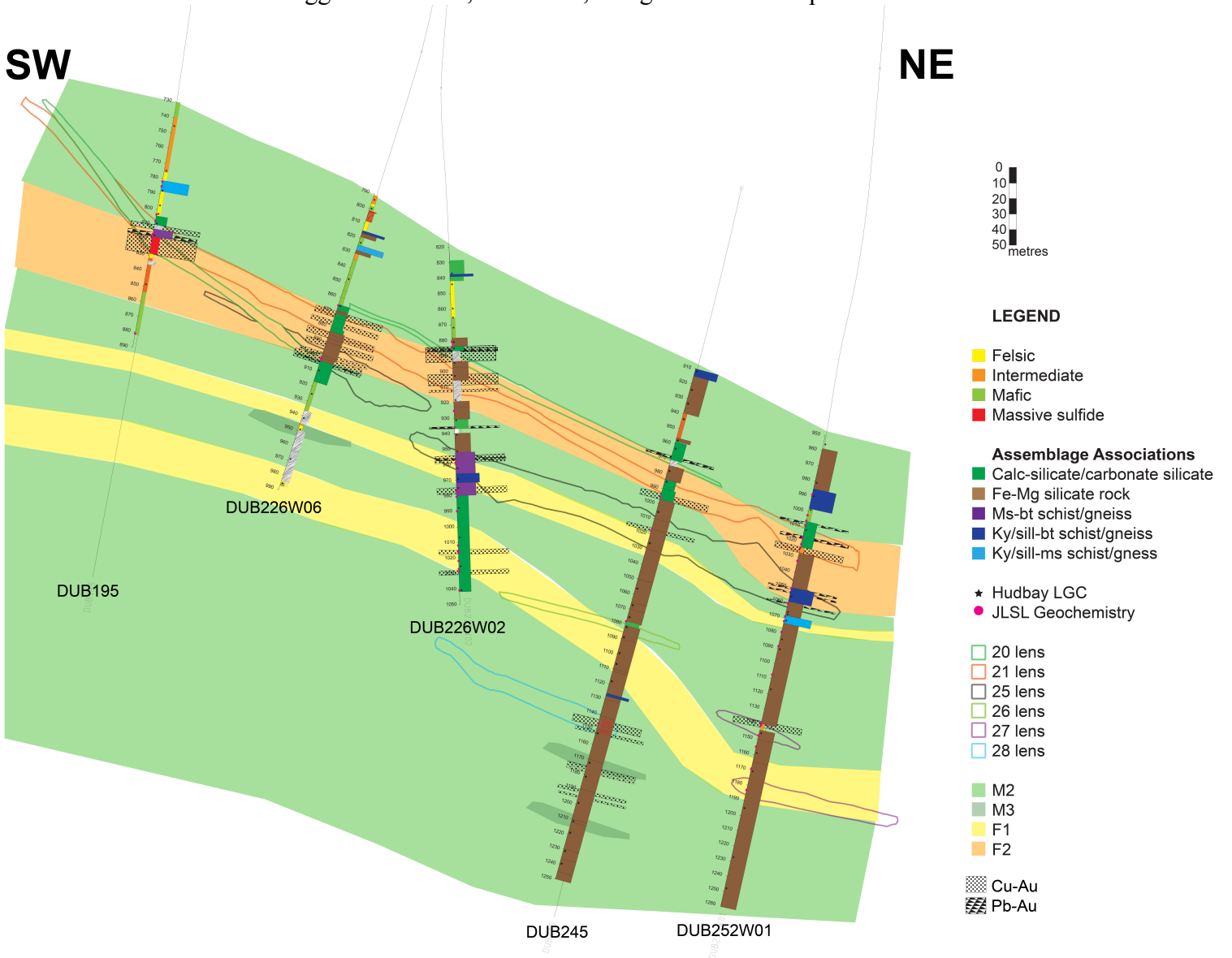

Figure 32: Pb vs. various elements (As, Bi, Hg, Sb, Se, Te) and Au tenor; sub-selected from Figure 25. The elements exhibit similar chemical behavior as gold (Phillips and Powell, 2010) and were selected to evaluate a correlation with Pb. Samples exceeding the upper detection limits are plotted at those limits (As 500 ppm, Sb 50 ppm).

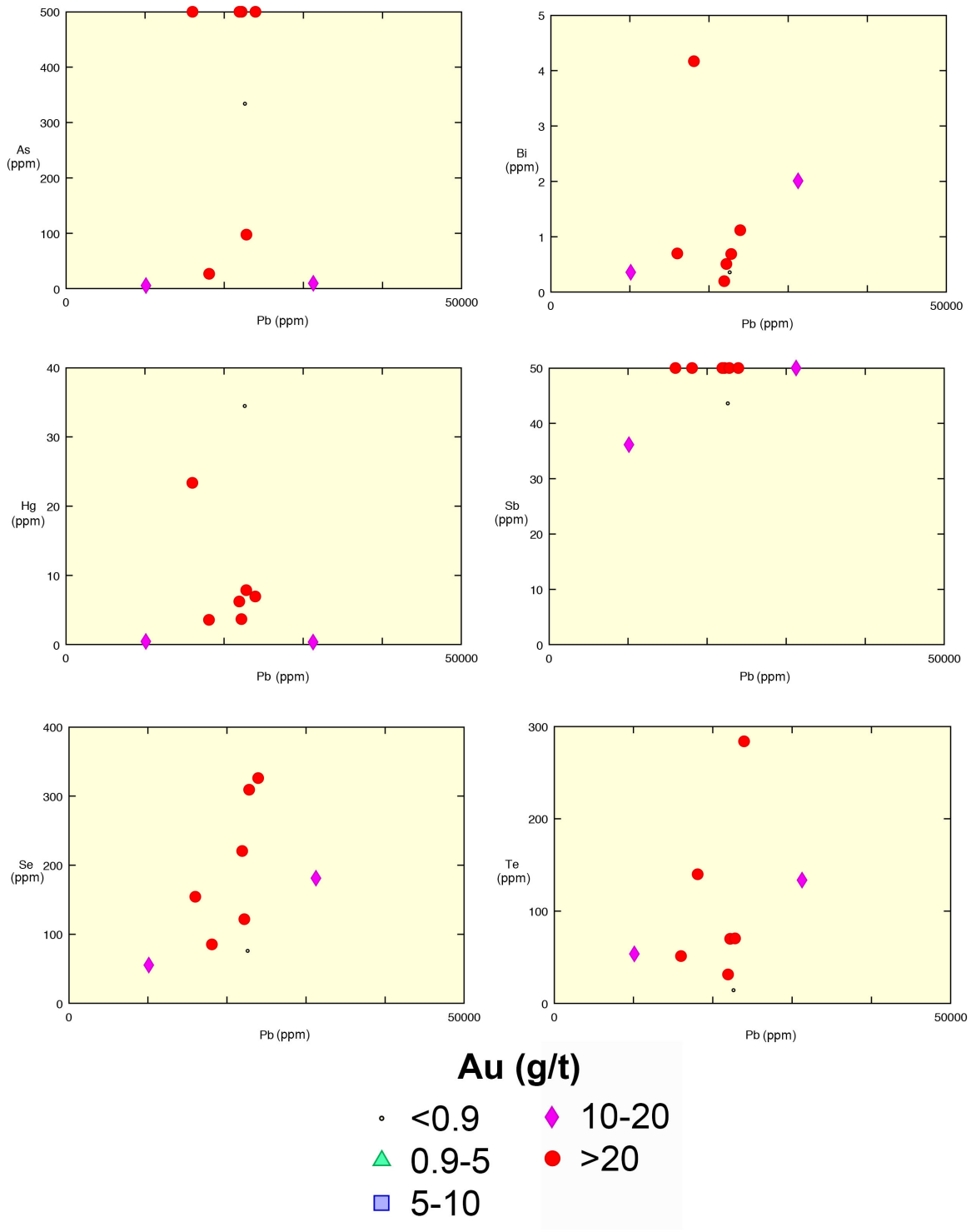

Figure 33: Cu vs. various elements (As, Bi, Hg, Sb, Se, Te) and Au tenor; sub-selected from Figure 25. The elements exhibit similar chemical behavior as gold (Phillips and Powell, 2010) and were selected to evaluate a correlation with Cu. Samples exceeding the upper detection limits are plotted at those limits (As 500 ppm).

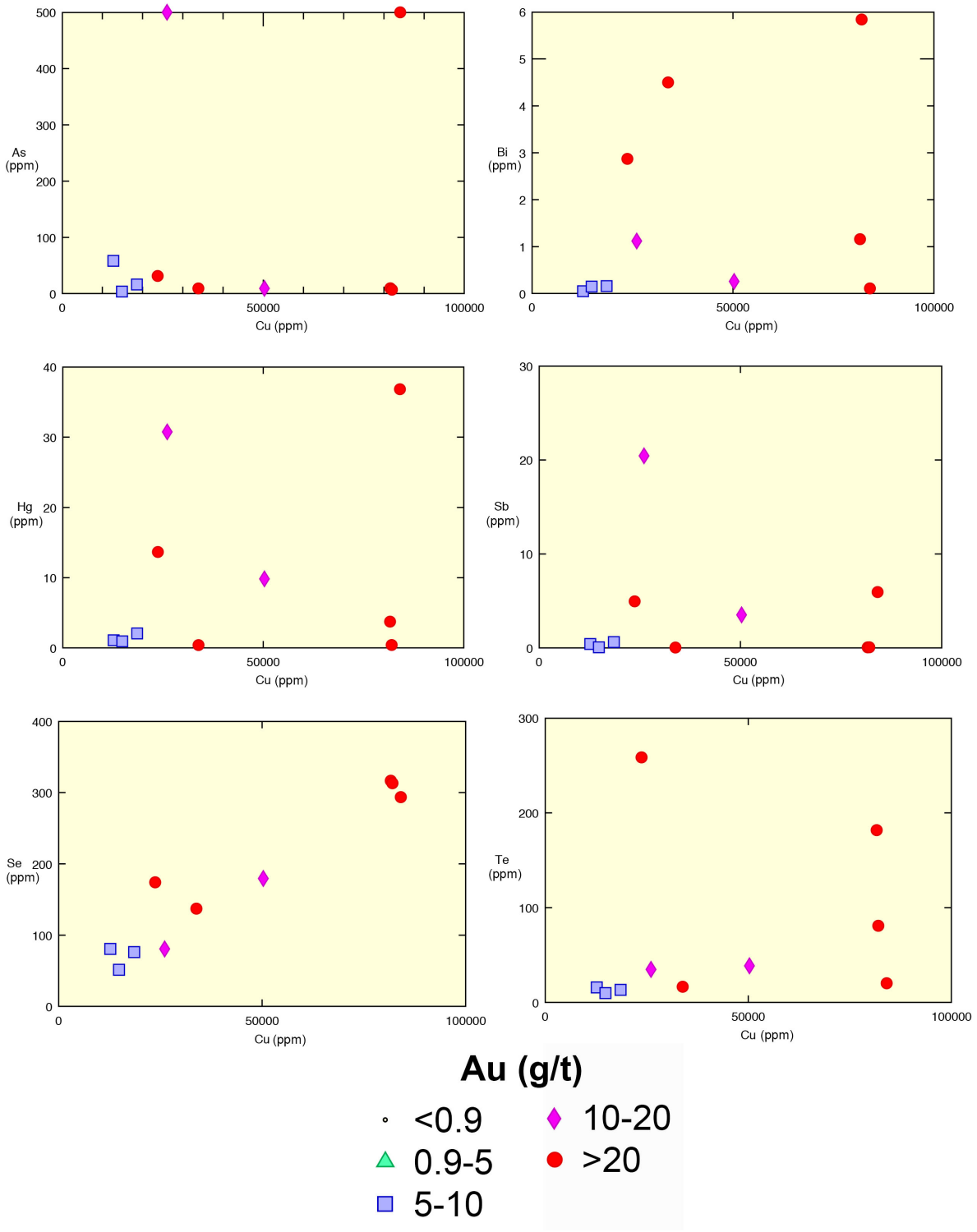

Figure 34: Au vs. various elements (As, Bi, Hg, Sb, Se, Te) and Au tenor (JLSL samples). The elements exhibit similar chemical behavior as gold (Phillips and Powell, 2010) and were selected to evaluate a correlation with Au. Samples exceeding the upper detection limits are plotted at those limits (As 500 ppm, Sb 50 ppm).

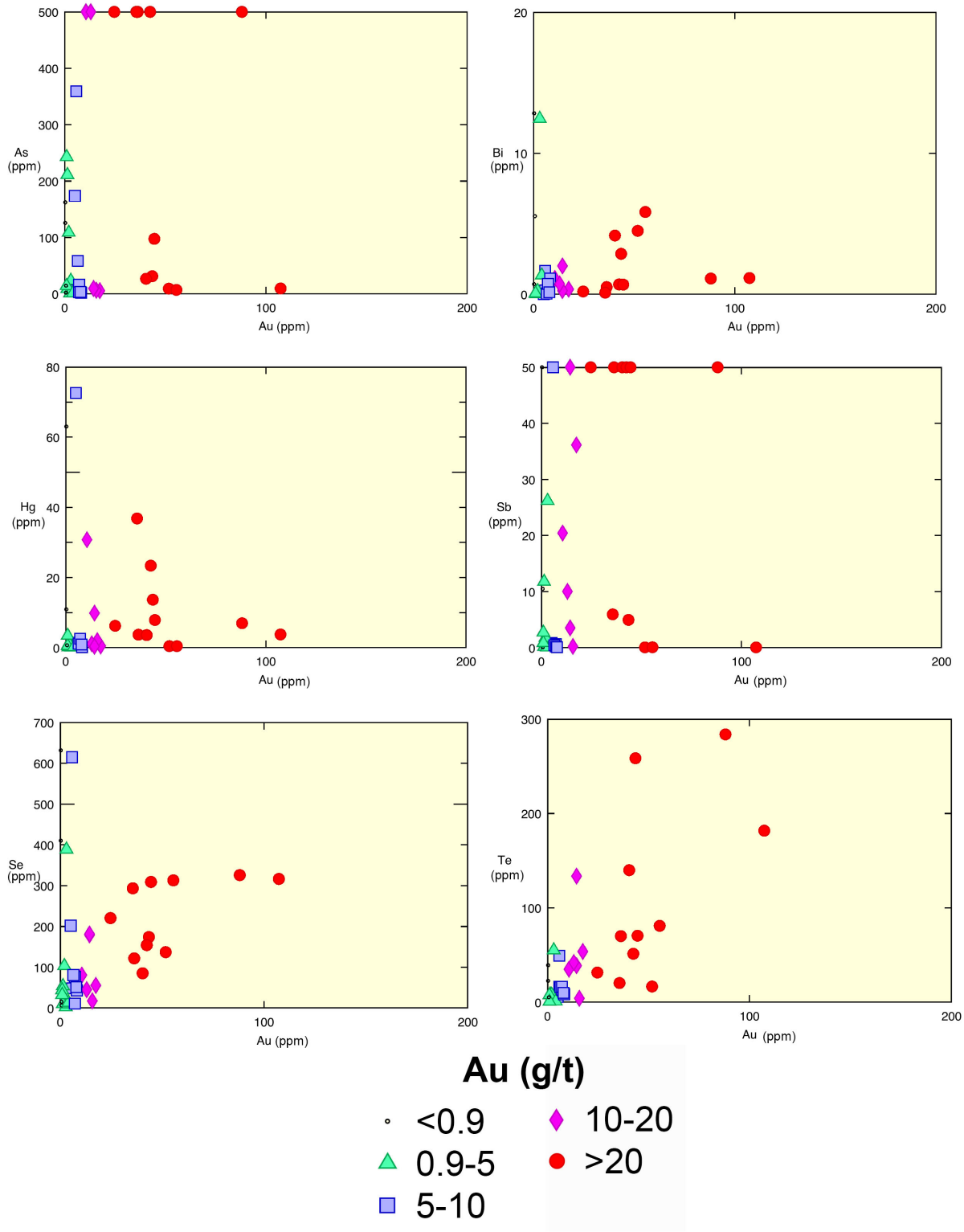

Figure 35: Ag vs. various elements (As, Bi, Hg, Sb, Se, Te) and Au tenor (JLSL samples). The elements exhibit similar chemical behavior as gold (Phillips and Powell, 2010) and were selected to evaluate a correlation with Ag. Samples exceeding the upper detection limits are plotted at those limits (As 500 ppm, Sb 50 ppm).

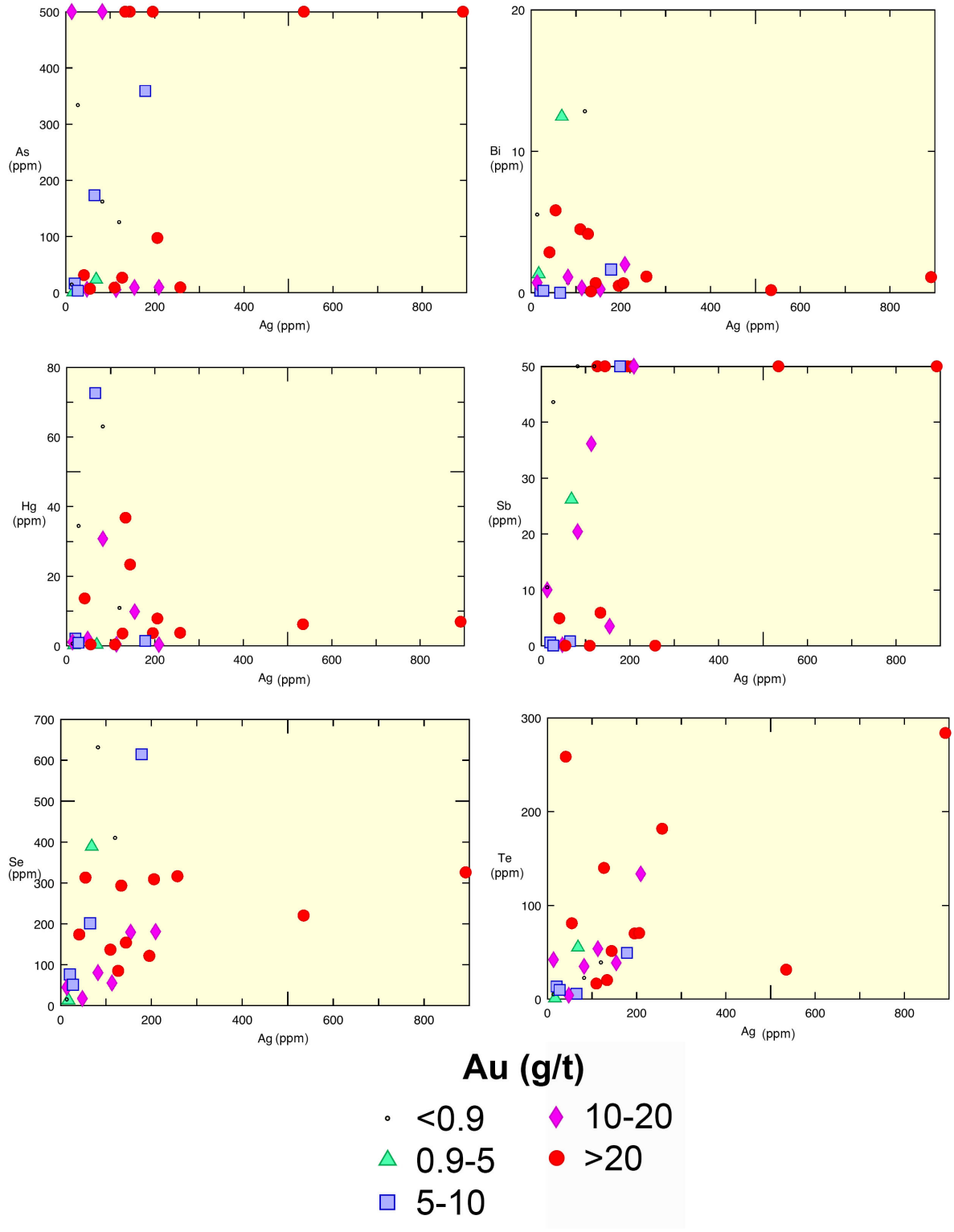

Figure 36: Photomicrograph examples of Ky/Sil-Ms-Bt rocks: Prograde metamorphic assemblage A) Ky-Bt ± Ms (JLSL-27100 from LP0008 ~139 m) and peak metamorphic assemblage B) Sil-Bt ± Ms (JLSL-27011 from DUB172 ~939 m). Where Ky and Sil are present, Sil is replaces Ky (C, JLSL-27021 from DUB172 ~1002 m). Staurolite occurs in some samples as a prograde phase that is reacting out, and forming Ky in this case (D, JLSL13-034 from DUB191 ~1032 m).

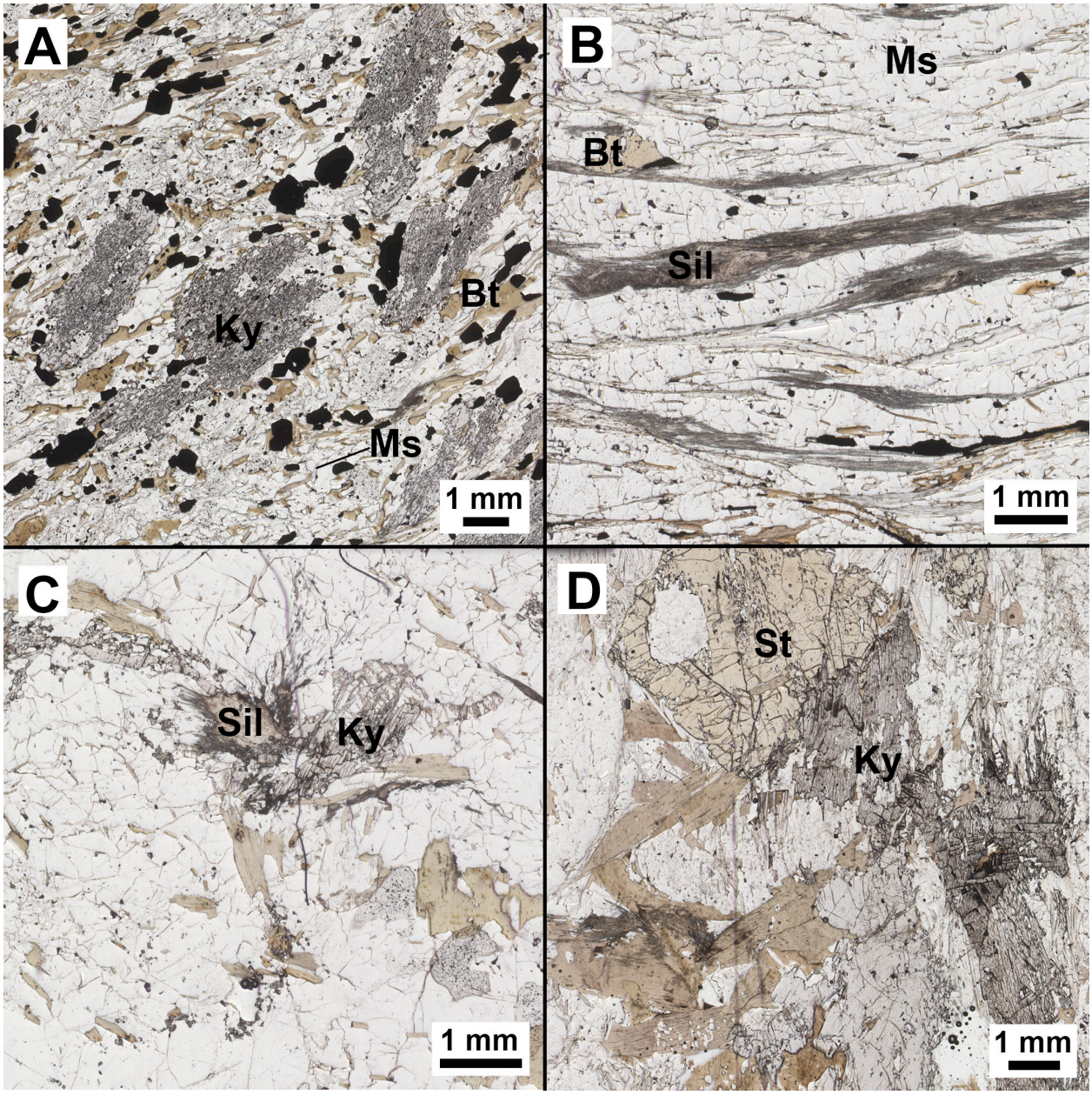

Figure 37: Photomicrographs of metamorphosed Fe-Mg altered rocks: A) Grt-St-Bt-Crd-Ath-Chl (JLSL-26090 from DUB252W01 ~1155 m), B) "Transitional" Fe-Mg altered rocks like Grt-St-Bt-Chl (JLSL-27149 from LP0017 ~83 m), and C) Strong Fe-Mg altered rocks: Grt-Ath-Crd (JLSL-26093 from DUB252W01 ~1169 m).

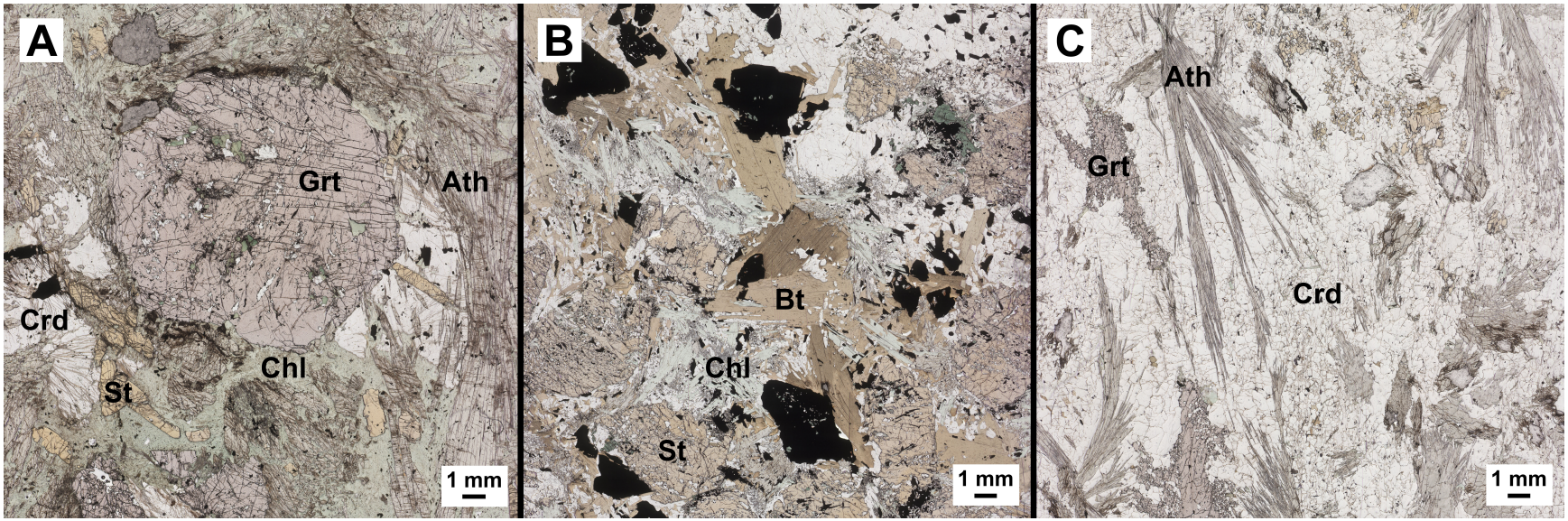

Figure 38: Photomicrographs of calc-silicate to carbonate silicate rocks. Peak metamorphic assemblages are shown in PPL and XPL for A), B) Cc-Tr-Chl ± Di ± Tlc (JLSL-27126B from DUB250 ~827 m) and C), D) Act-Ep (JLSL-27122 from DUB250 ~712 m).

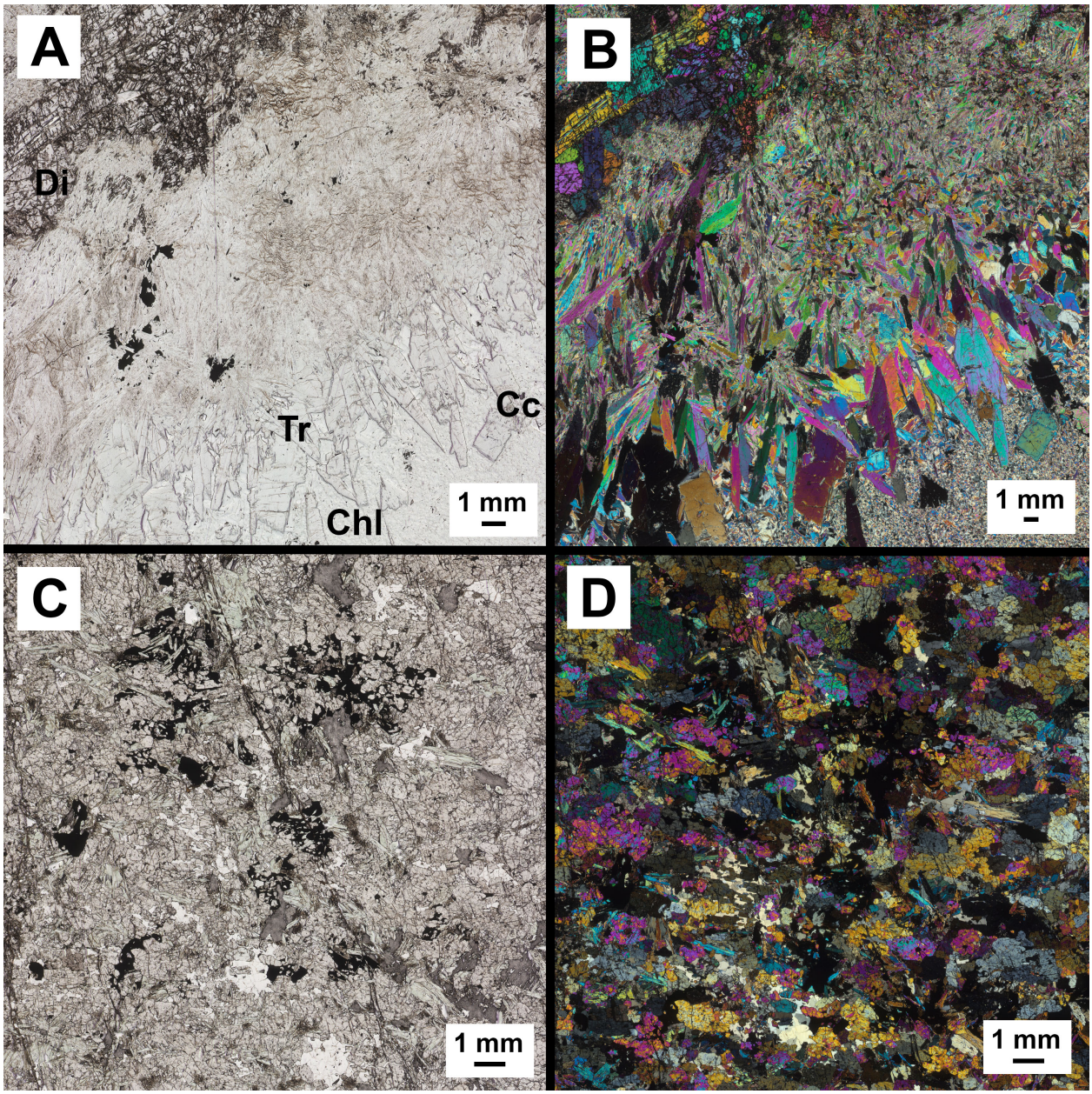

Figure 39: Remnant dolomite indicates that decarbonation reactions have occurred. Example shown is JLSL-26069 (from DUB252W01 ~1022 m): A) In drill core, B) In thin section – PPL, and C) In thin section – XPL.

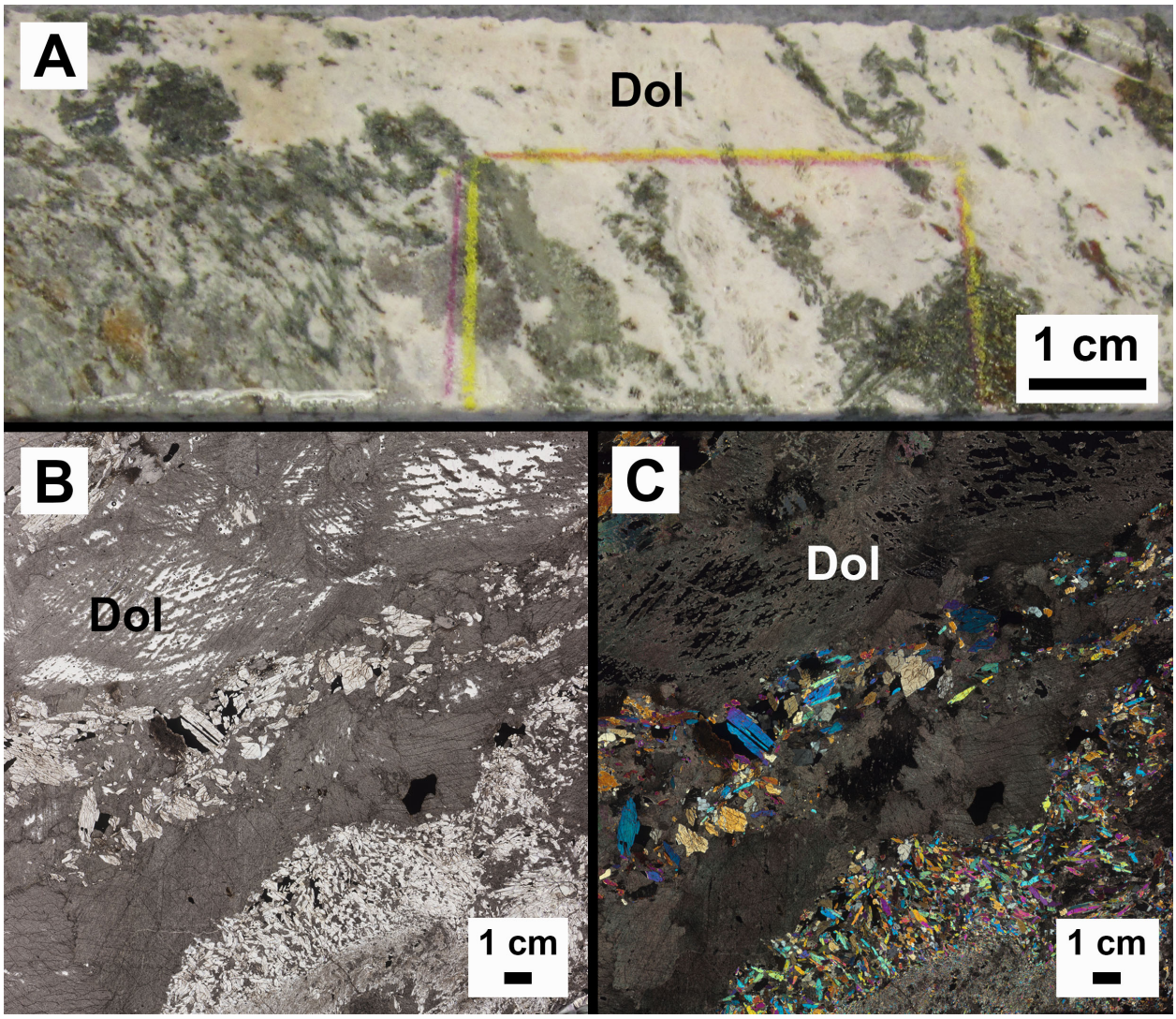

Figure 40: Calcic amphiboles (actinolite) occur as stable porphyroblasts in a Fe-Mg altered rock (JLSL-27083 from LP0008 ~35 m) in A) PPL and B) XPL.

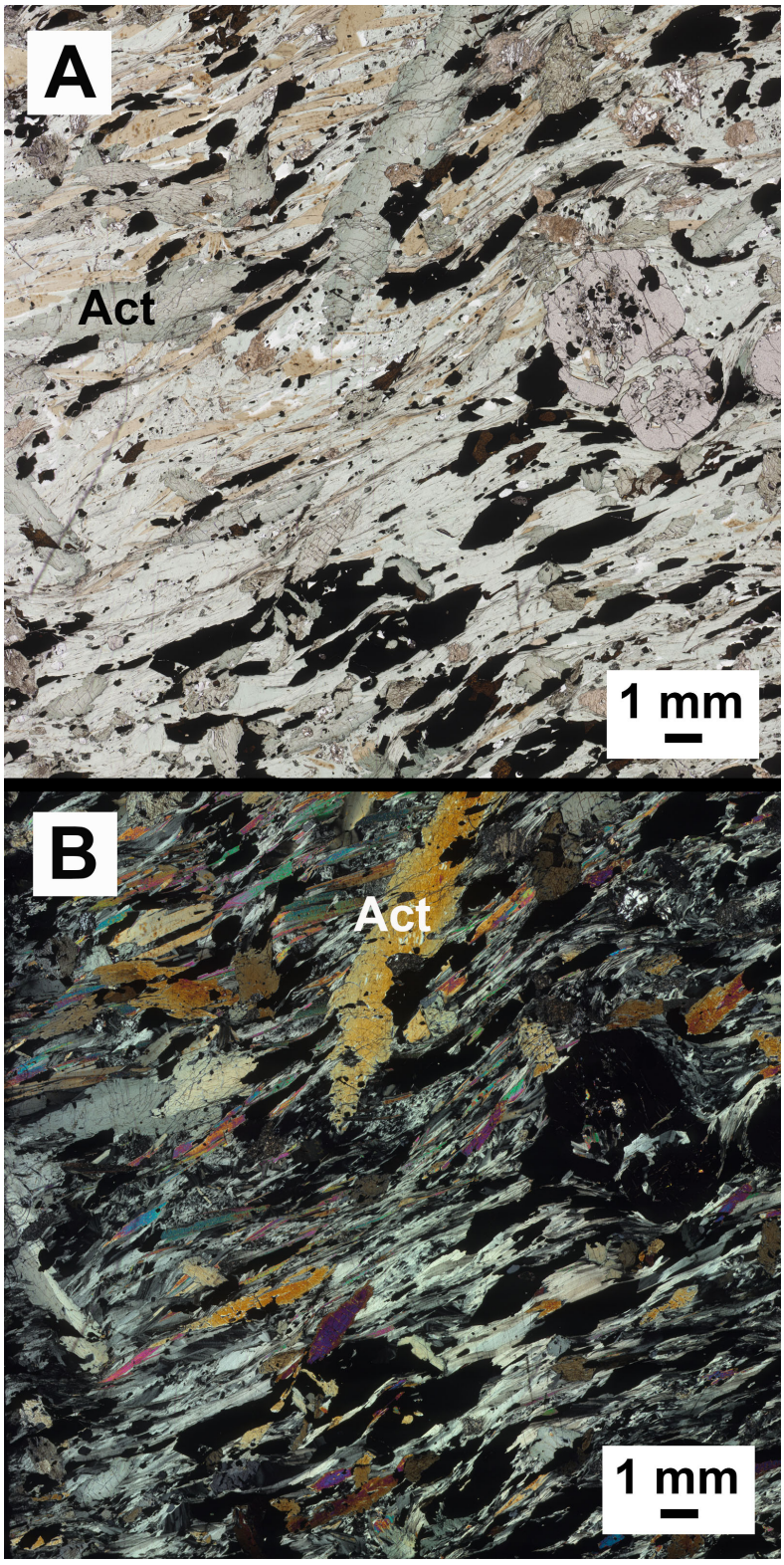

Figure 41: Anhydrite appears to be stable in a Fe-Mg altered rock (JLSL-27083B from LP0008 ~35 m), but it is often found as a remnant phase as in A) PPL and B) XPL.

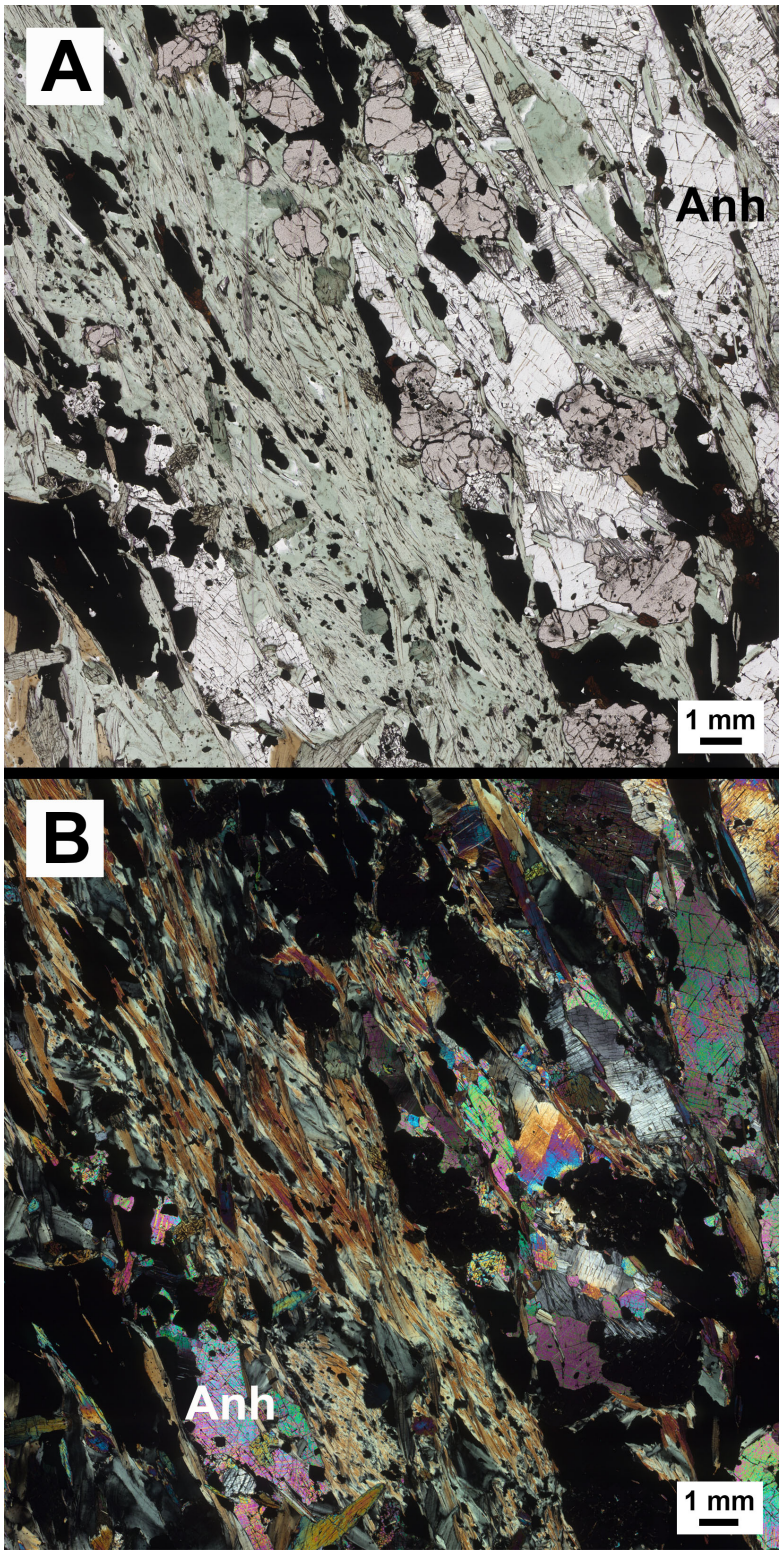

Figure 42: Sulfides observed in drill core: Pyrite, Chalcopyrite, Pyrrhotite, Sphalerite, Galena, and Arsenopyrite (A: JLSL-27094 from LP0008 ~113 m, B: JLSL-27097 from LP0008 ~121 m).

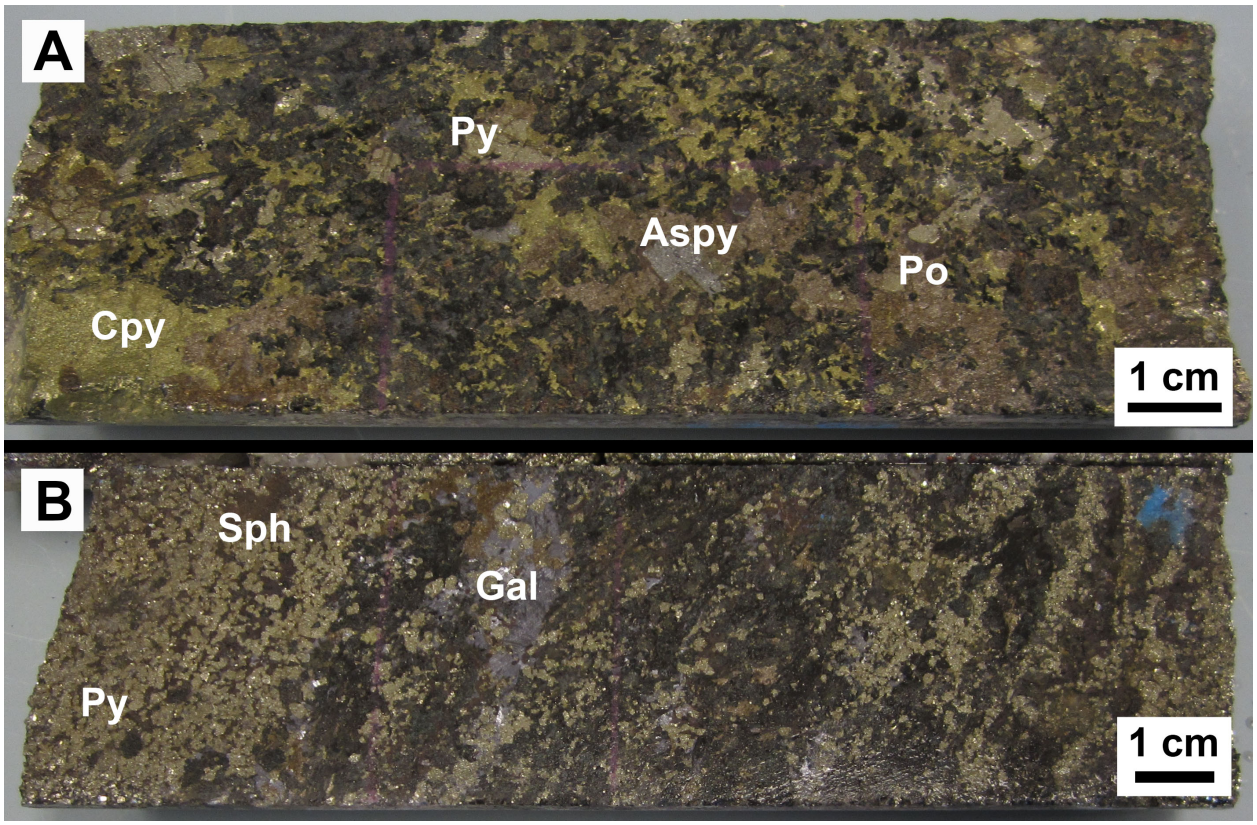

Figure 43: Photomicrographs of gahnite forming from A) the breakdown of sphalerite (JLSL-27148A) and to a lesser extent, B) the breakdown of staurolite (JLSL-27010). Euhedral gahnite occurs with mottled sphalerite and staurolite, indicating it is forming at the expense of those minerals.

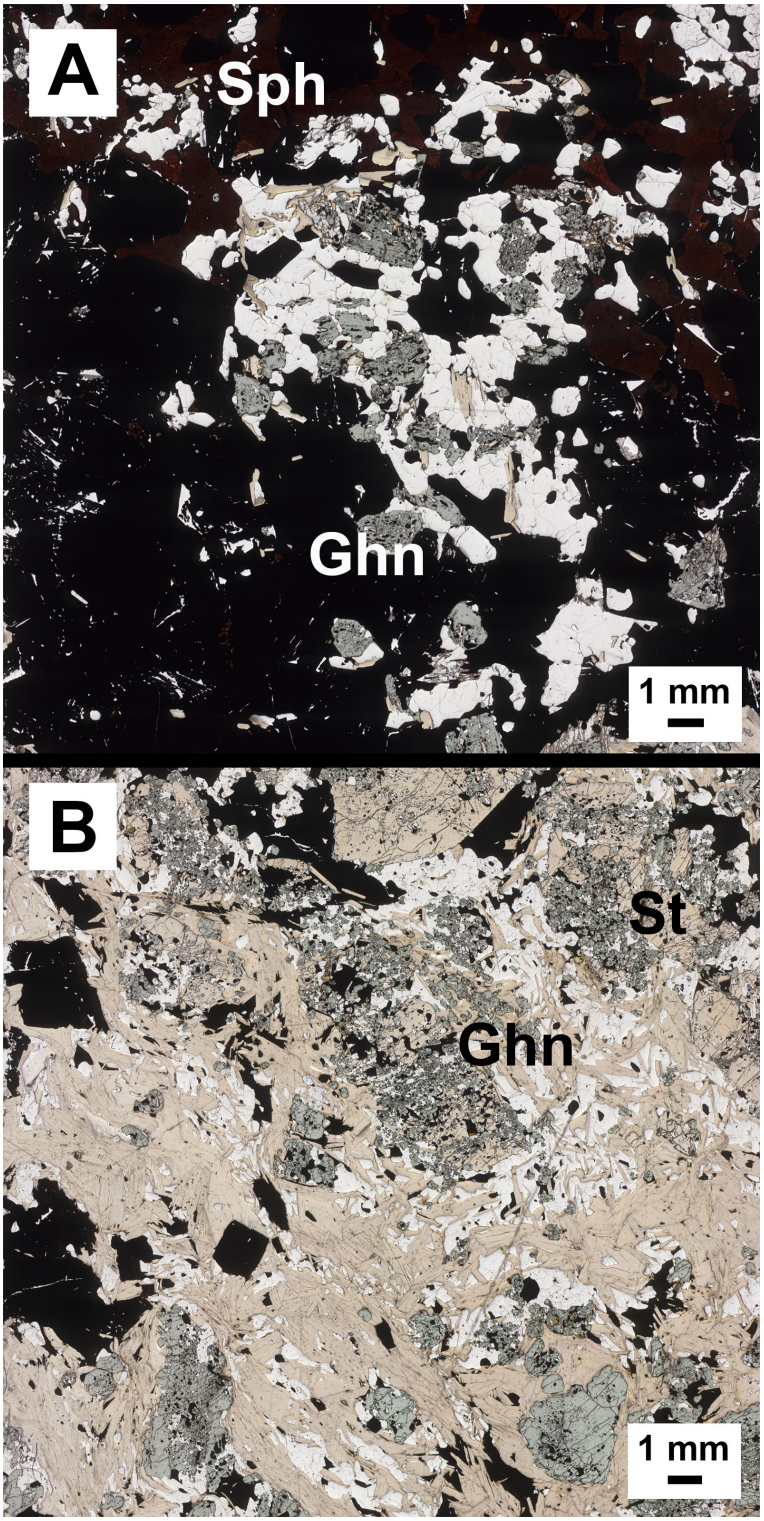

Appendices

The appendix consists of five sections. Appendix 1 contains the graphic logs for section 5200N, 5400N and 5600N. The graphic logs are for the drill holes logged and include the locations of Hudbay delineated ore zones within each drill hole. Appendix 1.1 consists of the logged drill holes along section 5200N, including the underground drill holes. Appendix 1.2 consists of the graphic logs for logged drill holes along section 5400N and 5600N. Appendix 2 is a petrography table that contains the petrography data for all the thin sections made and studied.

The rest of the appendix comprises: 3) Major element geochemistry data; 4) Summary tables of ore zones (base metal and gold); and 5) Drill hole reports. Appendix 3 is a table of the major element geochemistry of samples that were selected for research grade analyses. Appendix 4 is a summary table of the Hudbay delineated ore zones encountered during logging and their characteristics (depth, host rock, mineralization style, and metal associations as per assays). Appendix 5 consists of summary reports for each drill hole logged, as well as descriptions of the intervals within the drill hole where assay data indicated gold mineralization.

Appendix 1.1: Graphic logs from the 5200N section

5200N Section: Underground Drilling

*Hole drilled upwards at a shallow angle from the footwall of the 10 lens

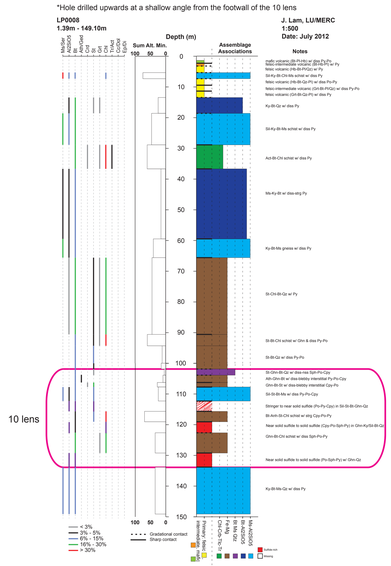

*Hole drilled upwards at a high angle from the footwall of the 10 lens

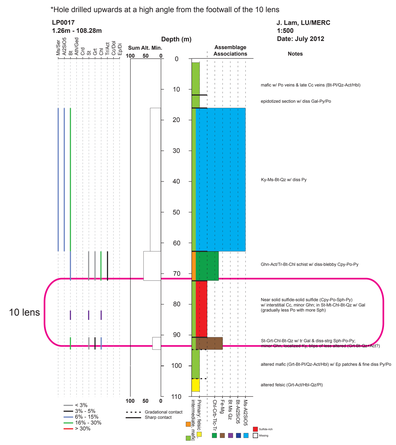

*Hole drilled down at a shallow angle from the footwall of the 10 lens

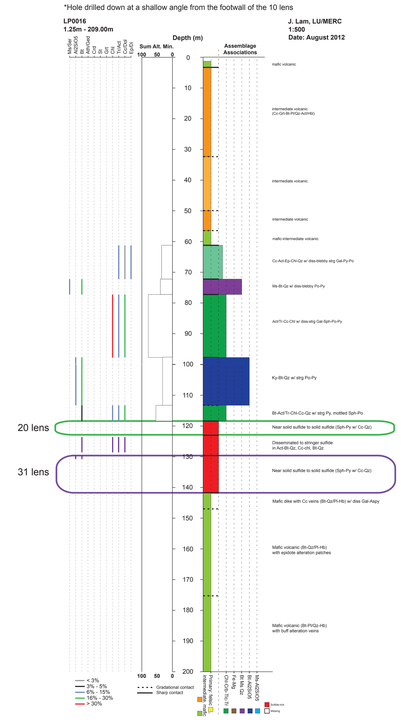

*Hole drilled down at a high angle from the footwall of the 10 lens

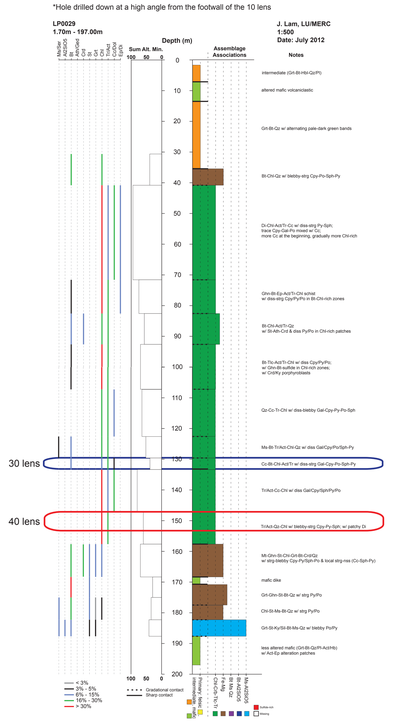

5200N Section

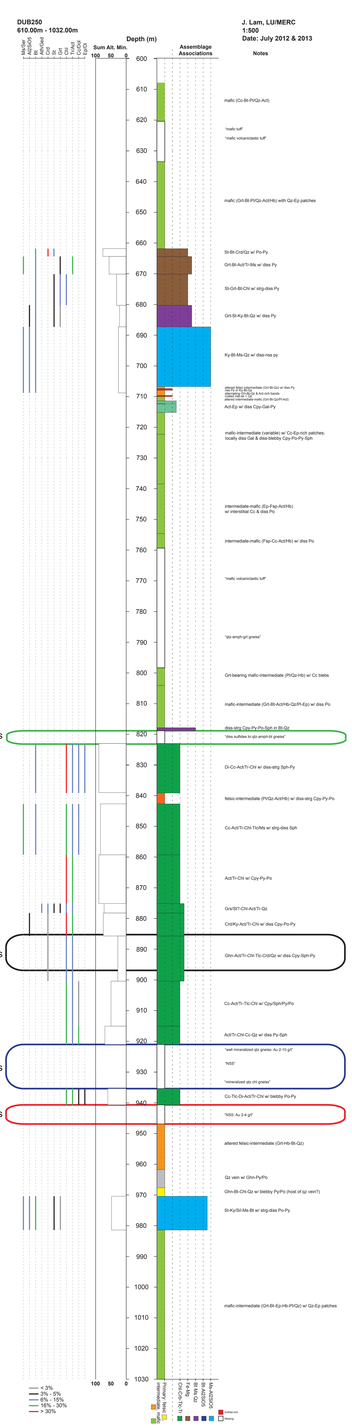

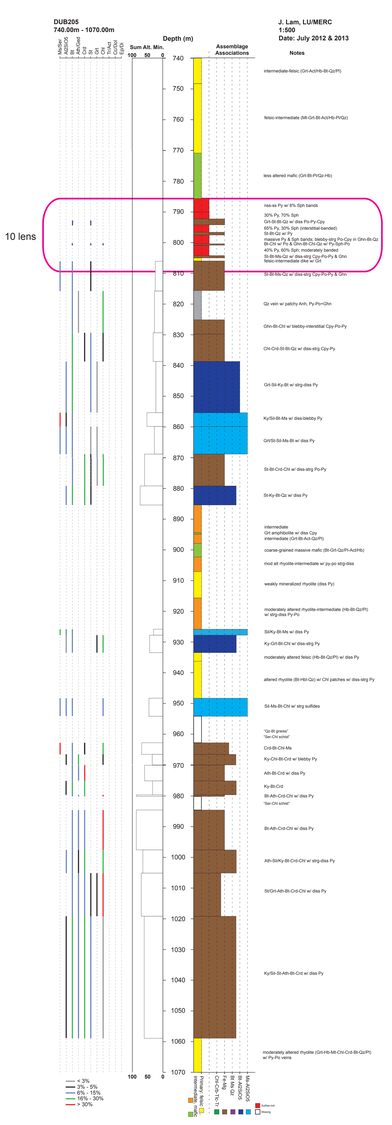

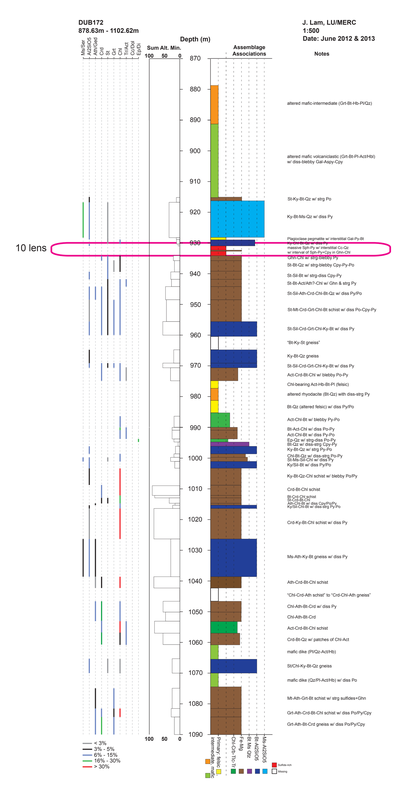

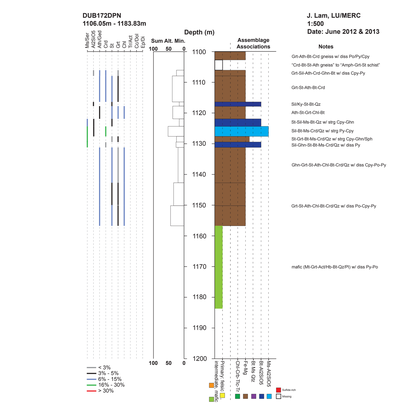

Appendix 1.2: Graphic logs from the 5400N and 5600 sections

5400N Section

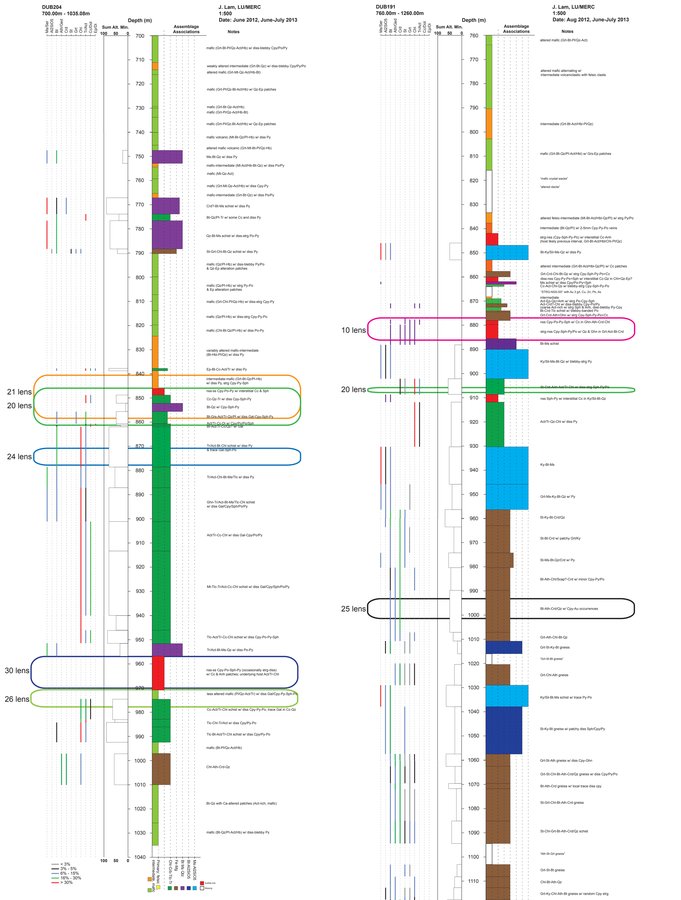

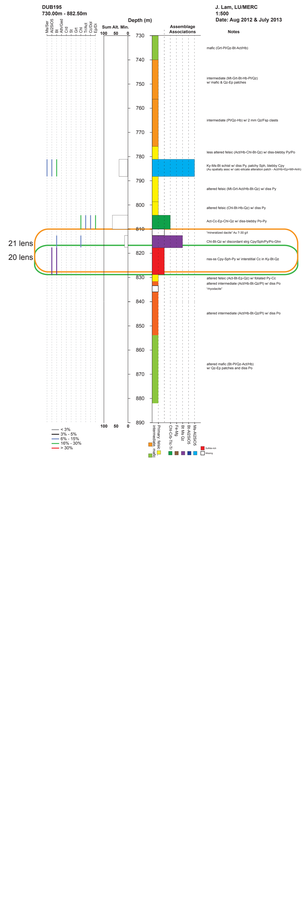

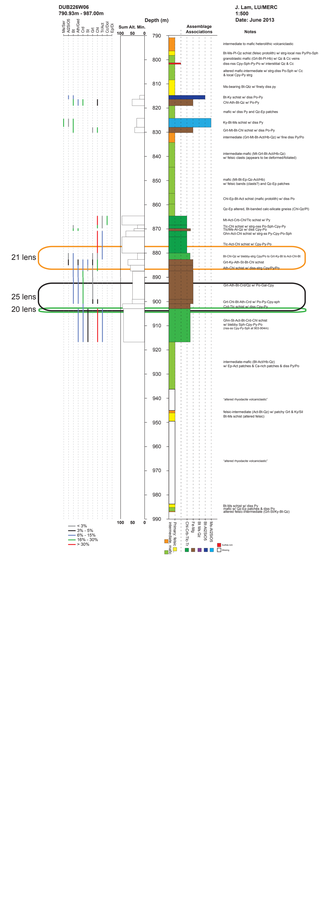

5600N Section

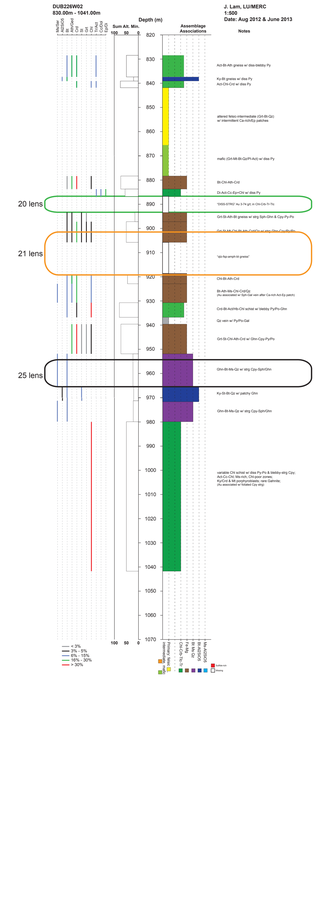

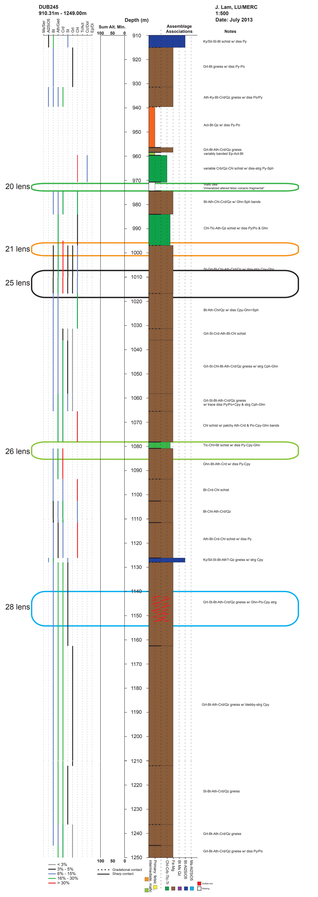

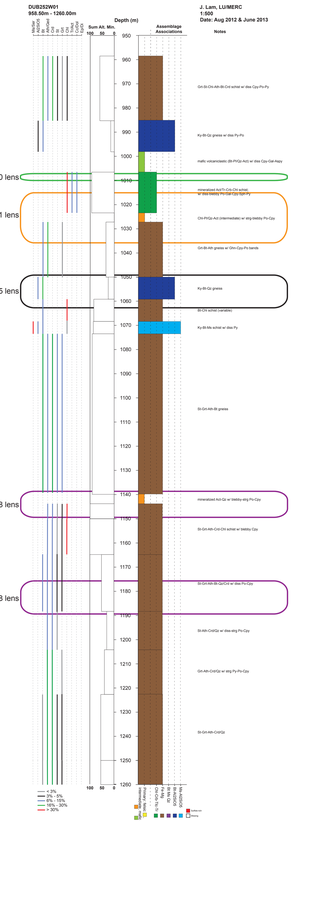

Appendix 2: Petrography Table

Sample	27002	27003	27006	27007A	27007B	27008	27010	27011	27015	27018A	27018B	27020
DDH	DUB172	DUB172	DUB172	DUB172	DUB172	DUB172	DUB172	DUB172	DUB172	DUB172	DUB172	DUB172
Depth (m)	906.78	909.08	923.89	928.15	928.15	932.46	935.16	939.38	944.02	974.97	974.97	1000
Location	5200N, HW10	5200N, HW10	5200N, HW10	5200N, HW10	5200N, HW10	5200N, 10 lens	5200N, FW10	5200N, FW10	5200N, FW10	5200N	5200N	5200N
Logged Rocktype	mafic volcaniclastic	mafic volcaniclastic	ky-bt-ser + diss sulf	plagioclase pegmatite	plagioclase pegmatite	ghn-chl w/ blebby sulf	ghn-st-bt-qz	sil-bt-ms + diss-fol cpy-po	ghn-bt-sulf	ep-grs-anh-cc	ep-grs-anh-cc	chl-bt-qz + diss-strg po-py
Assemblage Association	mafic	mafic	Ky-Bt-Ms			FeMg	FeMg	Sil-Bt-Ms	FeMg	Ca-altered	Ca-altered	FeMg (crd-pinite?-sulf)
LGC		x		x	x							
SEM	x			x		x						
Ath-Ged												
Cumm-Gru												
Tr-Act												
Act-Hbl	20	20							x	?	tr	
Chl	tr	tr				35			x			x
Tlc												
Bt	7	2		5	20	3	20	5	x			x
Wmca			5					10			x	
Ky			10									
Sil			7					15				
And												
Crd												x
Grt	1	2								x		
St							2	2	x			
Carb.						tr						
Cal										x		
Dol												
Ank												
Ep									5	x	x	
Zo/Czo												
Di												
Scp												
Anh										x	x	
Ttn												
Kfsp				x								
Pl	30	35	35	80	60	20						x
Qtz	35	25	12		3	15	40	50	50	2	x	
Ap		3										
Ghn						8	10		x			
Opaques	8	12	31	6		15	18	12	12			tr
SUM	101	99	100			96	90	94				
Ilm/Hem												
Rt												
Mt										x	x	
Sph			1			2			x			
Ccp	2	5	tr	2	x	3	5	1	x			tr
Py		tr	30	1	x	1	3	3	x	2	5	tr
Po	2	1		tr	x	9	10	7	x			tr
Gn	4	7		3	x							
Apy	x	x										
Sum Sulf	8	13		6		15	18	11				
Other Notes	no obv foln, Au 8 gt	grt cluster w/ blebby sulfides; sulfides in grain boundaries & included into grts, Au 24 gt	py follows foliation; ky porphyroblasts; sil-ky appear to be stable	Bt occurs interstitially, sulfides appear to be in fractures (late), Fsp sericitized		sulfides occur in primarily in fractures and as inclusions within ghn	sulfides occur dominantly included into Ghn+St but also in grain boundaries and cleavages	sulfides occur in main foliation; st likely prograde, not longer stable looking	ep occurs assc with Camp			
Paragenesis	minzn occurs diss-blebby - appears to be syn-post as it occurs between grains and in fractures	minzn occurs in fractures & grain boundaries thus syn-post; pro Grt subhedral, retro Chl euhedral	euhedral py indicates minzn occurs post-tectonic, but occurs in foliation so likely syn			sulfides are pre-peak met ghn formation, syn- Bt	sulfides occur pre-Ghn formation; possibly syn-post Bt	sulfides appear to be syn-post peak met				

Appendix 2: Petrography Table

Sample	27021	27023	27024	27025	27028	27029	27029A	27033	JLSL13-043A	JLSL13-043B	27102	27103
DDH	DUB172	DUB172	DUB172	DUB172	DUB172	DUB172	DUB172	DUB172	DUB172	DUB172	DUB205	DUB205
Depth (m)	1002.66	1012.37	1014.29	1106.15	1123.32	1127.52	1127.52	1156.49	1088.2	1088.2	787.22	804
Location	5200N	5200N	5200N	5200N	5200N	5200N	5200N	5200N	5200N	5200N	5200N, 10 lens	5200N, 10 lens
Logged Rocktype	ky-sill-bt-qz w/ diss py/po	bt-crd-chl	st-crd-bt-chl	ghn-chl-ath-qz +cpy	grt-sill-bt-qz +cpy	Sil-Bt-Ms-Crd/Qz +cpy	Sil-Bt-Ms-Crd/Qz +cpy	Grt-St-Ath-Chl-Bt-Crd/Qz	grt-ath-bt-crd	grt-ath-bt-crd	pyritized ky-ser-bt schist	bt-qz rich w/ strg-nss cpy
Assemblage Association	Ky/Sil-Bt	FeMg	FeMg	FeMg	Sil-Bt	Ms-Qz	Ms-Qz	FeMg (anh-pinite?-crd)	FeMg	FeMg	Ky-Ms-Bt	MS
LGC												
SEM												
Ath-Ged				x					30	20		
Cumm-Gru												
Tr-Act												
Act-Hbl								x				
Chl	x	x	x	x				x				
Tlc												
Bt	x	x	x	x	25	8	8	x	1		x	5
Wmca						7	5	x			x	
Ky	x		x								x	
Sil	x										x	
And												
Crd		x		x				x				
Grt			x									
St	?					3	2					
Carb.					x							
Cal												
Dol												
Ank												
Ep												
Zo/Czo												
Di												
Scp												
Anh								x				
Ttn												
Kfsp												
Pl	x									10	x	
Qtz	x		x	x	50	70	70		25	10	x	75
Ap												
Ghn					7		5		15	2		1
Opaques	tr				10	12	8		14			9
SUM					92	100	98		85			90
Ilm/Hem												
Rt												
Mt	tr							x				
Sph				tr	2	1	1		1		x	1
Ccp				x	7	9	5		10	2	x	5
Py	tr	x	tr	x	tr		tr	x	tr	tr	x	tr
Po			2	x	1	2	2	x	3	3	x	3
Gn												
Apy												
Sum Sulf												
Other Notes	st looks unstable / or is it inclusion-rich ky	bt growing off chl; crd porphyroblasts			Au 2 gt; mod-wk fol; loc qz vein, loc cc vein; sulfide diss-strg	Au 1 gt; strg cpy/sulf loc in foln; ghn likely from sph breakdown; some st occurs w/ no inclusions	Au 1 gt; sulfides loc in bt (80%) rich part; st looks remnant; ghn from sph breakdown		sulfides occur prox to ghn (like bc was prev sph) and in grain boundaries	wk foln; some sulfides occur in inclusions or veins		Au 10 gt; mod fol; qz-rich
Paragenesis					sulfides concd around veins so likely later; bt is peak; ghn forms at peak from sph breakdown	sulfides in foliation and occ in fractures; loc so syn-post met; st prograde, bt-ms peak +ghn	sulfides occur loc to bt-rich feature; bt appears to be peak so sulfides are likely syn					bt-ghn peak assemblage; sulfides are syn-post

Appendix 2: Petrography Table

Sample	27104	27109	27110	27114	27118	27121A	27122	27123	27124	27125	27126A	27126B
DDH	DUB205	DUB205	DUB205	DUB250	DUB250	DUB250	DUB250	DUB250	DUB250	DUB250	DUB250	DUB250
Depth (m)	811.87	1017.84	1018.78	661.18	667.04	711.45	712.67	714.85	749	799.2	827.25	827.25
Location	5200N, FW10	5200N	5200N	5200N	5200N	5200N	5200N	5200N	5200N	5200N	5200N, FW20	5200N, FW20
Logged Rocktype	st-bt-qz +ms	ath-bt-crd-chl w/ diss py	ath-bt-crd-chl w/ diss py	diss cpy-py in qz vein	st-chl-bt-qz w/ anh-py/po	act-ep	ep-act	ep-act	crb in po-ep-act	cc in grt-bt-amph	di-cc-act/trm-chl +sph-py	di-cc-act/trm-chl +sph-py
Assemblage Association	FeMg	FeMg (anh-pinite?-sulf)	FeMg	felsic	FeMg	Ca-altered	Ca-altered	Ca-altered	mafic	mafic	Calc-Crb	Calc-Crb
LGC												
SEM												
Ath-Ged			x									
Cumm-Gru												
Tr-Act											x	
Act-Hbl				x			x	x	x	x		
Chl		x	x	x	x						x	
Tlc												
Bt	4	x	x	x			x					
Wmca											x	
Ky	tr											
Sil	3											
And												
Crd			x									
Grt					x					x		
St	2	x			x							
Carb.											x	
Cal						x	x		x	x	x	
Dol												
Ank												
Ep						x	x	x	x	x		
Zo/Czo												
Di						x						
Scp												
Anh		x			x							
Ttn												
Kfsp												
Pl				x					x	x		
Qtz	70	x	x	x	x	x	x	x		x		
Ap					x							
Ghn	2	x	x									
Opaques	15			10								
SUM	96											
Ilm/Hem				?	?							
Rt												
Mt												
Sph	tr	x				x						
Ccp	2		x	x		2	x	x	x	x	x	
Py	12	x	x	x	x	4	x	x			x	
Po	1	x	x	x	x	3		x	x	x		
Gn				x		1		x				
Apy							x					
Sum Sulf												
Other Notes	Au 2 gt; diss sulfides in foliation; ghn-st loc to cpy vein			Au 3 gt, qz-rich phase in matrix w/ Gn		Au 26 gt; diss cpy-py (sulfides), ghn-sulf vein	Au 8 gt; diss Gn	Au 2 gt; qz vein in ep-act w/ blebby Po-Gn				
Paragenesis	sulfides pre-peak; sil form after ky; bt also peak											

Appendix 2: Petrography Table

Sample	27127	27128	27129	27131	27132	27133	27133B	27134	27135	27136	27137	27138
DDH	DUB250	DUB250	DUB250	DUB250	DUB250	DUB250	DUB250	DUB250	DUB250	DUB250	DUB250	DUB250
Depth (m)	829.33	843.55	839.51	879.92	889.86	896.3	896.3	1012	975.77	962.58	938.11	920.81
Location	5200N, FW20	5200N	5200N	5200N	5200N, 25 lens	5200N, 25 lens	5200N, 25 lens	5200N	5200N	5200N	5200N, bw 30 40	5200N, HW30
Logged Rocktype	di-cc-act/trm-chl +sph-py	cc-act/trm-chl-tlc/ms	ep-altered	crd/ky-act/tr-chl	ghn-act/tr-chl tlc-crd/qz	tlc-ghn-chl	tlc-ghn-chl	interlayered bt- vs act-rich	grt-st-ky-bt	qz vein w/ ghn+sulf	cc-tlc-di-act/tr-chl +py/po	act/tr-chl-cc-qz +sph-py
Assemblage Association	Calc-Crb	Calc-Crb	Ca-altered	FeMg to Calc-Crb	FeMg to Calc-Crb	FeMg to Calc-Crb	FeMg to Calc-Crb	mafic	Ky-Bt-Ms		Calc-Crb	Calc-Crb
LGC												
SEM												
Ath-Ged												
Cumm-Gru												
Tr-Act	x				x						x	x
Act-Hbl			1					x				
Chl	x			x	x	x				x	x	x
Tlc		x				x						
Bt		tr			x	x		x		x		
Wmca		x		x	x						x	
Ky					?							
Sil												
And												
Crd		x		x	x	x						
Grt								x				
St												
Carb.												
Cal	x									x		x
Dol												
Ank												
Ep			25									?
Zo/Czo			25									
Di												
Scp												?
Anh	x											x
Ttn												
Kfsp												
Pl			20					x				
Qtz		x	20									
Ap												
Ghn					x	x				x		
Opaques			8									
SUM			99									
Ilm/Hem												
Rt												
Mt												
Sph	x				x	x						x
Ccp	x		tr	x	x	x						x
Py	x	x	1	x	x					x	x	x
Po		x	7	x	x	x		x		x	x	x
Gn	x											x
Apy												
Sum Sulf			8									
Other Notes			well-foliated (incl diss-strg sulfides); Au 8 gt		Au 11 gt; diss cpy	Au 9 gt						
Paragenesis												

Appendix 2: Petrography Table

Sample	27140	27141	27078	27081	27082	27083	27083B	27085	27086	27089	27090	27091
DDH	DUB250	DUB250	LP0008	LP0008	LP0008	LP0008	LP0008	LP0008	LP0008	LP0008	LP0008	LP0008
Depth (m)	905.4	904.32	4.28	24.51	32.64	35.12	35.12	61.36	68.32	93.91	105.06	106.52
Location	5200N, FW25	5200N, FW25	5200N, FW10	5200N, FW10	5200N, FW10	5200N, FW10	5200N, FW10	5200N, FW10	5200N, FW10	5200N, FW10	5200N, 10 lens	5200N, 10 lens
Logged Rocktype	tlc-ser-qz	crb-chl w/ blebby py-cpy	Ky-Bt-Qz	Sil/Ky-Bt-Ms +py	crd-chl	anh-py-chl	anh-py-chl	ky-bt-ms	st-chl-bt +ky/sil+py	ghn-chl-anh-crd	ghn-ath +cpy	st-bt-qz +py-cpy
Assemblage Association	FeMg to Calc-Crb	Calc-Crb	Ky-Bt	Sil/Ky-Bt-Ms	FeMg	FeMg	FeMg	Ky-Bt-Ms	FeMg (anh ok w/ grt-chl?)	FeMg	FeMg	FeMg
LGC												
SEM												
Ath-Ged											15	
Cumm-Gru												
Tr-Act		x										
Act-Hbl						x			x			
Chl	x	x			x	x			x			
Tlc	x											
Bt				x		x			x		20	8
Wmca	x											
Ky				x								
Sil				x								
And												
Crd	x					x						
Grt				x		x			x			
St												15
Carb.												loc in vein
Cal		x							x			
Dol												
Ank												
Ep												
Zo/Czo												
Di												
Scp												
Anh						x			x			
Ttn												
Kfsp												
Pl												
Qtz	x										tr	40
Ap												
Ghn											10	
Opaques												
SUM												
Ilm/Hem												
Rt												
Mt				x	x							
Sph		x		x	x	x					x	x
Ccp	x	x		x	x	x					x	x
Py	x	x		x	x	x			x			x
Po	x	x		x	x						x	x
Gn												
Apy												
Sum Sulf												
Other Notes	Au 2 gt	Au 5 gt		ky w/ bt rims							cpy bleeds into bt cleavages	
Paragenesis												

Appendix 2: Petrography Table

Sample	27092	27093	27094	27095	27097A	27097B	27098	27099	27100	27167	27168	27172
DDH	LP0008	LP0008	LP0008	LP0008	LP0008	LP0008	LP0008	LP0008	LP0008	LP0016	LP0016	LP0016
Depth (m)	109.96	111.67	113.17	117.6	121.1	121.1	126.81	127.85	139.28	41.78	67.23	79.33
Location	5200N, 10 lens	5200N, 10 lens	5200N, 10 lens	5200N, 10 lens	5200N, 10 lens	5200N, 10 lens	5200N, 10 lens	5200N, 10 lens	5200N, HW10	5200N	5200N	5200N
Logged Rocktype	mafic +anh+cpy	sill-st-bt-ms (high silica)	NSS	bt-anh-st-crd-chl	gln+sulf in qz vein	gln+sulf in qz vein	qz vein w/ gln	ghn-bt-chl-qz +sulf	Ky/Sill-Ms-Bt	cc in grt-bt-amph	diss gln+ep prox qz vein	act/tr-cc-chl +di-anh
Assemblage Association	mafic	Sil-Bt-Ms	Sulfide-rich	FeMg (chl-grt-bt-sulf rel)	prox MS	prox MS	in FeMg	FeMg	Ky-Bt-Ms	intermediate	Ca-altered	Calc-Crb
LGC												
SEM												
Ath-Ged												
Cumm-Gru												
Tr-Act											x	?
Act-Hbl	17							x		x		
Chl				x								?
Tlc												
Bt	3	5	10	x		20		x	x	x		
Wmca									x			
Ky									x			
Sil		15										
And												
Crd												
Grt	tr			x						x		
St			5					x	x			
Carb.												
Cal										x	x	x
Dol												
Ank												
Ep											x	
Zo/Czo												
Di												
Scp												
Anh	8			x							x	x
Ttn												
Kfsp												
Pl	5						tr	x	x			
Qtz	40	70	20		90	10	x	x	x			
Ap												
Ghn			7	x		15	x	x				
Opaques												
SUM												
Ilm/Hem												
Rt												
Mt									x			
Sph	x	tr	x	x	x	x	x	x				tr
Ccp		x	x	x	x		x	x		tr	tr	tr
Py	x	x	x	x	x	x	x	x	x	tr		x
Po	x		x	x	x	x	x	x			x	x
Gn					3	x					x	x
Apy												
Sum Sulf												
Other Notes		fol by Sil-Bt										
Paragenesis												

Appendix 2: Petrography Table

Sample	27174	27175	27176	27177	27178	27179	27181	27184	27185	27142	27143	27144
DDH	LP0016	LP0016	LP0016	LP0016	LP0016	LP0016	LP0016	LP0016	LP0016	LP0017	LP0017	LP0017
Depth (m)	87.91	108	114.73	126.35	129.44	137.65	145.24	142.42	130.34	12.65	26.45	33.29
Location	5200N	5200N	5200N, HW20	5200N, bw 20 31	5200N, bw 20 31	5200N, 31 lens	5200N, FW31	5200N, FW31	5200N, 31 lens	5200N	5200N	5200N, HW10
Logged Rocktype	gal vein in act/tr-cc-chl	py-bt-qz	bt-act/tr-chl-cc-qz	chl-crb in MS	MS transition w/ gln	MS w/ gln	mafic dike	mafic dike	cc-act +cpy-aspy	ep w/ diss gln	ky/sill-ms-bt	py-bt-qz
Assemblage Association	Calc-Crb	Ky-Bt-Qz +Py/Po	Calc-Crb	Calc-Crb		Sulfide-rich	mafic	mafic		mafic	Ky-Ms-Bt	Ky-Ms-Bt
LGC												
SEM												
Ath-Ged												
Cumm-Gru												
Tr-Act	x			x	x	x						
Act-Hbl							50	30	x			
Chl	x		x	x	x	x						
Tlc												
Bt		x			x			10				
Wmca									x			
Ky		x										
Sil												
And												
Crd												
Grt												
St												
Carb.												
Cal	x			x		x		x	10			
Dol												
Ank												
Ep												
Zo/Czo												
Di												
Scp												
Anh	x		x									
Ttn												
Kfsp												
Pl		x	x		x			x	3			
Qtz						x	20	40	60			
Ap												
Ghn												
Opaques												
SUM												
Ilm/Hem												
Rt												
Mt												
Sph					x	x						
Ccp			tr		x	tr	2	x	x			
Py	tr	15	x	tr	x	x	tr		x			
Po	tr		tr	x	x	x			x			
Gn	x					x	5	x	x			
Apy							1	x				
Sum Sulf												
Other Notes							Au 71 gt; discontinuous cc veins, fol by act-hb	Au 5 gt; blebby sulfides	Au 7 gt			Au 1 gt
Paragenesis												

Appendix 2: Petrography Table

Sample	27147	27148A	27148B	27149	27150	26038	26039	26040	26044	26046	26047	26048
DDH	LP0017	LP0017	LP0017	LP0017	LP0017	LP0029	LP0029	LP0029	LP0029	LP0029	LP0029	LP0029
Depth (m)	67.13	84.83	84.83	83.52	94.42	32.53	56.14	70.1	115.74	129	138.07	152.22
Location	5200N, HW10	5200N, 10 lens	5200N, 10 lens	5200N, 10 lens	5200N, FW10	5200N, HW20	5200N, FW20	5200N, FW20	5200N, HW30	5200N, HW30	5200N, FW30	5200N, 40 lens
Logged Rocktype	ghn-act/trm-bt-chl	ghn-sph-po-py +gal	ghn-sph-po-py +gal	rep FeMg	st-grt-chl-bt-qz; gal in qz	minzn in qz vein	chl-act/tr-cc +di	anh-cc-trm-chl	qz-cc-trm-chl +sulf	act-crb-ep	tr/act-cc-chl +gln-cpy	di-cc-act/trm
Assemblage Association	Calc-Crb	Sulfide-rich	Sulfide-rich	FeMg in Sulfide-rich	FeMg	intermediate	Calc-Crb	Calc-Crb	Calc-Crb	Calc-Crb	Calc-Crb	Calc-Crb
LGC												
SEM												
Ath-Ged												
Cumm-Gru												
Tr-Act												
Act-Hbl												
Chl												
Tlc												
Bt												
Wmca												
Ky												
Sil												
And												
Crd												
Grt												
St												
Carb.												
Cal												
Dol												
Ank												
Ep												
Zo/Czo												
Di												
Scp												
Anh												
Ttn												
Kfsp												
Pl												
Qtz												
Ap												
Ghn												
Opaques												
SUM												
Ilm/Hem												
Rt												
Mt												
Sph												
Ccp												
Py												
Po												
Gn												
Apy												
Sum Sulf												
Other Notes							Au 2 gt; diss sph	Au 1 gt; diss cpy		Au 1 gt; blebby py	Au 11 gt; diss gln-cpy	
Paragenesis												

Appendix 2: Petrography Table

Sample	26049	26050	26053	27188	27190	27191	27192A	27192B	27193	27194	27195	27196
DDH	LP0029	LP0029	LP0029	DUB191	DUB191	DUB191	DUB191	DUB191	DUB191	DUB191	DUB191	DUB191
Depth (m)	160.09	162.49	183.11	848.29	879.67	905.03	911.58	911.58	919.61	925.9	937.53	957.83
Location	5200N, FW40	5200N, FW40	5200N, FW40	5400N, HW10	5400N, 10 lens	5400N	5400N, 20 lens	5400N, 20 lens	5400N, FW20	5400N, FW20	5400N	5400N
Logged Rocktype	chl-act-sulf	mt-ghn-st-chl-grt-bt-crd/qz	ghn-sph vein in silica-rich	py-ms-qz	ghn-act-grt-st-bt	anh-crd-act/tr-chl	MS	MS	tlc?-sil-chl-ms	anh-ep patch in qz	Ser +grt+sph-ghn	crd-ky-st-bt gneiss
Assemblage Association	FeMg	FeMg		Ky-Bt-Ms	FeMg	Calc-Crb to FeMg	Sulfide-rich	Sulfide-rich	Calc-Crb to FeMg	Calc-Crb	Ky-Bt-Ms	FeMg
LGC												
SEM												
Ath-Ged												
Cumm-Gru												
Tr-Act					x							
Act-Hbl						15						
Chl						69	tr	tr				
Tlc												
Bt					x		3	62				
Wmca				25		2		2				
Ky				1			5	5				
Sil				3			3	3				
And												
Crd					20	2	x					
Grt					tr							
St							tr					
Carb.												
Cal												
Dol												
Ank												
Ep												
Zo/Czo												
Di												
Scp												
Anh					tr							
Ttn						2						
Kfsp												
Pl				10			x	8				
Qtz				20								
Ap												
Ghn					2							
Opaques												
SUM												
Ilm/Hem												
Rt												
Mt												
Sph					5	3						
Ccp				tr	20	tr						
Py				20	x	1	50	20				
Po					12	7						
Gn												
Apy												
Sum Sulf												
Other Notes				strongly fol by ms - crenulated	Au 13 gt; blebby po-cpy							
Paragenesis												

Appendix 2: Petrography Table

Sample	27198	27199	26002	26004	26005	JLSL13-004	JLSL13-034	JLSL13-062	27037	27039	27040	27043
DDH	DUB191	DUB191	DUB191	DUB191	DUB191	DUB191	DUB191	DUB191	DUB204	DUB204	DUB204	DUB204
Depth (m)	988.57	1001.43	1153.55	1156.3	1158.53	762.07	1032.84	860.29	761.24	773.82	765.73	838.28
Location	5400N, HW25	5400N, 25 lens	5400N, 40 lens	5400N, 40 lens	5400N, FW40	5400N	5400N	5400N	5400N	5400N	5400N	5400N
Logged Rocktype	green-ath +qz	grt-ghn-ath-qz +cpy	ghn-chl-qz +cpy-sph	act-chl +cpy-po	grt-mt-chl	grt amphibolite	st to ky in ms-bt	ep?	grt-hbl +sulf	ser-bt contact w/ Ca rich	gal in qz vein in mafic	ep-bt-cc-act/trm
Assemblage Association	FeMg	FeMg	FeMg	Calc-Crb	Calc-Crb	mafic	ky/sil-bt-ms	Ca-altered	mafic	Ca-rich	mafic	Calc-Crb
LGC												
SEM												
Ath-Ged												
Cumm-Gru												
Tr-Act												
Act-Hbl						40			15			
Chl							1					
Tlc												
Bt						7	5					
Wmca							25					
Ky							3					
Sil							1					
And												
Crd												
Grt						3			1			
St							2					
Carb.												
Cal									tr			
Dol												
Ank												
Ep								69				
Zo/Czo												
Di												
Scp												
Anh								1				
Ttn												
Kfsp												
Pl						40		5	50			
Qtz						10	63	5	20			
Ap												
Ghn												
Opaques												
SUM												
Ilm/Hem												
Rt												
Mt												
Sph												
Ccp						1		2	6			
Py							tr	1	1			
Po						5	1	17	4			
Gn									2			
Apy												
Sum Sulf												
Other Notes		Au 19 gt				grts appear to be post-tectonic; rx likely still original	diss sulfides	plag repl zoisite	Au 5 gt, diss-blebby sulfides			
Paragenesis												

Appendix 2: Petrography Table

Sample	27044	27046	27047	27051	27052	27054	27056	27057	27058	27059	27062	27066
DDH	DUB204	DUB204	DUB204	DUB204	DUB204	DUB204	DUB204	DUB204	DUB204	DUB204	DUB204	DUB204
Depth (m)	840.12	849.06	852.14	860.78	861.4	869.19	875.32	844.3	882.45	888.63	919	954.26
Location	5400N, HW21	5400N, 20/21	5400N, 20 lens	5400N, 20 lens	5400N, FW20	5400, HW24	5400N, 24 lens	5400N, 20/21	5400N, FW24	5400N, FW24	5400N	5400N, HW30
Logged Rocktype	act-crd-chl	cc-act-plg	bt-qz +sulfides	di in chl-crb	gln in act-trm	brown min?-tlc-chl	act-chl-crb	bt-act-plg-qz	act-tlc-chl	ghn-tr-bt-ms/tlc-chl	mt-cc-chl	silica-ser
Assemblage Association	Calc-Crb	Ca-altered	Bt-Qz	Calc-Crb	Calc-Crb	Calc-Crb	Calc-Crb	intermediate	Calc-Crb	Calc-Crb	Calc-Crb	Ms-Bt Qz
LGC												
SEM												
Ath-Ged												
Cumm-Gru												
Tr-Act							15					
Act-Hbl								25				
Chl							10					
Tlc												
Bt								15				
Wmca												
Ky												
Sil												
And												
Crd												
Grt												
St												
Carb.												
Cal							tr					
Dol												
Ank												
Ep												
Zo/Czo												
Di												
Scp												
Anh												
Ttn												
Kfsp												
Pl								30				
Qtz								30				
Ap												
Ghn												
Opaques												
SUM												
Ilm/Hem												
Rt												
Mt												
Sph							tr	tr				
Ccp							10	3				
Py							1	tr				
Po							1	5				
Gn							7	1				
Apy												
Sum Sulf												
Other Notes	Au 1 gt	Au 5 gt	Au 1 gt				Au 68 gt	Au 27 gt	Au 2 gt	Au 2 gt		
Paragenesis												

Appendix 2: Petrography Table

Sample	27067	27068	27069	27072	27073	27074	27076	JLSL13-048	26031	26032	26033	26034
DDH	DUB204	DUB204	DUB204	DUB204	DUB204	DUB204	DUB204	DUB204	DUB195	DUB195	DUB195	DUB195
Depth (m)	955.26	950.1	963.3	966.76	971.1	972	972.48	975.19	782.58	785.33	804.63	809.43
Location	5400N, HW30	5400N, HW30	5400N, 30 lens	5400N, 30 lens	5400N, 30/26	5400N, 26 lens	5400N, 26 lens	5400N, 26 lens	5600N, HW20/21	5600N, HW20/21	5600N, HW20/21	5600N, HW20/21
Logged Rocktype	Ca-rich	chl-crb +sulf	mafic +gln vein	anh in chl-act-crb	gln vein in mafic	anh-sph in act-chl	?-cc-mt-act	cc-act/trm-chl +sulf	rep ser schist	anh-act-ep +gln-py	act-cc-ep/chl-qz	act-cc-ep/chl-qz
Assemblage Association	Ms-Bt Qz	Calc-Crb	mafic	Calc-Crb	mafic	Calc-Crb	mafic	Calc-Crb	Ky-Ms	Ky-Ms-Bt	Calc-Crb	Calc-Crb
LGC												
SEM												
Ath-Ged												
Cumm-Gru												
Tr-Act												
Act-Hbl												
Chl												
Tlc												
Bt												
Wmca												
Ky												
Sil												
And												
Crd												
Grt												
St												
Carb.												
Cal												
Dol												
Ank												
Ep												
Zo/Czo												
Di												
Scp												
Anh												
Ttn												
Kfsp												
Pl												
Qtz												
Ap												
Ghn												
Opaques												
SUM												
Ilm/Hem												
Rt												
Mt												
Sph												
Ccp												
Py												
Po												
Gn												
Apy												
Sum Sulf												
Other Notes		Au 4 gt	Au 6 gt					Au 11gt xcutting vein		Au 11 gt		
Paragenesis												

Appendix 2: Petrography Table

Sample	26035	26035B	26036	26037	JLSL13-044	26009	26010	26011	26012	26016	26019	26020
DDH	DUB195	DUB195	DUB195	DUB195	DUB195	DUB226W02	DUB226W02	DUB226W02	DUB226W02	DUB226W02	DUB226W02	DUB226W02
Depth (m)	816.61	816.61	819.27	823.2	881.45	880.57	884.01	926.15	936.96	959.2	977.41	980.23
Location	5600N, 21 lens	5600N, 21 lens	5600N, 20/21	5600N, 20/21	5600N	5600N, HW20	5600N, HW20	5600N, FW21	5600N, FW21	5600N, 25 lens	5600N	5600N
Logged Rocktype	chl-bt-qz +sulf	chl-bt-qz +sulf	py-ky-bt-qz	MS	bt-plg/qz-act/hbl	bt-chl-ath-crd	di-act-cc-ep	bt-ath-ser-chl-crd/qz	qz vein w/ gal	ghn-bt-ms-qz +tlc	crb-chl +cpy	act-chl-crd
Assemblage Association	Bt-Qz	Bt-Qz	Sulfide-rich	Sulfide-rich	mafic	FeMg	FeMg	FeMg		Bt-Qz	Calc-Crb	Calc-Crb
LGC												
SEM												
Ath-Ged												
Cumm-Gru												
Tr-Act												
Act-Hbl				1	60							
Chl											70	
Tlc												
Bt												
Wmca				tr								
Ky												
Sil												
And												
Crd												
Grt												
St												
Carb.												
Cal				5							loc	
Dol												
Ank												
Ep					1							
Zo/Czo											2	
Di											1	
Scp				tr								
Anh				tr								
Ttn												
Kfsp												
Pl					20							
Qtz				3	20							
Ap												
Ghn												
Opaques												
SUM												
Ilm/Hem												
Rt												
Mt												
Sph				15							1	
Ccp				10	1						7	
Py				10							tr	
Po				1	2						5	
Gn												
Apy												
Sum Sulf												
Other Notes	Au 36 gt	Au 36 gt	Au 3 gt	Au 25 gt	disseminated sulfides; appear to be discrete						Au 20 gt	
Paragenesis												

Appendix 2: Petrography Table

Sample	26022	26023	26024	26025	26026	26027	26028	26029	JLSL13-017	JLSL13-020A	JLSL13-020B	JLSL13-021
DDH	DUB226W02	DUB226W02	DUB226W02	DUB226W02	DUB226W02	DUB226W02	DUB226W02	DUB226W02	DUB226W06	DUB226W06	DUB226W06	DUB226W06
Depth (m)	990	1012.19	1016.83	1017.31	1022.47	1027	1029.39	1040.78	886.06	901.45	901.45	902.22
Location	5600N	5600N	5600N	5600N	5600N	5600N	5600N	5600N	5600N, 21 lens	5600N, 25 lens	5600N, 25 lens	5600N
Logged Rocktype	anh in chl schist	chl-crb + ath-crd	mt-po-cpy in act-chl	cc-chl +cpy	ghn-mt-cc-chl	transition to clasts in chl	mt-ghn-act-chl	bt w/ rims	ath-chl schist	crd-tlc schist	crd-tlc schist	tlc schist
Assemblage Association	Calc-Crb	Calc-Crb	Calc-Crb	Calc-Crb	Calc-Crb	Calc-Crb	Calc-Crb	Calc-Crb	FeMg	FeMg	FeMg	FeMg
LGC												
SEM												
Ath-Ged												
Cumm-Gru												
Tr-Act									7			
Act-Hbl										tr		
Chl				20								3
Tlc												15
Bt									tr	5		
Wmca												15
Ky												
Sil												
And												
Crd												20
Grt												
St												
Carb.												
Cal				35								
Dol												
Ank												
Ep				40					5		2	
Zo/Czo												
Di				15								
Scp												
Anh				5					tr	2	7	
Ttn												
Kfsp												
Pl									60		5	20
Qtz				10						20	10	5
Ap												
Ghn												
Opaques												
SUM												
Ilm/Hem												
Rt												
Mt												
Sph				1					1	5	2	
Ccp				3					23	2	10	2
Py				tr						1	7	
Po				1					3	40	40	5
Gn				tr						tr		
Apy												
Sum Sulf												
Other Notes			Au 41 gt	Au 23 gt	Au 12 gt		Au 13 gt		Au 73 gt	Au 278 gt	Au 278 gt	
Paragenesis												

Appendix 2: Petrography Table

Sample	JLSL13-081	JLSL13-086	JLSL13-089	JLSL13-090	26059	26060	26063	26064	26066	26069	26072	26076
DDH	DUB245	DUB245	DUB245	DUB245	DUB252W01	DUB252W01	DUB252W01	DUB252W01	DUB252W01	DUB252W01	DUB252W01	DUB252W01
Depth (m)	995.95	1018.42	1078.31	1146.21	989.58	1003.26	1017.71	1017.29	1024.21	1022	1060.82	1069.69
Location	5600N, HW21	5600N, 25 lens	5600N, 26 lens	5600N, 28 lens	5600N	5600N, HW20	5600N, 21 lens	5600N, 21 lens	5600N, 21 lens	5600N, 21 lens	5600N, 25 lens	5600N, FW25
Logged Rocktype	chl-tlc-ath-qz	ghn-cpy in qz vein	ghn-sulf	ghn-cpy	py-ky-bt-qz	mafic +aspy	act-cc-chl w/ qz+gln	qz vein w/ sulf	act-plag/crd-qz	dol?-cc-act +cpy	crb-chl +gln-cpy	bt-ms-qz +ky
Assemblage Association	Calc-Crb	FeMg	FeMg	FeMg	FeMg	mafic	Calc-Crb	Calc-Crb	intermediate	Calc-Crb	FeMg	Ky-Bt-Ms
LGC												
SEM												
Ath-Ged	80		10	5								
Cumm-Gru												
Tr-Act												
Act-Hbl												
Chl												
Tlc												
Bt				1								
Wmca												
Ky												
Sil												
And												
Crd			30	30								
Grt												
St												
Carb.												
Cal												
Dol												
Ank												
Ep												
Zo/Czo												
Di												
Scp												
Anh												
Ttn												
Kfsp												
Pl												
Qtz	10		30	30								
Ap												
Ghn	2		10	2								
Opaques												
SUM												
Ilm/Hem												
Rt												
Mt												
Sph				tr								
Ccp	3		7	20								
Py				5								
Po	2		3	5								
Gn												
Apy												
Sum Sulf												
Other Notes	Au 5 gt	Au 16 gt	Au 9 gt	Au 12 gt		Au 1 gt	Au 20 gt	Au 66 gt	Au 15 gt	Au 2 gt	Au 27 gt	
Paragenesis												

Appendix 3: Major element geochemistry data

Location	DDH	Depth (m)	Sample ID	SiO_2	Al_2O_3	$Fe_2O_3(T)$	FeO	MnO	MgO	CaO	Na_2O	K_2O	TiO_2	P_2O_5	LOI	Total
5400, 40	DUB191	1153.55	JLSL-26002	43.38	8.53	15.65	NA	0.272	7.3	0.27	0.04	0.06	0.374	0.13	4.77	80.79
5600, 20/21	DUB195	823.2	JLSL-26037	5.49	0.51	31.91	NA	0.127	0.29	6.72	0.01	< 0.01	0.016	< 0.01	15.25	60.33
5200	LP0029	70.1	JLSL-26040	22.88	3.56	10.6	NA	0.252	6.12	32.13	0.02	< 0.01	0.056	0.08	2.7	78.41
5200	LP0029	138.07	JLSL-26047	10.74	0.72	3.75	NA	0.614	19.07	27.82	0.04	< 0.01	0.029	< 0.01	35.37	98.18
5600	DUB252W01	1079.88	JLSL-26079	48.72	18.68	15.79	NA	0.223	10.66	0.99	0.18	0.9	0.686	0.29	1.61	98.71
5400, 20/21	DUB204	849.06	JLSL-27046	86.3	3.59	4.36	NA	0.073	3.33	1.29	0.04	0.2	0.077	0.01	1.5	100.8
5400, 21	DUB204	844.3	JLSL-27057	52.73	13.07	9.8	NA	0.133	6.29	12.23	0.31	0.06	0.515	0.11	1.65	96.88
5400, 30	DUB204	963.3	JLSL-27069	45.1	13.71	7.66	NA	0.217	9.47	10.91	1.29	0.09	0.468	0.09	2.96	91.96
5400, 26	DUB204	971.1	JLSL-27073	43.48	14.91	10.42	NA	0.229	10.58	12.44	0.57	0.11	0.54	0.1	2.5	95.88
5200, 10	LP0008	109.96	JLSL-27092	56.58	19.09	8.92	NA	0.193	2.66	7.83	0.66	2.04	0.79	0.41	0.48	99.67
5200, 10	LP0008	121.1	JLSL-27097	17.64	10.53	31.4	NA	0.111	4.32	0.26	0.14	1.47	0.442	0.09	15.88	82.29
5200, 10	DUB205	804	JLSL-27103	83.39	1.35	6.48	NA	0.038	0.72	0.21	0.01	0.43	0.245	0.07	4.95	97.89
5200	LP0017	12.65	JLSL-27142	38.96	14.56	10.33	NA	0.293	4.26	25.26	0.42	0.06	0.426	0.05	3.2	97.82
5200, 31	LP0016	137.65	JLSL-27179	22.6	2.09	18.25	NA	0.194	2.65	2.45	0.03	0.02	0.045	< 0.01	15.31	63.64
5400, 10	DUB191	879.67	JLSL-27190	31.09	19.02	18.53	NA	0.749	7.11	8.24	0.59	1.42	0.937	0.05	4.7	92.42
5400, 25	DUB191	1001.43	JLSL-27199	64.75	10.48	11	NA	0.25	9.72	0.31	0.05	1.21	0.304	0.14	2.44	100.6
5400	DUB191	762.07	JLSL13-004	53.33	14.25	15.7	NA	0.245	4.23	6.67	2.27	0.52	0.893	0.35	0.07	98.53

Appendix 3: Major element geochemistry data (continued)

Location	DDH	Depth (m)	Sample ID	SiO_2	Al_2O_3	$Fe_2O_3(T)$	FeO	MnO	MgO	CaO	Na_2O	K_2O	TiO_2	P_2O_5	LOI	Total
5600	DUB226W06	886.06	JLSL13-017	51.78	3.77	19.12	NA	0.138	2.93	2.18	0.04	0.03	0.052	0.03	7.04	87.11
5600, 25	DUB226W06	901.45	JLSL13-020	37.88	1.59	39.28	NA	0.066	1.06	2.35	0.02	0.04	0.021	0.04	9.96	92.3
5600, 25	DUB226W06	902.22	JLSL13-021	43.23	16.1	13.17	10.93	0.117	13.17	4.49	0.13	0.07	0.459	0.21	6.31	97.45
5200	DUB172	1088.2	JLSL13-043	51.4	14.24	11.5	NA	0.435	9.05	0.32	0.06	0.37	0.148	0.06	1.62	89.21
5600	DUB195	881.45	JLSL13-044	45.77	19.81	10.58	NA	0.139	6.07	14.84	1.33	0.08	0.47	0.18	0.65	99.92
5600, 26	DUB245	1078.31	JLSL13-089	58.29	8.75	16.37	NA	0.201	7.7	0.27	0.04	0.04	0.095	0.03	1.53	93.31
5600, 28	DUB245	1146.21	JLSL13-090	50.82	7.93	21.57	NA	0.175	7.21	0.46	0.04	0.16	0.228	0.08	4.07	92.75
5200	LP0029	56.14	JLSL-26039	11.83	6.59	2.91	NA	0.792	23.11	21.81	0.01	< 0.01	0.153	0.03	32.37	99.61
5600, 27	DUB252W01	1147.29	JLSL-26089	47.98	16.05	17.84	NA	0.261	14.9	0.65	0.18	0.16	0.653	0.28	1.24	100.2
5400	DUB191	1032.84	JLSL13-034	79.91	10.84	2.74	NA	0.053	2.38	0.13	0.17	2.32	0.232	0.09	1.21	100.1
5600, 21	DUB245	995.95	JLSL13-081	59.16	11.67	11.38	NA	0.311	15.11	0.66	0.05	0.05	0.785	0.33	1.12	100.6
5600, 26	DUB226W02	977.41	JLSL-26019	25.77	14.84	11.92	NA	0.126	23.34	5.84	< 0.01	< 0.01	0.555	0.22	10.59	93.2
5600, 21	DUB195	816.61	JLSL-26035	76.29	4.24	6.61	NA	0.062	2.73	1.05	0.1	0.26	0.089	0.02	2.13	93.58
5600, 20/21	DUB195	819.27	JLSL-26036	44.49	17.88	17.92	NA	0.05	3.44	1.03	0.66	0.67	0.398	0.03	9.29	95.86
5600, 21	DUB252W01	1024.21	JLSL-26066	38.47	14.19	13.65	NA	0.25	8.55	12.5	0.23	0.07	0.138	0.08	3.98	92.1
5600, 27	DUB252W01	1140.67	JLSL-26086	37.64	4.04	32.95	NA	0.032	2.47	3.51	0.2	0.43	0.005	0.02	6.76	88.07
5200	DUB172	909.08	JLSL-27003	50.59	13.95	15.04	NA	0.139	6.34	6.37	1.26	0.21	0.977	0.86	0.56	96.3

Appendix 3: Major element geochemistry data (continued)

Location	DDH	Depth (m)	Sample ID	SiO_2	Al_2O_3	$Fe_2O_3(T)$	FeO	MnO	MgO	CaO	Na_2O	K_2O	TiO_2	P_2O_5	LOI	Total
5200	DUB172	928.15	JLSL-27007	46.22	19.27	11.19	NA	0.041	2.41	5.16	5.16	1.06	0.106	0.3	6.45	97.37
5400, 24	DUB204	875.32	JLSL-27056	36.97	4.18	3.92	NA	0.374	19.74	18.14	0.13	0.02	0.092	0.02	7.45	91.04
5200, 10	LP0008	105.06	JLSL-27090	25.14	21.58	19.76	NA	0.396	12.2	0.38	0.73	1.5	0.533	0.05	4.22	86.48
5200, 10	LP0008	106.52	JLSL-27091	32.86	21.28	29.74	NA	0.249	2.35	0.26	0.05	0.74	0.762	0.05	6.24	94.59
5200, 10	LP0008	111.67	JLSL-27093	80.73	9.32	4.05	NA	0.035	0.8	1.79	0.28	0.47	0.365	0.05	3.01	100.9
5200, 10	LP0008	113.17	JLSL-27094	15.01	8.09	39.36	NA	0.065	1.63	0.97	0.08	0.63	0.256	0.02	11.49	77.61
5200	DUB250	712.67	JLSL-27122	45.07	15.86	8.5	NA	0.458	4.14	20.52	0.08	0.02	0.425	0.1	2.69	97.85
5200, 25	DUB250	889.86	JLSL-27132	35.6	16.13	13.25	NA	0.231	20.95	3.37	0.08	0.03	0.83	0.73	7.25	98.46
5200, 25	DUB250	896.3	JLSL-27133a	28.01	18.83	14.85	10.07	0.246	20.29	1.56	0.08	0.02	0.325	0.12	8.44	92.78
5200, 25	DUB250	896.3	JLSL-27133b	49.54	16.23	11.82	10.11	0.253	15.11	1.94	0.12	0.51	0.635	0.27	2.73	99.17
5200, 25	DUB250	905.4	JLSL-27140	76.74	7.01	4.51	3.87	0.238	7.98	1.2	0.08	0.33	0.171	0.02	1.8	100.1
5200, 25	DUB250	904.32	JLSL-27141	45.23	9.21	9.4	NA	1.404	14.61	10.87	0.16	0.03	0.202	0.07	4.57	95.74
5200	LP0016	145.24	JLSL-27181	39.91	13.84	8.75	NA	0.162	9.91	14.06	1.22	0.28	0.333	0.09	5.59	94.16
5200, 10	LP0017	84.83	JLSL-27148	19.54	6.75	39.87	NA	0.057	1.6	0.24	0.05	0.43	0.252	0.08	10.59	79.45
5600	DUB252W01	1169.82	JLSL-26093	77.19	7.44	8.41	NA	0.253	5.05	0.14	0.07	0.04	0.112	0.02	0.32	99.04
5200	LP0008	4.28	JLSL-27078	33.28	21.52	16.53	NA	0.176	8.86	2.48	1.12	4.53	0.671	0.16	8.56	97.89
5200	LP0008	61.36	JLSL-27085	59.28	15.23	10.43	1.23	0.072	2.41	0.68	0.34	3.72	0.722	0.4	6.13	99.41

Appendix 3: Major element geochemistry data (continued)

Location	DDH	Depth (m)	Sample ID	SiO_2	Al_2O_3	$Fe_2O_3(T)$	FeO	MnO	MgO	CaO	Na_2O	K_2O	TiO_2	P_2O_5	LOI	Total
5200	LP0008	93.91	JLSL-27089	22.36	18.61	23.23	NA	0.576	18.12	1.25	0.07	0.19	0.94	0.04	12.38	97.78
5200	DUB250	677.04	JLSL-27118	54	15.33	16.15	NA	0.297	4.4	3.35	1.46	0.6	0.734	0.49	3.85	100.7
5200	DUB250	827.25	JLSL-27126	53.08	1.6	2.85	NA	0.689	18	19.99	0.14	0.03	0.028	< 0.01	1.85	98.27
5200	DUB250	975.35	JLSL-27135	70.69	13.73	6.46	NA	0.257	4.05	0.21	0.1	2.53	0.311	0.08	1.02	99.42

Appendix 4.1: Summary table of base metal zones

10 Lens	**DUB172**	**DUB205**	**LP0008**	**LP0017**	**DUB191**
Depth	930-934.10m	786.45-809.75m	102-134m	71.89-93.15m	877-886m
Host rock	Massive sulfide; Ghn-Chl Schist	Transitional Fe-Mg: St-Bt-Qz+Chl	Transitional Fe-Mg: St-Bt-Qz, Bt-Ghn-Ath, Chl-Bt-St-Qz, Sil-St-Bt-Ms, Bt-Chl	N/A	Variable Fe-Mg: Ghn-St-Bt, Grt-St-Bt-Chl-Crd, Chl+Ghn-Act
Mineralization style	NSS-SS Cpy-Sph-Py	STRG-NSS Cpy-Po-Sph-Py	Massive intervals Po-Py-Cpy+Sph/Ghn; DISS-STRG Cpy-Sph-Po+Ghn+Py	Massive Cpy-Po-Sph-Py +Gal+Ghn+Cc	Blebby-NSS Cpy-Po-Py-Sph +Cc+Qz+Anh
Metal association	Cu-Zn-Au	Zn-Au+Pb, Cu-Au	Cu-Au	Cu, Cu-Zn, Zn	Cu-Zn-Au

20 Lens	**LP0016**	**DUB191**	**DUB204**	**DUB195**	**DUB226W06**	**DUB252W01**
Depth	118.29-123m	905.70-908m	846.01-861.11m	817-829m	903-905m	1007.49-1010m
Host rock	Bt-Cc-Chl, Ky-Bt-Qz	Crd-Act-Chl schist	Massive, Silica-rich w/ sulfides, Ca-rich	Py-Ky-Bt-Qz	St-Act-Bt-Chl +patchy Crd-Ath	Chl schist
Mineralization style	Massive Py-Sph +Cc+Qz+Gal	Diss-strg Sph-Py-Po+Cpy	Massive Cc-Sph-Py+Cpy+Po	NSS-SS Cpy-Sph-Py w/ Cc	NSS-SS Py-Sph+Cc, blebby Sph-Cpy-Py-Po	Diss Cpy-Gal+Ghn+Sph, Py-Cpy, blebby Sph-Cc
Metal association	Zn	Zn	Cu-Zn-Au+Pb	Zn-Au+Cu	Zn	Zn
Missing: DUB250 (819.00-823.00m), DUB226W (887.73-893.38m)						

	LP0029	**DUB204**	**LP0016**	**LP0029**	**DUB191**
Lens	30	30	31	40	40
Depth	128.85-133.96m	957-970m	129.66-141.62m	147.04-152.58m	1153.46-1156.11m
Host rock	Cc-Bt-Chl-Act/Trm-Qz	Act/Trm-Chl +Cc-Anh	Bt-Cc-Chl, Ky-Bt-Qz	Act/Trm-Qz-Chl schist	Ghn-Bt-Ath to Ghn-Ath-Ms/Qz
Mineralization style	Diss-Strg Cpy-Gal-Po-Sph-Py	NSS-SS Cpy-Po-Sph-Py (also Strg-Diss)	Massive Py-Sph +Cc+Qz+Gal	Blebby-Strg Cpy-Py-Sph	Massive Py-Sph to NSS Sph
Metal association	Not obvious w/ Au	Zn	Zn	Cu-Pb-Au	Zn-Au
Missing: DUB250 (30: 921.00-936.34m and 40: 940.53-947.00m)					

Appendix 4.2: Summary table of gold zones

21 Lens	DUB204	DUB195	DUB226W06	DUB245	DUB252W01	DUB226W02
Depth	839.4-861.11m	810-828m	877.57-886.29m	995.9-1001.18m	1015-1036m	901.43-919.13m (905.85- 918.56m)
Host rock	Int-Maf, Massive, Silica-rich w/ sulfides, Ca-rich	Altered felsic, Py-Ky-Bt-Qz	Tlc-Act-Chl	Chl-Tlc-Ath-Qz, Ath-Crd+Bt	Act-Cc-Chl, Chl-Plag/Qz-Act, Grt-Bt-Ath, Act-rich	Grt-St-Chl-Bt-Ath-Qz/Crd
Mineralization style	Diss-Strg Cpy, Po, Py, Sph +Aspy+Gal	Strg Ghn+ Gal-Cpy-Py/Po, NSS-SS Cpy-Sph-Py+Cc	Diss Cpy, Py, Po	Diss-Strg Cpy-Ghn+Po	Diss-blebby Po-Gal-Cpy-Sph-Py; Strg Po-Cpy; Strg-Diss sulfides	Au is associated with Ghn+Po-Cpy veins
Metal association	Cu-Zn-Au+Pb	Cu-Au	Cu-Au+Zn	Cu-Au	Pb-Au, Cu-Au+Pb	Missing (metreage)

25 Lens	DUB250	DUB191	DUB226W02	DUB226W06	DUB245	DUB252W01
Depth	871-906m	993-1001.65m	954.23-965.61m	892.87-903m	1007.28-1018.63m	1049-1062.31m
Host rock	Act/Trm-Chl+Cc	Bt-Ath-Crd/Qz	Bt-Ms-Qz	Fe-Mg: Grt-Ath-Bt+Act, Grt-Chl-Bt-Ath-Crd, Crd-Tlc, Ghn-St-Act-Bt-Chl	Ath-Crd+Chl, Bt-Ath-Chl/Qz	Ky-Bt-Qz; Act-rich section
Mineralization style	Diss-stringer Cpy-Sph-Py	Blebby-Strg Cpy	Stringer Cpy-Sph/Ghn	Diss-Strg Cpy, Py, Po, Sph, +Gal	Diss-Strg Cpy-Ghn+Po, Cpy-Ghn	Diss Py; Diss-blebby Cpy-Gal
Metal association	Cu-Au	Cu-Au	Cu-Zn-Au+Pb	Cu-Zn-Au+Pb	Cu-Au+Zn	Pb-Au+Cu

	DUB204	DUB204	DUB245	DUB252W01	DUB252W01	DUB245
Lens	24	26	26	27	27	28
Depth	871-878m	970.68-978m	1078.14-1085.32m	1139.29-1161.61m	1176-1197.71m	1140.18-1154.49m
Host rock	Cc-Trm-Chl schist (Trm-Bt-Chl, Ghn-Trm-Bt-Ms/Tlc-Chl)	Mafic, Anh prox sulfides; act/tr-chl+cc, sulfides in Tr; mafic dike	Chlorite schist w/ patchy ath-crd; ath-crd+bt+ghn	Act-Qz, Fe-Mg altered rocks	St-Grt-Ath-Bt, St-Ath-Crd/Qz	Grt-St-Bt-Ath-Crd/Qz
Mineralization style	Diss Cpy-Sph-Po-Py, Sph-Gal-Py, Cpy, Gal	Diss to strg gln-cpy-py-sph-po; diss po-py	Bands of po-cpy-ghn; diss to stringer py-cpy	Blebby-Strg Cpy-Po	Diss-Strg Po-Cpy	Ghn-Cpy bands/stringers
Metal association	Pb-Au +Zn	Pb-Au ± Zn	Cu-Au ± Zn	Cu-Au	Cu-Zn-Au	Cu-Au

Appendix 5: Drill hole reports

DDH: DUB172
Location: 5200N, east
Logged: 876m-1090m
Zones: 10 lens at 930-934.10m

The logged section of the drill hole is dominantly in Ky/Sil-Bt schists and ferromagnesian altered rocks. There is hanging wall gold mineralization (above the 10 lens) as well as fairly continuous mineralization in intervals immediate to the 10 lens. Au generally appears to be associated with Cpy and Gal. Py and Po generally occur throughout the drill hole, typically disseminated and occasionally in the foliation.

Approximately 100m above the logged section, HudBay diamond drill logs indicate the occurrence of felsic fragmental units, silicified basalt units, and a rhyodacite interval leading into where logging began. Approximately 100m below the logged section, it is predominantly Fe-Mg alteration with an interval of diorite/gabbro.

Pb-Au+As, 906.77-915.24m: Au occurs associated with finely disseminated 3% Cpy, 1% Aspy, and trace Gal within an altered mafic volcaniclastic interval. Mineralization is associated with Grt porphyroblasts and mafic bands; some minor quartz veins have associated Ghn-Cpy.

Pb-Au, 928.17-928.45m: Au occurs associated with interstitial Gal and Py between plagioclase pegmatite crystals, which also contain interstitial coarse Bt.

Cu-Zn-Au, 930-934.1m, 10 lens: The 10 lens interval is massive sulfide (Cpy-Sph-Py) with Ghn. It appears to be fairly Py-rich (80%) with 5% interstitial Sph and minor Cc-Qz. Minor Cpy occurs in the interval, but becomes most concentrated at the end of the interval where it becomes less massive. Within the massive sulfide, there is also a small interval of a Ghn-Chl schist with 7% Po, 20% Sph-Py, and minor Cpy.

Cu-Au, 935-943.9m: Au occurs within dominantly Fe-Mg alteration (Chl-Crd-St-Bt, Chl-St-Bt, St-Sill-Bt, St-Act/Trm-Bt-Chl) associated with discordant to weakly foliated sulfides (Cpy-Py+Po+Ghn).

Appendix 5: Drill hole reports

DDH: DUB172DPN
Location: 5200N, east
Logged: 1100m-1184m
Zones: none

The drill hole consists of primarily Fe-Mg alteration with a window of Ky/Sil-Ms-Bt. The last section is appears to be an altered mafic rock. Au mineralization appears to be associated with discordant stringer Cpy localized in the section of Ky/Sil-Ms-Bt schists.

Approximately 100m below the logged section, there are Fe-Mg silicates, amphibole quartzofeldspathic schist, and a mafic polymodal fragmental (according to HudBay logs).

Cu-Au, 1121.87-1129.45m: Au occurs within a section of Ky/Sil-Ms-Bt-Qz associated with Cpy-Ghn stringers. There are three intervals that make up this section. First, St-Sil-Ms-Bt occurs with Ghn+Py/Po-Cpy stringers. Second, Sil-Bt-Ms-Crd occurs with trace Py and 1% 1-2mm vein/stringer Cpy. Third, St-Grt-Bt-Ms-Crd/Qz occurs with stringers of trace Sph, 1% Py, and 3% Cpy that have associated Ghn.

Appendix 5: Drill hole reports

DDH: DUB205
Location: 5200N, slightly east
Logged: 771.20m-1164.76m
Zones: 10 lens at 786.45-809.75m

The drill hole begins in a less altered felsic rock with quartz-epidote alteration patches (which also include grossular and anhydrite). It grades into a massive Cpy-Po-Sph-Py assemblage, which is the 10 lens. Au is found proximal to the lens, likely in association with Cpy. The sulfides are typically found disseminated, but occasionally occur as stringers; Py and Po occur throughout the drill hole. In the footwall of the 10 lens, the drill hole alternates between Al_2SiO_5-mica rocks, Fe-Mg altered rocks, and less altered felsic-intermediate rocks.

Approximately 100m above the logged interval, there are units of feldspar-phyric diorite, altered fragmental rhyolite, rhyodacite fragmental, argillite, rhyolite fragmental, and altered rhyolite/rhyodacite fragmental. Approximately 100m below the logged interval, there is an altered mafic fragmental.

Zn-Au+Pb, 792.4-803.9m; Cu-Au, 803.9-815.55m; 10 lens: Au occurs within a stringer-near solid sulfide zone, Cpy-Po-Sph-Py. Cpy occurs patchily and minor Ghn also occurs. Initially, there is more Sph than Cpy, but then there is more Cpy than Sph (typical VMS metal zoning). The underlying host rock is dominantly St-Bt-Qz+Chl (transitional Fe-Mg alteration) with minor quartz veining. A late dike is also present, but does not contain any mineralization.

Appendix 5: Drill hole reports

DDH: DUB250
Location: 5200N, slightly west
Logged: 634.49m-1032m
Zones: 20 lens at 819-823m; 25 lens at 885.67-897m; 30 lens at 921-936.34m; 40 lens at 940.53-947m

The logged section of this drill hole progresses from a less altered mafic to transitional Fe-Mg alteration to what appears to be wisps of the 10 lens in a pyritized Ky-Bt-Ms schist to an epidote altered/calc-silicate with blebby-vein Cpy and disseminated Gal. There is a gradational contact with a less altered mafic rock going into a mineralized zone with Chl-Crb alteration and ends in a less altered felsic-mafic sequence. At ~965m, there is a quartz vein with Ghn porphyroblasts as well as Py and Po; it may have ripped the material from surrounding rock as it was emplaced.

Approximately 100m above the logged interval, there are sections of mafic tuff, siliceous epidotized rhyolite, and mafic volcaniclastic tuff leading into the logged interval.

Pb-Au, 661-662m: Au is likely associated with a quartz vein in which disseminated Py-Po occurs, emplaced in an intermediate unit. Pb is present, but Gal was not observed in drill core.

Zn-Au, 664-664.46m: Au appears to be associated with disseminated Po-Py in St-Bt-Crd/Qz. Zn is present, though Sph was not observed in drill core.

Pb-Au+Zn, 709.85-715m: In a Mt-bearing, epidote-altered section (mafic-intermediate), Au is associated with disseminated Gal as well as blebby Cpy-Po-Py, Sph bands, and Qz veins. Cc is present in the groundmass as well as in veins. This is above a possible structure.

819.00-823.00m, 20 lens: MISSING FROM CORE BOXES

Pb-Au, 839-842.78m: Au appears to be associated with an intermediate dike and trace specks of Cpy and finely disseminated Py-Po in the presence of Cc veins. Gal was not obvious.

Cu-Au, 871-906m, 25 lens: Au occurs with disseminated to stringer sulfides (Cpy-Sph-Py) within a calc-silicate to carbonate silicate alteration assemblage. Interstitial Cc occurs patchily, while Tlc-Ghn appears with the sulfides.

Cu-Zn-Pb-Au, 921-948m: Missing 921-936.35m (30 lens) and 940.53-947m (40 lens). In 936.35-940.53m, there are no Au occurrences. At 947-948m, there is 2.263 g/t of Au in Chl schist with foliated Bt and blebby Py.

Appendix 5: Drill hole reports

DDH: LP0008
Location: 5200N (underground)
Logged: 1.39m-149.10m
Zones: 10 lens at 102-134m

The first part of the drill hole occurs in less altered felsic to mafic rock. Next, there are Ky/Sil-Ms/Bt schists with disseminated Py, with a small section of Act-Chl schist. There is a thick section of variable Fe-Mg altered rocks in the footwall of the 10 lens and blips of it throughout. Disseminated to blebby sulfides occur in these intervals, typically in the foliation; Py is the most abundant with Po, small amounts of Sph and Cpy, and very minor Gal. In the massive sulfide sections, the minerals are much more porphyroblastic. Au mineralization appears to be related to the appearance of Cpy, and possibly porphyroblastic minerals.

88-102m: The 112 lens occurs predominantly in Fe-Mg alteration; St-Chl-Bt with Cpy-Po-Py + Ghn.

Cu-Au, 95-122.55m: Au occurs associated with disseminated to blebby Cpy-Po ± Py within Fe-Mg alteration, as well as a section of Sil-St-Bt-Ms proximal to the massive sulfide lens. Au grades gradually decrease with Cu and an increase in Zn.

102-134m: The 10 lens occurs as predominantly massive sulfide with showings of altered rocks. First, it is in St-Bt-Qz with disseminated Py-Sph-Po-strg Cpy and Ghn. The next section is a Ghn-Ath rich zone with interstitial Cpy-Bt and some Po-richer parts. Then there is an interval of Chl-Bt-St-Qz with disseminated-stringer Py-Cpy-Po. Fourth, there is a Sil-St-Bt-Ms schist with Ghn-Cpy-Po as well as minor disseminated Py (12% total sulfides). There is an interval of stringer-near solid sulfide with trace carbonate and anhydrite; sulfides are 5% blebby Po, 10% euhedral-blebby Py, 15% interstitial blebby Cpy, and trace Aspy. Trace Sph also occurs though most of it has likely turned into 10% Ghn. The next interval is Bt-Chl schist with 7% Ghn, 15% disseminated Py in foliation, 10% Cpy-Sph-Po, and Gal+Py/Po occurs with quartz veins. The last interval is massive sulfide (generally Py with interstitial Sph, trace Gal), minor Po in less massive parts, trace Cpy, and Ghn.

Appendix 5: Drill hole reports

DDH: LP0016
Location: 5200N (underground)
Logged: 1.25m-209.00m
Zones: 20 lens at 118.29-123m, 31 lens at 129.66-141.62m

The drill hole begins in well foliated less altered felsic to intermediate rock with patchy Grt and Cc. The next interval is a Cc-Act/Trm-Chl assemblage with possible diopside and epidote. It is followed by a section of well-foliated Ms-Bt-Qz with Py and Po in the foliation, disseminated to blebby stringers. The next interval is back into Act/Trm-Cc-Chl, with parts that are richer in Chl being poorer in carbonate (and vice versa). The carbonate sections appear very mottled, with white/pink Cc and interstitial Chl imparting a green colour. It is also moderately foliated, with minor anhydrite and sulfides – stringer to blebby to disseminated Sph, Py, Po, and Gal. A section of moderately foliated Ky (patchy)-Py-Bt follows, with discordant stringer Py and Po. The next interval is a poor to moderately foliated Bt-Act/Trm-Chl-Cc/Qz. In the carbonate-poor Chl-rich zones, there appears to possibly be St or Crd. The sulfides in the section are stringer and mottled Py, Po, Sph and Cpy.

The next interval is massive sulfide, the 20 & 31 lens, which is comprised dominantly of Py cubes and Sph with interstitial Cc and Qz. There is also patchy Gal in the interval, appearing as blebs and stringers. Some sections of host rock appear in the lens; a section of Bt-Cc-Chl section and Ky-Bt-Qz.

The next interval in the drill hole is a well-foliated less altered mafic rock with epidote patches; at the beginning of this interval, there is also a section of fairly concordant discontinuous Cc veins with blebby stringer Aspy. It is followed by a well-foliated mafic rock with less epidote patches and the appearance of discordant quartz/ankerite veinlets.

Au mineralization in this drill hole is limited to the section of what appears to be less altered mafic rock (Bt, Plag/Qz, Act/Hbl) with foliated blebby Cc and disseminated Aspy & Gal. Au also occurs in two assays; within a section of pyritized Ky-Bt-Qz with minor blebby Po and at the top of the 31 lens (Cpy-Gal bearing, Sph-Py with Cc-Qz).

Cu-Pb-As-Au, 141.62-147m: Au occurs associated with disseminated Aspy, Gal, and Cpy within a mafic intrusive (sharp contact at the base of 31 lens) containing discontinuous foliated Cc veins.

Appendix 5: Drill hole reports

DDH: LP0017
Location: 5200N (underground)
Logged: 1.26m-108.28m
Zones: 10 lens at 71.89-93.15m

The drill hole starts in mafic rock with Po veins, and gradually progresses into a section that appears to be epidotized as well. In the epidotized section, there appears to be discordant veins and disseminations of Gal. It is followed by moderately to well-foliated Ky/Sil-Ms-Bt schist containing disseminated Py with rare Gal veins. Then there is an interval of Ghn-Act/Trm-Bt-Chl, which is followed by massive sulfide (10 lens, hosted in St-Mt-Chl-Bt). At the base of the 10 lens, there is an interval of St-Grt-Chl-Bt. The last section of the drill hole is less altered mafic rock.

Au mineralization in this drill hole appears to be spotty although other sulfides are prevalent.

Pb-Au+Cu, 33-35m, 43m: The gold occurs within Ky-Ms-Bt-Qz associated with locally disseminated Cpy-Gal and disseminated Py.

71.89-93.15m: Gold appears to be hosted in the massive sulfide environment (Cpy-Po-Py-Sph, rare Gal). The 10 lens is near solid sulfide to solid sulfide with interstitial Cc. There is 5% Cpy, 15% Po, 25% Sph, 30% Py, and minor Ghn. Trace Gal occurs within the less massive sections.

Appendix 5: Drill hole reports

DDH: LP0029
Location: 5200N (underground)
Logged: 1.70m-197.00m
Zones: 20 at 35.56-38.8m, 31 at 63-72m, 30 at 129.85-133.23m, 40 at 147.04-153.48m

The drill hole begins in an intermediate unit with a showing of a more mafic one. Then there is a small section of Fe-Mg altered rocks, which is followed by a thick section of Chl-Crb altered rocks. Next, there are Fe-Mg altered rocks with a small mafic interval sandwiched between the two. Ky/Sil-Bt/Ms schist occurs next and then another mafic interval occurs at the end of the drill hole.

Within the Chl-Crb section of the drill hole, diopside occurs patchily and mottled. The Act/Trm occurs mottled with Cc, as well as in Chl where it is carbonate-poor. There are also small patches of Fe-Mg alteration within the Chl-Crb interval. Tlc/Ms occurs very patchily, as well as Mt and Ghn.

Although there is no massive sulfide in the drill hole, mineralization occurs as Py, Po, Cpy, Sph, and Gal. Py and Po appear throughout, typically disseminated-blebby. Cpy occurs as disseminated-blebby stringers primarily in the Chl-Crb alteration, as far down as into the Fe-Mg at 168m; same with Sph up to 174m. Gal appears to be restricted to the Chl-Crb altered sections as stringers-disseminated. Au mineralization is restricted to the Chl-carbonate altered rocks.

- **Cu-Au, 56-57m, 69.88-71.65m:** Au occurs associated with disseminated-stringer Py-Sph, trace Cpy-Po-Gal mixed in with Cc within Act/Trm-Cc-Chl schist.
- **79.9-87m:** Au occurs associated with disseminated-blebby Py-Po in Bt-Chl rich zones with Ghn in an Act/Trm-Chl to Ath-Crd/Qz host.
- **Cu-Au, 95.5-104m:** Au occurs associated with disseminated Cpy-Py-Po with Ghn in Bt-Tlc-Act/Trm-Chl schist.
- **Cu-Pb-Au, 106.4-107.2m:** Au occurs associated with disseminated Cpy-Py-Po with Ghn in Bt-Tlc-Act/Trm-Chl schist.
- **Pb-Au, 107.85-108.22m:** Au occurs associated with disseminated-blebby Gal-Cpy-Py-Po-Sph in a Qz-Cc-Trm-Chl schist; assay is over a Qz/Cc-rich section with obvious Gal.
- **116.68-119.75m:** Au occurs in low sulfide content section within a Qz-Cc-Trm-Chl schist containing disseminated-blebby Gal-Cpy-Py-Po-Sph.
- **129.85-133.25m:** The 30 lens is disseminated-stringer sulfides with Cc, in a host of Cc-Bt-Chl-Act/Trm-Qz. The sulfides are 2% Cpy, 2% Gal, 5% Po, 8% Sph, 10% Py. Au mineralization is also present, but there is no obvious relationship with other sulfides.
- **Cu-Pb-Au, 138-139m:** Au occurs associated with disseminated Gal-Cpy-Sph-Py-Po within a Trm/Act-Cc-Chl host.
- **Cu-Pb-Au, 147.04-152.58m:** The 40 lens is within a host of Act/Trm-Qz-Chl schist containing blebby-stringer sulfides; 2% Cpy, 5% Py, and 7% Sph. There are a few diopside patches and late Cc veins.

Appendix 5: Drill hole reports

DDH: DUB191
Location: 5400N, slightly east
Logged: 764.00m-1260.00m
Zones: 10 lens at 877-886m, 20 lens at 905.7-908m, 25 lens at 993-1001.65m, 40 lens at 1153.46-1156.11m

The drill hole starts in less altered intermediate to mafic rock. The hanging wall sequence to the 10 lens is fairly variable with sulfide-rich intervals. The 10 lens itself is semi-massive and hosted in Fe-Mg altered rocks. It is followed by a section of Bt/Ms-Qz+Ky/Sil. Then there is the massive sulfide 20 lens sandwiched between Chl-Crb altered rocks. Another interval of Bt/Ms-Qz+Ky/Sil follows, and the rest of the drill hole is Fe-Mg altered rocks with small intervals of Bt/Ms-Qz+Ky/Sil. However, in the proximal footwall of the 40 lens, there is Fe-Mg alteration that contains actinolite.

Approximately 100m above the logged section, there are a few intervals of rhyolite fragmental, rhyolite tuff, plagioclase porphyritic diorite, dacite fragmental to lapilli tuff, and mafic fragmental.

The mineralization is predominantly stringer sulfides – Sph-Py-Po. Au is likely associated with Cpy, but not restricted to the sections of stringer sulfides.

- **837.65-846.95m:** The interval is possibly a sub-economic part of the 11/10 lens containing 2% Cpy, 8% Sph (patchy), 12% Py, and 20% Po. Calcite and anhydrite occur interstitially with the sulfides. The host is Grt-Bt-Qz+Ghn with local Chl+Ms and 30% stringer Cpy-Po+Sph+Py and a Ghn-Bt-Chl patch with stringer sulfides in Ms-rich sections.
- **877.00-886.00m, 10 lens:** The 10 lens is composed of 30% blebby stringers to near solid sulfides, Cpy-Po-Py-Sph. Sphalerite occurs on its own while Cpy-Py-Po are typically found together. Calcite is present with the sulfides, as well as quartz and anhydrite veins. The host Fe-Mg assemblage is a bit variable: Ghn-St-Bt, Grt-St-Bt-Chl-Crd, and Chl+Ghn-Act.
    - **Cu-Zn-Au, 864-880m:** Au occurs within a sulfide-rich section: stringer Cpy-Sph-Py-Po with Cc and stringer to near solid Cpy-Po-Py-Sph, within Ghn-Act-Grt-St-Bt.
- **905.70-908.00m:** The 20 lens interval is comprised of 10% disseminated to stringer Sph in foliation with Py-Po 12% and trace Cpy within the Chl schist host. Anhydrite veins occur, often with Sph. The host rock appears to be Crd-Act-Chl with possibly St.
- **928.8-929.97m:** Au occurs with disseminated Py in Act/Trm-Chl.
- **Cu-Au, 982.85-983.6m:** Au occurs associated with Cpy-Py/Po in Bt-Ath-Chl/Scap-Crd.
- **Cu-Au, 993.00-1001.65m, 25 lens:** The 25 lens is comprised of blebby to stringer Cpy proximal to late orange (ankerite) veins but not directly associated. It is hosted in a well-foliated Bt-Ath-Crd/Qz rock with trace St-Grt and bands of Bt/Chl occurring with Py-Cpy.
- **1005-1006m, 1009.56-1011.09m:** Au occurs with Cpy in Fe-Mg alteration; Ath-Crd/Qz and Grt-Ath-Chl-Bt. Grt has Bt in its pressure shadows, and sulfides in and proximal to it.
- **Cu-Au, 1059.1-1060.95m:** Au occurs with disseminated Cpy and Ghn in a Grt-St-Ath gneiss.
- **Cu-Au, 1063.65-1063.94m, 1067-1068m:** Au occurs with disseminated Cpy-Py-Po in a Grt-St-Chl-Bt-Ath gneiss, where Grt has sulfides in its fractures and Bt increases proximal to sulfides.
- **Cu-Au, 1070-1071m:** Au occurs associated with local disseminated Cpy in Bt-Ath-Crd.
- **Cu-Au, 1109.16-1109.34m:** MISSING
- **1153.46-1156.11m, 40 lens:** The 40 lens is massive sulfide (40-50% Sph with 15% Py cubes) that appears to be hosted in Ghn-Bt-Ath assemblage. It starts in an increase in Bt-Ghn-Sph bands (also with disseminated to blebby 5% Cpy-Sph-Py/Po). Gradationally, it ends as Ghn-Ath-Ms/Qz (possibly some talc) with near solid sulfide Sph patches/bands.
    - **Zn-Au, 1149.82-1157m:** Au occurs proximal to and within a sulfide-rich interval; diss-blebby sulfides+Ghn in St-Ath-Bt, 40 lens, and diss Sph/Po/Py in Grt-Mt-Crd-Act/Trm-Chl.

Appendix 5: Drill hole reports

DDH: DUB204
Location: 5400N
Logged: 740.22m-1035.08m
Zones: 20 lens at 846.01-861.11m, 21 lens at 840.92-858.72, 24 lens at 871-878m, 30 lens at 957-970m, 26 lens at 970.68m-978m

The drill hole begins in less altered rock leading into massive sulfide, into a thick section of Chl-Crb, and then back into massive sulfide and less altered rock. The 20/21 and 30/26 lenses occur within the thick sequence of Chl-Crb altered rocks with decent gold mineralization associated with disseminated/vein Sph-Gal+Cpy. Stringer/blebby/disseminated Py and Po occur throughout the drill hole, in and discordant to the foliation.

Approximately 100m above the logged section, there is a mafic tuff unit and a basalt unit. Approximately 100m below the logged section, there is a mafic fragmental unit and a Bt-schist unit.

Cu-Pb-Au, 761-765.68m: Au occurs associated with disseminated Cpy-Gal+Py within a mafic volcaniclastic with banded, alternating Ca-altered clasts (Act-Grt).

Cu-Zn-Au+Pb, 839.4-863.58m, 21 lens (overlaps with 20): First, there is a weakly altered mafic-intermediate rock (Grt-Bt-Qz/Plag-Hbl) with 10% disseminated-stringer sulfides in the foliation (Cpy-Py-Po-Sph). It is followed by an interval of near solid sulfide to solid sulfide Cc-Sph-Py+Cpy+Po and then Cc-Qz-Trm with disseminated Cpy-Sph-Py+Aspy. Next, there is a silicified/quartz rich interval with 1mm Py-Bt bands, blebby Cpy-Sph-Py, and 20-30cm bands of Py-Sph+Cc+Cpy+Aspy. The last few intervals are calc-silicate to carbonate silicates; Bt-Grs-Trm-Qz/Plag with disseminated Gal-Cpy-Sph-Py, Bt-Act/Trm-Cc/Qz with Gal+Sph in late veins, Bt-Act-Qz with 20-30% stringer to near solid sulfide Cpy-Py-Sph, and Act/Trm-Cc-Di with Cpy-Py-Po-Sph,

846.01-861.11m, 20 lens (overlaps with 21): First, it is massive Py with interstitial Sph and Cc as well as 5% Cpy-Po. Second, disseminated-vein Cpy<Sph<Py (15%) occurs in Cc-Trm-Qz. Third, there is a silicified/quartz-rich interval with Py-Bt+Cpy+Sph bands. Fourth, in a dominantly Ca-rich interval (Bt-Grs-Trm-Qz/Plag), disseminated-stringer Gal-Cpy-Sph-Py occur (with Gal in late veins, sometimes with Sph). Fifth, there is an interval of Trm-Cc-Di with 12% Sph-Po-Py-Cpy.

871.00-878.00m, 24 lens: The 24 lens is a chlorite dominated interval with calcite veins and silica-rich sections. Calcite veins commonly have Qz/Ep, Gal, Crd, Cpy-Py-Po, and at the margins, Chl or Act/Trm. A section of higher Au assays is in a Chl poor, Trm-Cc rich section with disseminated Gal and Cpy. Sulfides are typically patchy and disseminated (Cpy-Sph-Po-Py, Sph-Gal-Py).
Pb-Au±Zn, 871-889m: Au occurs in calc-silicate to carbonate silicate assemblages; Trm/Act-Bt-Chl schist with disseminated Py and Ghn-Trm/Act-Bt-Ms/Tlc-Chl schist with disseminated sulfides.

Zn-Au, 900-950m: Au occurs with disseminated sulfides in Ghn-Trm/Act-Bt-Ms/Tlc-Chl schist, Act/Trm-Cc-Chl with disseminated Gal-Cpy-Po-Py, and Mt-Tlc-Trm/Act-Cc-Chl schist with disseminated sulfides.

- **940.53-947.00m, 40 lens:** MISSING

Pb-Au±Zn, 963.2m-978.38m, 30 & 26 lens: Au occurs in near solid sulfide-solid sulfide Cpy-Po-Sph-Py, sometimes stringer-disseminated, with Cc-Anh patches in Act/Trm-Chl (30 lens), then in a less altered mafic dike with disseminated sulfides and a Cc-Act/Trm-Chl schist with disseminated Cpy-Py-Po, trace Gal in Cc-Qz (26 lens).

Appendix 5: Drill hole reports

DDH: DUB195
Location: 5600N, west
Logged: 740.41m-831.67m
Zones: 20 lens at 817-829m, 21 lens at 810-828m

For the most part, the drill hole is in less altered felsic to intermediate to mafic rock (in the hanging wall and foot wall). There is patchy Mt, Grt, and Chl in these rocks. There are also quartz-epidote patches with associated grossular and anhydrite. Calcite veins occur with actinolite and epidote at the end of the drill hole. There is sparse disseminated-blebby Py and Po in the less altered rocks. The first section of altered rocks is Ky-Ms-Bt-Qz+St+Grt within a sequence of felsic rocks; disseminated Py occurs with Sph veins and Cpy blebs. The second interval of altered rocks is Chl-Crb+Act+Ep with Py-Po in and overprinting the foliation. It is followed by an interval of Chl-Bt-Qz+Ghn with discordant sulfides (including Gal). Next, the 20/21 lens contains Py cubes with interstitial Sph and Cc and Ky-Bt-Qz. Cpy also occurs in the interval, likely what Au occurrences are associated with.

Approximately 100m above the logged section, there are intervals of silicified amygdaloidal basalt and Fe-Mg alteration. Approximately 100m below the logged section, there are intervals of rhyodacite, weakly altered basalt, and altered basalt.

Pb-Au+Zn+Cu, 784-786m: Au is spatially associated with a local patch of calc-silicate alteration within Ky-Ms-Bt schist with disseminated Py and patchy Sph-Cpy.

810.00-828.00m, 21 lens (overlaps with 20): MISSING 810-812.60m.
The 21 lens is an interval of well-foliated high silica rock with Bt/Chl with 3% foliated Gal-Cpy-Py/Po stringers associated with Ghn; it appears to be a felsic unit with quartz veins in the foliation. It grades into near solid sulfide to solid sulfide, Cpy-Sph-Py with interstitial Cc, in a Py-Ky-Bt-Qz host that occurs in little windows.

- **Cu-Au, 810-817m:** Au appears to be related to stringer Cpy-Sph-Py-Po+Ghn in Chl-Bt-Qz.

Zn-Au+Cu, 817.00-829.00m, 20 lens (overlaps with 21): In the 20 lens, there is predominantly near solid sulfide to solid sulfide (Cpy-Sph-Py) with interstitial Cc; Au appears to be associated with the massive sulfide. Two quartz veins are also present in the massive sulfide, one with Chl in it. The Py-Ky-Bt-Qz host also occurs in little windows through the section.

Appendix 5: Drill hole reports

DDH: DUB226W02
Location: 5600N, center
Logged: 878.35m-1041.58m
Zones: 20 lens at 887.73-893.38m, 21 lens at 901.43-919.13m, 25 lens at 954.23-965.61m

The drill hole is fairly variable with Fe-Mg altered rocks that contain calcic phases (commonly Act). It starts in Act-Bt-Ath, then Ky-Bt, then Act-Chl-Crd, then altered felsic-intermediate, and then mafic-intermediate. Next, there is a sequence of mostly altered Fe-Mg rocks; a quartz vein occurs with Gal-Py-Po in between lenses 21 and 25 in this section. Next is the 25 lens, which is comprised of Ghn-Bt-Ms with foliated stringer Sph-Cpy in the foliation, and possibly disseminated Gal. Ghn is associated with the Sph. Minor Ath occurs as well. The interval is cut by Ky-St-Bt+Ghn in the middle.

Last, there is a thick section of well-foliated chlorite schist with variable mineralogy. Sulfides occur within the foliation as stringer-blebby Cpy and finely disseminated Py-Po. Patchy calcite occurs and appears to be overprinting chlorite. Unknown bluish porphyroblasts appear locally – possibly Crd pseudomorphs after Ky. Minor Act and Mt also occur patchily. A short interval of ellipsoid clasts occurs, smaller ones at the edges and larger ones in the middle. In the Chl-poor zones, other minerals such as Ms or Crd/Ath are in greater abundance. Bt and St occur at the end of the section.

Approximately 100m above the logged interval, there are units of mafic volcaniclastics, a quartz vein, Ms-Bt-Qz schist, Py-Bt-Qz schist, and Bt-amphibole-Qz gneiss.

- **Cu-Zn-Au±Pb, 887.23-892.22m:** MISSING
- **Cu-Zn-Au, 892.22-893.38m:** MISSING
- **Cu-Zn-Au, 894.6-894.8m:** Au occurs in Grt-St-Ath-Bt with Cpy-Py and Sph-Ghn stringers.
- **Cu-Au, 896.19-896.51m:** Au occurs in Grt-St-Ath-Bt gneiss.
- **898.47-898.77m:** Au occurs with stringer Cpy-Py-Po+Ghn in Grt-St-Mt-Chl-Bt-Ath-Crd/Qz.
- **901.43-919.13m, 21 lens:** MISSING 905.85-918.56m. In the 21 lens, there is Grt-St-Chl-Bt-Ath-Qz/Crd with veins of Ghn+Po-Cpy that Au is likely associated with.
- **901.43-901.65m:** Au occurs with stringer Cpy-Py-Po+Ghn in Grt-St-Mt-Chl-Bt-Ath-Crd/Qz.
- **Cu-Zn-Au, 902.74-908.68m:** MISSING 905.5-908.68m. Au appears to be associated with Cpy-Py-Po+Ghn stringers within Grt-St-Mt-Chl-Bt-Ath-Crd/Qz.
- **Cu-Au, 909.67-910.49m:** MISSING
- **Cu-Zn-Au±Pb, 911.72-919.13m:** MISSING
- **Cu-Zn-Au±Pb, 926.11-927m:** Au is associated with a Sph-Gal vein proximal to a Ca-rich patch within Bt-Ath-Ms-Chl-Crd/Qz.
- **931.72-932.38m:** Au occurs associated with blebby Py/Po-Ghn in Crd-Bt-Act-Chl schist.
- **939.58-942.36m, 947.8-951.47m:** Au occurs associated with Ghn-Cpy-Py/Po in Grt-St-Chl-Ath-Crd; proximal to a Qz vein with Py/Po-Gal but no Au mineralization.
- **Cu-Zn-Au±Pb, 954.23-965.61m, 25 lens:** The 25 lens is a mineralized well-foliated Bt-Ms-Qz where Au is associated with Cpy-Sph/Ghn stringers.
- **Cu-Zn-Au, 969.87-970.32m:** Au is associated with Cpy-Ghn-Sph-Bt stringers in Ky-St-Bt-Qz.
- **Cu-Zn-Au, 971.55-972.83m, 977.23-978.41m:** Au occurs associated with stringer Cpy-Sph/Ghn in Bt-Ms-Qz.
- **Cu-Zn-Au, 1013-1037.65m:** Au occurs associated with Cpy stringers and finely disseminated Py-Po within a variable Chl-schist containing Act-Cc, Ghn, Ky/Crd and Mt porphyroblasts.

Appendix 5: Drill hole reports

DDH: DUB226W06
Location: 5600N, center-west
Logged: 790.93m-987.00m
Zones: 21 lens at 877.57-887m, 25 lens at 892.87-904.18m, 20 lens at 903-905m

The logged section of this drill hole contains weakly altered volcanics and strongly altered rocks. Au mineralization primarily limited to the strongly altered calc-silicates to carbonate silicates and Fe-Mg altered rocks. The weakly altered volcanics occur above and below the altered rocks, dominantly mafic with small sections of felsic (Ms-bearing) and intermediate rocks. In the hanging wall weakly altered rocks, there are two 5m occurrences of Ky-Bt+Ms schists overlying a Fe-Mg altered rock.

Cu-Zn-Au, 808-808.36m: Au occurs associated with stringer-disseminated Po-Sph in altered mafic with local Cpy-Py. It occurs proximal to a section of near solid sulfide.

Cu-Zn-Au, 871.89-873.25m: Au occurs associated with stringer-solid sulfide Py-Cpy-Po-Sph in a Ghn-Act-Chl schist; below a section of near solid sulfide.

Cu-Au+Zn, 877.57-886.29m, 21 lens: The 21 lens is variable in this section. It begins in a Tlc-Act-Chl schist with Cpy<<Py<Po within the foliation which is shallow then steep. It grades into a section where there may be evidence of a shear zone; Bt-Chl-Qz to Grt-Ky-Bt with blebby-stringer trace Py, 3% Po/Cpy to Act-Chl-Bt+Qz/Plag and trace sulfides (Cpy-Po). An interval of Grt-Ky-Ath-St-Bt-Chl schist is next (no sulfides). Last, there is an Ath-Chl schist with 3% disseminated Py/Po-Cpy and stringer Cpy with anhydrite.

886.29-892.87m: Au occurs associated with disseminated-stringer Cpy-Py/Po in Ath-Chl schist (part of 21 lens) and Po-Gal-Cpy in Grt-Ath-Bt.

Cu-Zn-Au+Pb, 892.87-905.00m, 25 lens: The 25 lens is primarily in Fe-Mg alteration (in calc-silicate to carbonate silicates where it overlaps with the 20 lens). It starts in a Grt-Ath-Bt with 10% sulfide stringers (Py-Gal-Sph-Po-Cpy) in which Act is also often present. The next interval is Grt-Chl-Bt-Ath-Crd with disseminated Py-Cpy in Bt bands as well as Py-Po-Cpy-Sph stringers to near solid sulfide in Act-Tlc-Qz; 5% total sulfides. The following section is a Crd-Tlc schist with 5% disseminated Cpy-Py. The last section is a Ghn-St-Act-Bt Chl schist with blebby sulfides (trace Sph, 2% Cpy, 3% Py, 5% Po) and near solid sulfide to solid sulfide (Cc-Py-Sph, 20 lens).

903.00-905.00m, 20 lens: There is a section of near solid sulfide to solid sulfide of Py-Sph+Cc as well as quartz veins rimmed by Bt. The general lithology is St-Act-Bt Chl schist with patchy Crd-Ath and blebby sulfides; trace Sph, 2% Cpy, 3% Py, 5% Po.

908-910m: Au occurs associated with blebby Sph-Cpy-Py-Po in Ghn-St-Act-Bt-Crd-Chl schist

Appendix 5: Drill hole reports

DDH: DUB245
Location: 5600N, center-east
Logged: 910.31m-1249.00m
Zones: 20 lens at 971.78-974.26m, 21 lens at 995.9-1001.18m, 25 lens at 1007.28-1018.63m, 26 lens 1078.14-1085.32m, 28 lens at 1140.18-1154.49m

The logged section of this drill hole contains primarily Fe-Mg altered rocks with calc-silicates/carbonate silicates, an intermediate rock, and two occurrences of Ky/Sil-St-Bt rocks (at the beginning and deep in the alteration). The strong Fe-Mg altered rocks dominate the section from a depth of 1000m and on; though there is also a small section near the beginning of the interval. Gold is associated with the presence of Cpy-Ghn stringers, sometimes with Po as well.

Pb-Au, 963.21-963.97m: Au occurs within a carbonate/quartz-Chl schist, likely associated with Py-Sph stringers mixed in with Cc-Qz. (No visible Gal)

971.78-974.26m, 20 lens: MISSING FROM CORE BOXES

Cu-Au, 995.90-1001.18m, 21 lens: The 21 lens occurs across two intervals; the bottom of a Chl-Tlc-Ath-Qz schist and mostly in Ath-Crd+Bt overprinting Chl where gold is associated with disseminated to stringer Cpy-Ghn+Po.

Cu-Au+Zn, 1007.28-1018.63m, 25 lens: The 25 lens occurs in Fe-Mg alteration; dominantly in Ath-Crd overprinting Chl where gold is associated with disseminated to stringer Cpy-Ghn+Po, and the top of the next interval of weaker Fe-Mg alteration (Bt-Ath-Chl/Qz) where gold is associated with Cpy-Ghn.
Cu-Au+Zn, 1019.50-1026.85m: Au occurs in an interval of Bt-Ath-Chl/Qz, likely associated with 5% Cpy-Ghn+Sph bands.

1061.02-1070.68m: Au occurs in a Grt-St-Bt-Ath-Crd/Qz gneiss and appears to be associated with trace disseminated Py-Po+Cpy and Ghn+Cpy-Qz stringers.
Cu-Au, 1078.14-1085.32m, 26 lens: The 26 lens occurs in Fe-Mg alteration, crossing over two intervals. The first interval is in Chl schist with patchy Ath-Crd with Po-Cpy-Ghn bands. The second interval is Ath-Crd+Bt+Ghn with 10% disseminated to stringer Py and Cpy.

Cu-Au, 1123.04-1129.48m: Au occurs in three intervals in this section. It is in an Ath-Bt-Crd-Chl schist with Ghn+Cpy-Po, Ky/Sil-St-Bt-Ath gneiss with 2% Cpy stringers in buff alteration, and Grt-St-Bt-Ath-Crd/Qz gneiss with Ghn-Cpy stringers.
Cu-Au, 1140.18-1154.49m, 28 lens: The 28 lens is in Fe-Mg alteration, within a section of Grt-St-Bt-Ath-Crd/Qz gneiss. Gold appears to be associated with an increase in Ghn-Cpy stringers/bands. Ath appears to be randomly oriented within the section and becomes foliated again near the end.
Cu-Au, 1160-1201.67m: Au mineralization occurs across two intervals; at the end of a Grt-St-Bt-Ath-Crd/Qz gneiss likely associated with Cpy-Po stringers and primarily in a Grt-Bt-Ath-Crd/Qz gneiss with 1-2% blebby-stringer Cpy that is likely associated with Au (with and without quartz veins).

Appendix 5: Drill hole reports

DDH: DUB252W01
Location: 5600N, slightly east
Logged: 958.50m-1235.73m
Zones: 20 lens at 1007.49-1010m, 21 lens at 1015-1036m, 25 lens at 1049-1062.31m, 27 lens at 1139.29-1149.12m & 1176-1189.39m

The drill hole begins in Fe-Mg alteration with patchy Mt-Sil and minor disseminated-blebby Py-Po. The next interval is a Py-Ky-Bt-Qz ± Ms assemblage, and then a less altered mafic volcaniclastic with disseminated arsenopyrite. The following interval is Cc-Act-Chl with disseminated Gal and Cpy; dolomite appears to present as well. Next is a moderately foliated Act/Hbl-Crd/Qz interval with stringer Cpy. The rest of the drill hole is overall Fe-Mg alteration, with varying degrees of intensity; St, Grt, Bt, Ath, and Crd are the main minerals that occur. Within the strong Fe-Mg altered rocks, there are zones of mineralization with calcic amphiboles/plagioclase-quartz.

Approximately 100m above the logged interval, there are sections of mafic fragmental, muscovite altered Bt schist, and Fe-Mg alteration leading into the logged interval. Approximately 100m below the logged interval, there is a continuation of Fe-Mg alteration until the end of hole.

- **As-Au, 1003-1004m:** Au occurs with disseminated Cpy-Gal-Aspy in a mafic volcaniclastic.
- **Zn-Pb-Au, 1006-1007m:** The assay is across the contact between a mafic volcaniclastic with disseminated Cpy-Gal-Aspy and a mineralized Act/Trm-Cc-Chl schist with disseminated-blebby Po-Gal-Cpy-Sph-Py. Sharp contacts appear to be bounded by Bt.
- **1007.49-1010.00m, 20 lens:** The 20 lens is in a Chl-schist with disseminated Cpy-Gal+Ghn+Sph, blebby Sph-Cc, and disseminated Py-Cpy.
- **Pb-Au, 1015-1020m; Cu-Au+Pb, 1020-1036m; 21 lens:** The 21 lens begins in an Act/Trm-Cc-Chl schist with disseminated-blebby Po-Gal-Cpy-Sph-Py. Then there is Chl-Plag/Qz-Act with foliated stringer-blebby Po-Cpy; locally sulfides are1 parallel to the core axis. The next interval is Grt-Bt-Ath gneiss with Ghn-Sph-Py/Py/Cpy-Po-Sph stringers and then there is an Act-rich section with disseminated Cpy-Gal as well as minor talc bands with Ghn and blebby sulfides.
- **1049.00-1062.31m, 25 lens:** The 25 lens interval is a Ky-Bt-Qz gneiss with trace disseminated Py. There is an Act-rich section with local disseminated-blebby Cpy-Gal, bounded by a quartz vein and approximately 15cm of Ms-Tlc. It is also partially in a variable Bt-Chl schist.
    - **Pb-Au+Cu, 1049-1056m:** Au occurs in Grt-Bt-Ath and in Ky-Bt associated with a bleb of Cpy-Gal bleb in an Act-rich section.
- **Cu-Pb-Au, 1060-1061m:** Au occurs within a variable Bt-Chl schist.
- **1072.93-1076.84m:** Au occurs in Ky-Bt-Ms with disseminated Py and St-Grt-Ath-Bt gneiss.
- **1079.84-1080.84m, 1089.45-1099.58m:** Au occurs in St-Grt-Ath-Bt gneiss.
- **1139.29-1149.12m, 27 lens:** The 27 lens is an Act-Qz interval with blebby to stringer Cpy±Po which also occurs in Fe-Mg alterated rocks. There are also quartz veins with associated sulfides that occur parallel to foliation, proximal to and within the Fe-Mg altered rocks.
    - **Cu-Au, 1139.29-1166.61m:** Au occurs in dominantly Fe-Mg altered rocks; St-Grt-Ath-Bt gneiss, mineralized Act-Qz with blebby to stringer Po-Cpy, St-Grt-Ath-Crd-Chl schist with blebby Cpy, and St-Grt-Ath-Bt with disseminated Po-Cpy.
- **Cu-Zn-Au, 1176-1195.71m, 27 lens:** Au occurs in Fe-Mg altered rocks; St-Grt-Ath-Bt with disseminated Po-Cpy and St-Ath-Crd/Qz with disseminated to stringer Po-Cpy.
- **Cu-Zn-Au, 1215-1215.33m, 1221.84-1222.17m:** Au occurs in Fe-Mg altered rocks; Grt-Ath-Crd/Qz with stringer Po-Cpy and St-Grt-Ath-Crd/Qz.